LBL-13518

Lawrence Berkeley Laboratory
UNIVERSITY OF CALIFORNIA

Materials & Molecular Research Division

RECEIVED
LAWRENCE
BERKELEY LABORATORY
FEB 10 1982
LIBRARY AND
DOCUMENTS SECTION

MARTENSITIC TRANSFORMATIONS IN ZrO_2:
NUMERICAL METHODS AND APPLICATIONS

Ming-Der Donald Huang
(Ph.D. thesis)

May 1981

TWO-WEEK LOAN COPY

This is a Library Circulating Copy which may be borrowed for two weeks. For a personal retention copy, call Tech. Info. Division, Ext. 6782

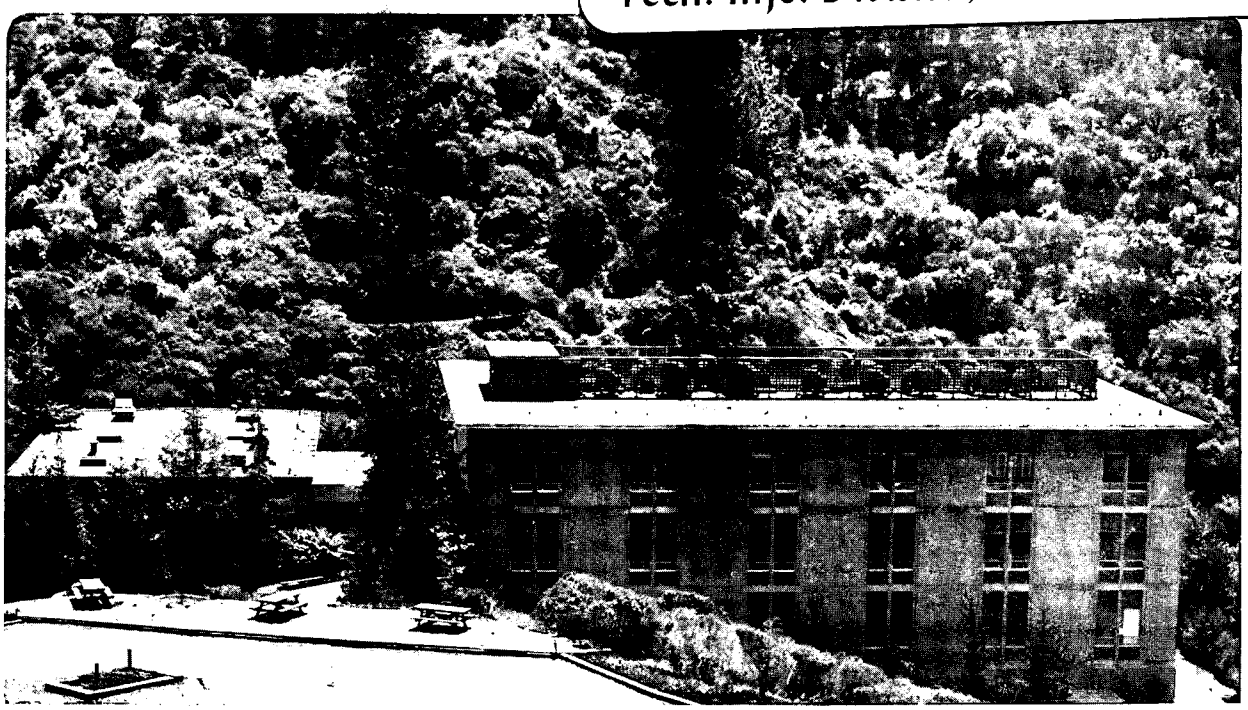

LBL-13518 c.2

Prepared for the U.S. Department of Energy under Contract W-7405-ENG-48

DISCLAIMER

This document was prepared as an account of work sponsored by the United States Government. While this document is believed to contain correct information, neither the United States Government nor any agency thereof, nor the Regents of the University of California, nor any of their employees, makes any warranty, express or implied, or assumes any legal responsibility for the accuracy, completeness, or usefulness of any information, apparatus, product, or process disclosed, or represents that its use would not infringe privately owned rights. Reference herein to any specific commercial product, process, or service by its trade name, trademark, manufacturer, or otherwise, does not necessarily constitute or imply its endorsement, recommendation, or favoring by the United States Government or any agency thereof, or the Regents of the University of California. The views and opinions of authors expressed herein do not necessarily state or reflect those of the United States Government or any agency thereof or the Regents of the University of California.

LBL-13518

MARTENSITIC TRANSFORMATIONS IN ZrO_2: NUMERICAL METHODS AND APPLICATIONS

Ming-Der Donald Huang

Ph.D. Thesis

May 1981

Materials and Molecular Research Division
Lawrence Berkeley Laboratory
and Department of Materials Science and Mineral Engineering
University of California
Berkeley, CA 94720

This work was supported by the Director, Office of Energy Research, Office of Basic Energy Sciences, Materials Science Division of the U. S. Department of Energy under Contract No. W-7405-ENG-48

Dedicated

To my parents

MARTENSITIC TRANSFORMATIONS IN ZrO_2: NUMERICAL METHODS AND APPLICATIONS

Contents

ABSTRACT vii

PART I: FINITE ELEMENT CALCULATIONS OF THE STRAIN ENERGY OF TWINNED MARTENSITE (THEORY)

Abstract 2

1. INTRODUCTION 3

1.1 Martensitic Transformations 3

1.2 Significance of the Martensitic Transformation 5

1.3 Martensite Theories 6

2. THE STRAIN ENERGY OF MARTENSITE 11

2.1 Strain Energy Formulations 13

2.2 The Finite Element Formulation 16

2.2.1 Introduction 16

2.2.2 The Phase Transformation Problem 18

2.2.3 The Strain Energy Formulation 25

2.2.4 Examples of the Finite Element Calculation . . . 28

3. CONCLUSION 32

Appendix A: The Equivalent Inclusion Method 33

Appendix B: Twins and Uniformity 43

Appendix C: Symbols and Notations 44

Appendix D: Decomposition of R^o to Surface and Body Force Terms . 47

Appendix E: The Strain Energy of a Spherical Inclusion, In a Spherical Matrix, Subject to Uniform Expansion . . . 49

REFERENCES 55

TABLE 59

FIGURE CAPTIONS 60

FIGURES 61

PART II: STRAIN ENERGY OF TWINNED ZrO_2 MARTENSITE

Abstract 66

1. INTRODUCTION 67

1.1 Zirconia and Transformation Toughening 67

1.2 The Role of Strain Energy in Transformation Toughening . 69

1.2.1 Strain Energy and Transformation Zone 69

1.2.2 Strain Energy and Optimal Size for Toughening . . 69

1.2.3 Strain Energy and Transformation Toughening . . . 70

2. STRAIN ENERGY CALCULATIONS 71

2.1 Elastic Constants 71

2.2 The Stress-Free Strain 72

2.2.1 The Lattice Constants 73

2.2.2 Boundary Coherency 74

2.2.3 Lattice Correspondence 75

2.2.4 Orientation Relationship 77

2.2.5 The Stress-Free Strain 78

2.3 Twinning 79

2.4 The Shape of the Precipitate 80

2.5 Finite Element Calculations 80

2.5.1 Additivity of the Strain Energy 80

2.5.2 Symmetry Properties 81

2.5.3 Finite Element Mesh 82

3. RESULTS 82

3.1 Influence of Twinning 83

3.2 Precipitate Shape Effects 84

3.3 Effect of the Shearing Plane 84

3.4 Differences Between Transformation in Single Crystal (Large Grained) ZrO_2 and ZrO_2 Precipitates in PSZ . . . 85

3.5 The Effect of the Matrix 85

4. DISCUSSION 86

4.1 Bounds on the Strain Energy 86

4.2 The Twin Boundary Energy 87

4.3 Size Effects 90

4.4 The Twin Thickness 90

4.5 The $(110)_m$ Twinning 91

5. CONCLUSIONS 92

Appendix A: The Scaling Factor for the Strain Energy Calculation 94

Appendix B: An Interative Method to Determine the Unconstrained Lattice Parameters of the (t)-ZrO_2 97

Appendix C: Listing of a Computer Program for Strain Energy Calculation Based on Eshelby Method 99

REFERENCES 105

TABLES 108

FIGURE CAPTIONS 116

FIGURES 118

ACKNOWLEDGMENTS 137

MARTENSITIC TRANSFORMATIONS IN ZrO_2: NUMERICAL METHODS AND APPLICATIONS

Ming-Der Donald Huang

Materials and Molecular Research Division
Lawrence Berkeley Laboratory
and Department of Materials Science and Mineral Engineering
University of California
Berkeley, CA 94720

ABSTRACT

Part I

The strain energy formulation for systems undergoing phase transformations has, for the first time, been established by the finite element method. The primary advantages of this method over others are the removal of limitations based on elastic isotropy or homogeneity, and its applicability to all types of stress-free strain (including twinning). This method has been applied to study the strain energy changes associated with the phase transformation of a spherical inclusion. The result indicates that good numerical accuracy can be obtained with a reasonably small number of elements.

Part II

The strain energy of an inhomogeneous (m)-ZrO_2 precipitate embedded in the (c)-ZrO_2 matrix has, for the first time, been determined using the finite element method. It was found that the total strain energy can be decoupled into two parts, one contributed by the diagonal stress free strain and the other by the shear stress free strain. These two strain energies are additive for an isotropic system. Twinning was found to reduce the shear strain energy and was

thus justified as a relaxation mechanism. It was found that for a given precipitate, the orientation relationship which gave the minimum strain energy changed when twinning occurred. Thus twinning can not be neglected when making predictions based on the minimum energy approach. The active transformation mode was found to be predetermined by the precipitate shape and thus quite different from that in a larger grained pure ZrO_2. For PSZ, the minimum strain energy is related to the orientation relationship $(001)_m \| (001)_c$, $[100]_m \| [100]_c$; the lattice correspondence LCC, and the twinning mode $(001)_m$.

A minimum energy approach was used to estimate the bounds on the twinning boundary energy. It was found that $0.36 \leq \gamma_T \leq 0.89\ Jm^{-2}$. The twin width was found to be relatively insensitive to the particle size based on the free energy approach, consistent with the experimental observation.

Part I

FINITE ELEMENT CALCULATIONS OF THE STRAIN ENERGY OF TWINNED MARTENSITE (THEORY)

ABSTRACT

The strain energy formulation for systems undergoing phase transformations has, for the first time, been established by the finite element method. The primary advantages of this method over others are the removal of limitations based on elastic isotropy or homogeneity, and its applicability to all types of stress-free strain (including twinning). This method has been applied to study the strain energy changes associated with the phase transformation of a spherical inclusion. The result indicates that good numerical accuracy can be obtained with a reasonably small number of elements.

1. INTRODUCTION

1.1 Martensitic Transformations

Martensitic transformation is a polymorphic phase transition, which consists of the regular rearrangement of the crystal lattice by a diffusionless cooperative movement of the constituent atoms. The product phase is known as martensite. It usually exhibits specific geometrical and kinetic characteristics. These characteristics may differ for different materials and under different conditions, but some common morphological, thermodynamic and kinetic features do exist.

1) The transformations are shear-like or displacive in nature. Little diffusion or interchange of atoms is involved in the process. This is to be contrasted to some diffusion-controlled solid state transformations (such as eutectoid decomposition) in which the atoms undergo random diffusional movements of a relatively long range nature. Moreover, being largely diffusionless, the martensite inherits the composition of the parent phase.

2) The transformation is accompanied by a change in shape of the transformed region. The parameters of the macrodeformation are constant for a given material. The shape change reveals itself as a characteristic relief effect on a plane surface.

3) There exists an orientation relationship between the lattices of the parent phase and the martensite. The orientation relationship is a constant characteristic of each material.

4) The martensites have a regular internal structure, usually a polysynthetic twin.

5) The martensite phase usually forms as a thin lenticular plate lying along a habit plane of the parent phase. The habit plane is irregular in general, i.e., the Miller indices are not simple.

6) Supercooling is required for the transformation to occur. When the supercooling is not great, only part of the specimen transforms; the amount of the martensite increases with the degree of supercooling. Thermal hysteresis effects are usually observed for the reverse transformation.

7) The rate of the martensite crystal growth is great ($\sim 10^4 - 10^5$ cm/sec), and displays no appreciable temperature dependence.

8) Both athermal and isothermal transformations can proceed in the same material. The nucleation rate for the former is large and does not display any temperature dependence. For example, martensite can form even at temperatures near absolute zero. The nucleation rate of an isothermal transformation is temperature dependent.

9) The morphology of the martensite and the temperature at which the transformation occurs are strongly influenced by the applied stress.

It is to be emphasized that the features cited above may also appear in other phase transitions in solids. Conversely, certain martensitic transformations do not exhibit all of the noted characteristics. These features should not therefore be regarded as necessary or sufficient for a martensitic transformation.

1.2 Significance of the Martensitic Transformation

The martensitic transformation has been found in many systems including metals and nonmetals.[1] It has been the subject of extensive research, because martensite has several important applications.

The occurrence of the martensitic transformation can drastically change the microstructure. Also, appreciable internal stress can be induced by the transformation strain. Hence the mechanical properties of the material are greatly influenced. The best known examples are the transformations that occur by quenching in the production of the ferrous martensites. This process generates steels with high hardness and other mechanical attributes. Certain martensitic transformations occurring near an advancing crack tip in a two phase system (such as partially stabilized zirconia[2,3] and austenitic FeNiAl-alloys[4]) have been found to enhance the fracture toughness. This process has been referred to as transformation toughening. Thus the martensitic transformation is of value for microstructural design. The advantages are especially evident for ceramics which are inherently brittle, and can experience order of magnitude increases in toughness.

The martensitic transformation has also been demonstrated to contribute to the following interesting phenomena: thermoelasticity, superelasticity and the shape memory effect.[5] These effects are now subject to intense investigation, because of their potential applications in shape-recovery devices, in heat engines and as acoustical damping materials.

Recently, a martensitic transformation has been found to precede the superconducting transition in a series of superconductors with high critical temperatures (of A-15 structure). An understanding of the martensitic transformation will elucidate the nature of the superconducting transition, and may offer a potential means of raising the critical temperature. This is most desirable for practical superconducting materials.

Diffusionless phase transformations are frequently associated with ferromagnetic transitions, paraelectric to ferroelectric transitions, semiconductor to metallic transitions and, order-disorder transitions. Development of the theory of the martensitic transformation will promote the understanding of the transitions mentioned above, and of their technological applications.

1.3 Martensite Theories

Because of the importance and complexities of the martensitic transformation, a large number of hypotheses, models and theories have been proposed to explain the peculiarities of the transformation. The historical evolution of the theories can be found in the review papers by Christian.[6,7] The modern martensite theories may be summarized as follows.

The crystallography is the most extensively developed aspect of the martensitic transformation, as independently established by Bowles and Mackenzie[8,9] and by Wechsler, Lieberman and Reed.[10,11] The models are based on an invariant plane strain assumption, which requires that the interface between a martensite plate and the parent

phase be an undistorted and unrotated plane. The theory is phenomenological because a postulated martensite substructure is used. Nevertheless, the model predicts the habit plane of an isolated martensite plate with reasonable accuracy (although the predictions[12] of shape change directions are usually less satisfactory). However, as is characteristic of most phenomenological theories, discrepancies often exist. Typical examples include the detection of different martensites in the same alloy and sometimes in the same sample, and often with a variable internal structure. Various attempts have been made to explain the scattering of the habit planes. These include the introduction of a dilation parameter δ,[9,13] a double shear mechanism,[14,15] and an accommodation strain[15] (in parent crystals). However, these explanations are still phenomenological and none of them are completely satisfactory. In addition to its phenomenological nature, the crystallographic theory has the following limitations. Firstly, the theory might not be applicable to the transformation of spheroidal precipitates with a finite number of internal twins, because the resulting martensite is not plate-like and there is no parent-martensite interface present in the final structure. Secondly, the interaction of martensite plates is not considered and therefore, the theory can not explain the spatial arrangement of the martensite within the parent phase.

Another approach, the minimum strain energy approach, was advocated by Khachaturyan,[17] and used by Shibata and Ono[18] among others, to explain the crystallography of martensite. Reasonable

success has been claimed. Yet none of these treatments have considered the effect[19] of twinning, which will change the strain energy minimum, and shift the habit plane away from predicted values. Recently, two dimensional computer simulations based on Khachaturyan's approach have been conducted by Chen.[20] Many features of the martensitic transformation, including twinning, were successfully revealed. However, further work along similar lines is needed in order to address the three dimensional character of typical martensite transformations.

As for the thermodynamics and kinetics of the martensitic transformation, four major theories have been developed:[38]

1. The mechanism of lattice softening.[21-24] According to this approach, the martensitic transformation occurs due to the loss of mechanical stability of the parent phase, resulting from the softening of some generalized shear elastic constant (e.g., $c' = (c_{11} - c_{12})/2$) in the vicinity of the transition temperature. Mechanisms of phonon nucleation[26] and elastic spinodal decomposition[24,25] have been proposed to explain the nucleation of martensite. Experimental evidence of the lattice softening has been obtained in A-15 compounds, such as V_3Si, Nb_3Sn and V_3Ga; and other alloys like In-Tl, Au-Cd, and Ti-Ni systems etc. However, the experimental support is limited to either second-order phase transitions or first-order transitions with little discontinuity (transformation strain $<10^{-2}$).

2. The classical nucleation and growth theory: The martensitic transformation is treated as a first order phase transition and its characteristics are explained in the framework of the classical and

nucleation and growth theory. There are two nucleation theories: homogeneous[27,28] and heterogeneous.[29,30] The former correctly indicates that the isothermal nucleation rate varies with temperature in a C-curve fashion, increasing to a maximum with decreasing temperature and then diminishing with further decrease in temperature. However, the calculated activation energy is far too high to be overcome by thermofluctuation, and the homogeneous nucleation theory can not explain the athermal transformation at temperatures in the vicinity of absolute zero.[31]

The heterogeneous nucleation theory has employed a spectrum of pre-existent embryos to account for the athermal transformation, but there are quantitative difficulties (the activation energy is far too high for the transformation to occur[32]) when the theory is applied to isothermal kinetics. Additionally, the martensite embryo has never been experimentally observed.

3. Defect assisted nucleation and growth theory: The quantitative difficulties encountered with the classical nucleation and growth theory have stimulated the formulation of theories that explain the transformation peculiarities using various dislocation mechanisms. This approach differs from the heterogeneous classical nucleation theory by allowing a monotonically decreasing free energy[31] (rather than an energy barrier). The embryos are surrounded by loops of dislocations,[33] and the growth of the embryo is achieved by expansion of the dislocation loops. Therefore, a dislocation

structure is developed during the growth process. In the classical theory, no such dislocation structure is assumed. Specific mechanisms have been proposed such as: pre-existing embryos of martensite surrounded by a dislocation loop,[33] the migration of dislocations into an interface to form the martensitic embryo,[31] nucleation by cooperative faulting from groups of existing dislocations,[34] and the interaction of dislocations with the transformation train.[35] However, the analysis of available experimental data concerning the influence of the initial state on the subsequent transformation[36] (such as the development of a trusslike substructure), and the studies of transformation in defect free crystals[37] suggest that the general features of the transformation can not be totally governed by the defect structure.

4. Strain phase transition.[38] This approach regards the martensitic transformation as the self-development of a first order phase transition (the so called strain transition). The theory is based on the assumed existence of a coherent contact between phases in heterophase systems. This coherence preservation results in the development of the internal stress which leads to the increase in strain energy. This strain energy increase is a function of the shape and the substructure of the transformed region and must be minimized. The tendency of the strain energy increase to become less plays the leading role in the formation of the heterophase structure. The

athermal and isothermal transformations are explained by the difference in activation energy resulting from the difference in product martensite structures. This approach, however, does not exclude the possibility of a combination with one of the other models mentioned above.

2. THE STRAIN ENERGY OF MARTENSITE

The central idea of the martensite transformation is based on a competition between the decrease in chemical free energy and the increase in the elastic strain energy during the course of the transition. In fact, in most of the martensite theories cited above, strain energy is considered to be the major restraining force, and is directly related to most features of the transformation. Hence, in order to actually apply the theories to real systems, an accurate determination of the strain energy is required. In addition, strain energy calculations provide a quantitative basis for evaluation of the theories. Consider, for example, internal twinning. According to the nucleation and growth theory (classical or defect assisted), the martensite embryos are not twinned; twins are formed during the growth process. Accordingly, before the twin forms, the embryos should be thermodynamically favorable (i.e., the free energy change for the formation of the embryos is negative). Twinning would occur as a subsequent process if the twinning further reduces the total free

energy* (the strain energy is reduced while the twinning surface energy increases, and the chemical free energy remains unchanged). Alternately, in the strain transition theory the condition that the embryo without twins be thermodynamically stable is not required, because twinning always occurs. However, the theory requires that the twin structure should give a minimum total free energy for the final configuration.

In other areas, such as transformation toughening, strain energy calculations are also very useful. For example, the strain energy change associated with the martensitic transformation near the crack tip is directly connected with the increase in fracture toughness. In addition, the optimal size of the second phase particle** involves strain energy considerations.

Important as the strain energy is, the available methods to evaluate it are not satisfactory. It is the object of the present study to develop a general scheme to determine the strain energy of martensite. A review of the available formulations for strain energy calculations is given in the next section followed by the development of the new approach.

---

*The final size of the martensitically transformed region is unknown to the embryo. Hence, the twin structure that minimizes the free energy in the embryo does not guarantee a minimum free energy for the final configuration. This situation arises because the strain energy is sensitive to the twin width and to the aspect ratio of the martensite crystal, both of which can change as the transformation progresses.

**The toughness depends upon size, with a peak toughness occurring at an optimum particle size.

2.1 Strain Energy Formulations

In the most general sense, the evaluation of the strain energy of twinned martensite should allow (1) the elastic constants of the particle and matrix to be anisotropic* and inhomogeneous,** (2) the stress-free strain to be arbitrary, (3) the particle shape to be arbitrary, (4) twins to have twin related elastic constants (i.e., elastic non-uniformity exists within the particle) and stress-free strains, and (5) interaction between the transformation induced stresses and the applied stress. None of the presently available formulations satisfy the aforementioned conditions. The principal difficulties arise because analytic formulations are incapable of allowing the twins to have anisotropic twin related elastic constants, while pure numerical formulations are not available. A review of the available procedures indicates the following limitations.

There are two basic formulations: one in real space and the other in reciprocal space. The former was established by Eshelby.[39] He

---

*The elastic constants are isotropic if their values at any given point in the domain under consideration are independent of the reference coordinate frame; otherwise, they are anisotropic. The isotropic elastic constants have two independent parameters. The anisotropic constants can have from three to twenty-one independent parameters, depending on the crystal symmetry.

**In general the elastic constants are considered to be homogeneous if they do not vary over the domain; otherwise, they are inhomogeneous. However, in common with prior literature on this topic, elastic inhomogeneity is used herein to indicate that the inclusion and the matrix have different elastic constants. The term elastic non-uniformity will be used to describe the case in which the elastic constants vary within the inclusion or in the matrix.

successfully solved the problem of an isotropic matrix containing an isotropic ellipsoidal inclusion which undergoes (in the absence of its surroundings), a uniform transformation strain. His procedure comprised a simple set of imaginary cutting, straining, welding and relaxation operations. Elastic inhomogeneity was nicely treated by employing an equivalent inclusion concept (for details see Appendix A).

Kinoshita and Mura[40] extended the problem to the case of inclusions in anisotropic media and thus satisfied the conditions of both elastic anisotropy and elastic inhomogeneity for the ellipsoidal inclusion. The Kinoshita and Mura treatment also applies to inclusion of arbitrary shape under the assumption of elastic homogeneity. However, removal of the elastic homogeneity requirement by using the equivalent inclusion concept restricts the analysis to ellipsoidal shapes. The restriction arises because, for arbitrary shapes, the stress within the inclusion is not necessarily uniform, and the equivalent inclusion does not exist.

These solutions are of limited merit for martensite calculations, because most martensites contain twins (or variants) and hence, the stress-free strains are non-uniform. Solutions that permit periodic stress-free strains are required for typical martensite transformations. Much effort has been devoted to the removal of the uniform stress-free strain requirements. Sendeckj[41] solved the isotropic inclusion problem for a linearly distributed stress-free strain; while Asaro and Barnett[42] obtained the solution for a polynomial stress-free strain in an anisotropic matrix. Subsequently, Mura, Mori, and Kato[43] established a formulation for evaluating the strain energy of

a uniformly anisotropic ellipsoidal inclusion with a periodically distributed stress-free strain, embedded in a matrix of the same anisotropic elastic constants. The solution for an inclusion with an arbitrary transformation strain can then be obtained by expressing the strain in terms of a Fourier series (or integral) and employing superposition procedures. Application of the equivalent inclusion method to the non-uniform-stress-free strain solution in order to remove the homogeneity requirement is described in Appendix A. However, extensive numerical effort is needed to establish and solve the simultaneous equations, and thus to determine the equivalent stress-free strain. Additionally, the Mura et al. treatment can not be applied to twinned martensite without restriction. The limitation arises because of the elastic uniformity requirement. For an anisotropic inclusion, the twins have different elastic constants (except in special cases when the elastic stiffness constants possess mirror symmetry with respect to the twinning plane (for details see Appendix B). Hence, the condition of elastic unformity within the inclusion is not generally satisfied for an anisotropic inclusion.

The reciprocal space formulation was established by Khachaturyan.[17,44] It applies to the transformation of inclusions (with uniform transformation strain) of arbitrary shape embedded in an anisotropic matrix under the assumption of elastic homogeneity. The Khachaturyan approach has the advantages that many inclusions are allowed and that the inclusion shape can be arbitrary. Thus, the twin related stress-free strains needed to analyze twinned martensite can

be considered by regarding each twin as a single entity. However, the Kachaturyan approach has the limitation that elastic homogeneity is required. Thus, even by considering each twin as a single inclusion, the twin related elastic constants can not be incorporated.

In summary, in the case of a uniform transformation strain, the real space formulation is limited by the assumption of an ellipsoidal inclusion shape; while the reciprocal space formulation is restricted by the elastic homogeneity requirement. In the case of twinned martensite, an additional restriction of elastic isotropy is required in either formulation.

In addition to these restrictions, extensive numerical effort is generally needed to obtain solutions using the above procedures. Analytic results can only be obtained for the simple cases of a uniform transformation strain and either an isotropic ellipsoidal inclusion (real space formulation) or an anisotropic plate inclusion (reciprocal space formulation). This has prompted us to develop a purely numerical scheme, which is not subject to the above restrictions.

2.2 The Finite Element Formulation

2.2.1 Introduction

The finite element method[45-47] is a general discretization procedure for solving continuum problems, posed by mathematically defined statements. This method has been successfully applied to problems in many fields, such as linear elasticity, nonlinear elasticity, plasticity, creep, fluid dynamics, diffusion, heat conduction, and electromagnetism. There are various finite element formulations.

A displacement formulation, most popular in linear elasticity, will be used in the present study. The displacement approach comprises the following basic precepts.

1. The continuum is regarded as an assembly of a finite number of elements separated by imaginary lines or surfaces.

2. The elements are interconnected at a discrete number of nodal points situated on their boundary. The displacements of these nodal points will be the basic unknown parameters of the problem.

3. A mathematical equation in integral form is established from the constitutive differential equations and boundary conditions either by determining the variational functional for which stationary form is sought or by the method of weighted residuals.[45,48]

4. Locally defined shape functions[49] are assumed for each element, through which the stress and strain in each element are related to the unknown nodal displacements.

5. Integrations of the constitutive integral equation are evaluated at the element level, and the governing equilibrium equations of the nodal displacements are established.

6. The solution of the governing equilibrium equation gives the nodal displacement, and then the stress and strain for the continuum are determined.

A finite element formulation for solving elasticity problems with an initial strain (which makes transformation problems so special) has already been established, in principle.[50] However, its major

application (as implanted in most finite element computer programs such as SAP IV[51]) has been limited to thermal stress analysis. The potential application to phase transformation problems has not been realized, and an adequate strain energy formulation has not been devised (perhaps because the strain energy is not of interest in thermal analysis). In the following section, the governing equilibrium equations will be established for a system involving a phase transformation under external loads. A comparison with Eshelby's treatment will be given. Finally, the strain energy formulation will be developed.

2.2.2 The Phase Transformation Problem

The elastic phase transformation problem is characterized by a non-zero initial strain, which can be a thermal strain, a plastic strain, a transformation strain, or any combination of these. The initial strain (which is the strain experienced in the absence of matrix constraint and when no external force is applied) will be called the stress-free strain, after Eshelby[39] and Robinson.[52] For a linear system, the stress-strain relation can be expressed as follows:

$$\sigma_{ij} = c_{ijkl}(e_{kl} - e^{o}_{kl}) \qquad (1)$$

where e_{kl} is the strain (with the unstrained matrix as the zero-strain state), and e^{o}_{kl} is the stress-free strain. (Note, this can be regarded as the definition of stress-free strain).

In Eshelby's treatment of cutting, straining, welding and relaxation operations,[39] a surface force of the magnitude $\sigma_{ij}n_j = C_{ijkl}e^o_{kl}n_j$; must be applied to the interface (as an imaginary load) during the relaxation operation. In the finite element formulation, however, the imaginary force term will emerge naturally from the analysis.

The finite element formulation is established following the procedure outlined in Section 2.2.1, and adopting the notation summarized in Appendix C. The continuum is subdivided into elements, with N nodes per element. The increase in internal strain energy of the system will be given in accord with the variational principle, by the potential energy of the external loads. Hence, for an arbitrary variation in strain $\delta\varepsilon$, the strain energy change is given by:

$$\int \delta\varepsilon^T \sigma dV = \int \delta U^T b dV + \int U^T t dS + \Sigma \delta A^i f^i \qquad (2)$$

where ε is the engineering strain array, $\varepsilon^T = (e_{11}\ e_{22}\ e_{33}\ 2e_{23}\ 2e_{13}\ 2e_{12})$, σ is the stress array, $\sigma^T = (\sigma_{11}\ \sigma_{22}\ \sigma_{33}\ \sigma_{23}\ \sigma_{13}\ \sigma_{12})$, U is the displacement array, $U^T = (u_1\ U_2\ U_3)$, b is the body force* array, $b^T = (b_1\ b_2\ b_3)$, t is the surface traction* array, $t^T = (t_1\ t_2\ t_3)$, f^i is the concentrated load* at node i, $f^{iT} = (f^i_1\ f^i_2\ f^i_3)$, A^i is the unknown nodal displacement,

---

*Body force, surface traction, and concentrated load are the force per volume, per surface area and at a given point respectively.

$e_{ij} = 1/2(\partial U_i/\partial x_j + \partial U_j/\partial x_i)$ and the superscript T stands for transposition.

The shape function which describes the spatial variation of the displacement U within an element, in terms of the nodal displacement $A^{(i)}$, is assumed to be a known function $H^{(i)}$ such that;

$$U = \sum_{i}^{N} \underline{H}_m^{(i)} \underline{A}_m^{(i)}$$

$$U = \underline{H}_m \underline{A}_m$$

$$U^T = \underline{A}_m^T \underline{H}_m^T$$

$$\delta U^T = \delta \underline{A}_m^T \underline{H}_m^T \tag{3}$$

By definition, $\varepsilon = LU$, where L is a strain operator, which can be expressed by the matrix,

$$L = \begin{bmatrix} \partial/\partial x & 0 & 0 \\ 0 & \partial/\partial y & 0 \\ 0 & 0 & \partial/\partial z \\ 0 & \partial/\partial z & \partial/\partial y \\ \partial/\partial z & 0 & \partial/\partial x \\ \partial/\partial y & \partial/\partial x & 0 \end{bmatrix} \tag{4}$$

It follows that,

$$\varepsilon = LU = L\underline{H}_m\underline{A}_m = \underline{B}_m\underline{A}_m \tag{5}$$

where, $\underline{B}_m \equiv L\underline{H}_m$. Thus,

$$\delta\varepsilon^T = \delta\underline{A}_m^T\underline{B}_m^T \tag{6}$$

The stress-strain relation, eqn (1), can be written in matrix notation as:

$$\sigma = \underline{C}_m(\varepsilon - \underline{\varepsilon}_m^o) \tag{7}$$

where $\underline{\varepsilon}_m^{o^T} = (e_{11}^o e_{22}^o e_{33}^o 2e_{23}^o 2e_{13}^o 2e_{12}^o)_m$ and $\underline{C}_m$ is the elastic stiffness matrix for element m, or

$$\sigma = \underline{C}_m\underline{B}_m\underline{A}_m - \underline{C}_m\underline{\varepsilon}_m^o \tag{8}$$

The strain energy relation (eqn (2)) can be rewritten such that the integration is evaluated at the element level,

$$\sum_m \int \delta\varepsilon^T\sigma dV_m = \sum_m \int \delta U^T b dV_m + \sum_m \int \delta U^T t dS_m + \sum_i \delta A^{(i)} f^{(i)} \tag{9}$$

Hence, by substituting eqns (3), (6), and (8) into eqn (9) the strain energy becomes;

$$\sum_m \delta \underline{A}_m^T \int (\underline{B}_m^T \underline{C}_m \underline{B}_m \underline{A}_m - \underline{B}_m^T \underline{C}_m \underline{\varepsilon}_m^o)\, dV_m$$

$$= \sum_m \delta \underline{A}_m^T \int \underline{H}_m^T\, b dV_m + \sum_m \delta \underline{A}_m^T \int \underline{H}_m^T\, t dS_m + \sum_i \delta A^{(i)^T} f^{(i)} \qquad (10)$$

Further, since $\underline{A}_m = \underline{J}_m A$, and $\delta A_m^T = \delta A^T \underline{J}_m^T$, introduction of eqn (10) gives;

$$\delta \underline{A}^T \sum_m \underline{J}_m^T \left(\int \underline{B}_m^T \underline{C}_m \underline{B}_m \, dVm \right) \underline{J}_m \underline{A}$$

$$= \delta \underline{A}^T \left[\sum_m \underline{J}_m^T \left(\int \underline{B}_m^T \underline{C}_m \underline{\varepsilon}_m^o \, dV_m \right) + \sum_m \underline{J}_m^T \left(\int \underline{H}_m^T \, dbV_m \right) \right.$$

$$\left. + \sum_m \underline{J}_m^T \left(\int \underline{H}_m^T \, t dS_m \right) + \underline{f} \right]$$

Then, because δA^T is arbitrary, the governing equilibrium equation becomes;

$$\underline{K}\ \underline{A} = \underline{R}^o + \underline{R}^b + \underline{R}^s + \underline{R}^c \equiv \underline{R} \qquad (11)$$

In this relation, $\underline{K}$ is the stiffness matrix of the element assemblage,

$$\underline{K} = \sum_m \underline{J}_m^T \left(\int \underline{B}_m^T \underline{C}_m \underline{B}_m \, dV_m \right) \underline{J}_m \quad ;$$

and the load vector $\underline{R}$ includes the effects of the element body force,

$$\underline{R}^b = \sum_m \underline{J}_m^T \int \underline{H}_m^T \, b dV_m$$

the surface traction,

$$\underline{R}^s = \sum_m \underline{J}_m^T \int \underline{H}_m^T \, t dS_m$$

the concentrated load,

$$\underline{R}^c = \underline{f}$$

and the stress-free strain,

$$\underline{R}^o = \sum_m \underline{J}_m^T \int \underline{B}_m^t \underline{C}_m \underline{\varepsilon}_m^o \, dV_m$$

The $\underline{R}^o$ term does not depend on the external load, and can thus be regarded as the imaginary load due to the stress free strain. It can be decomposed into an imaginary surface traction and a body force by partial integration (see Appendix D)

$$\underline{R}^o = \sum_m \underline{J}_m^T \left[\int \underline{H}_m^T \underline{n}_m \underline{C}_m \underline{\varepsilon}_m^o \, dS_m \right.$$

$$\left. - \int \underline{H}_m^T L^T (\underline{C}_m \underline{\varepsilon}_m^o) \, dV_m \right]$$

where,

$$\underline{n}_m = \begin{pmatrix} n_1 & 0 & 0 & 0 & n_3 & n_2 \\ 0 & n_2 & 0 & n_3 & 0 & n_1 \\ 0 & 0 & n_3 & n_2 & n_1 & 0 \end{pmatrix} ,$$

and the n_i's are the directional cosines of the outward normal. The quantity $\underline{n}_m \underline{C}_m \underline{\varepsilon}_m^o$ in the first term assumes the same role as the surface traction $\underline{t}$ in $\underline{R}^s$, and thus is the imaginary surface traction.

When expressed in tensor notation, the quantity $\underline{n}_m \underline{c}_m \underline{\varepsilon}_m^o$ gives $c_{ijkl} e_{kl}^o n_j$ or $\sigma_{ij}^o n_j$, which is the term used by Eshleby.[39] Similarly, the quantity $-L^T \underline{c}_m \underline{\varepsilon}_m^o$ in the second term can be identified with the imaginary body force, because it has the same effect as the body force b in $\underline{R}^b$. The components in $-L^T \underline{c}_m \underline{\varepsilon}_m^o$ can be expressed in tensor notation as $-\frac{\partial}{\partial x_j} C_{ijkl} e_{kl}^o$, or $-\frac{\partial}{\partial x_j} \sigma_{ij}^o$ as used by Asaro and Barnett[42] in the case of a nonuniform stress-free strain.

It is evident, therefore, that the finite element method is a real space approach. However, it has important advantages relative to available real space methods. Specifically, elastic inhomogeneity poses no restriction (since each element can have different elastic constants), the stress free strain is arbitrary, and external stresses can be imposed (through the surface traction t). When the method is applied to twinned martensite, each twin can consist of several elements, and the appropriate elastic constants and stress-free strains assigned to the elements. In this way, the stresses and strains in a twinned martensite may be determined.

2.2.3 The Strain Energy Formulation

The linear elastic strain energy is usually evaluated in accord with the following formula:

$$E_{el} = 1/2 \int_V \sum C_{ijkl} e_{ij} e_{kl} dV \tag{1}$$

However, for transformation problems in the presence of a stress-free strain, eqn (1) does not apply. For example, in the absence of external forces Eshelby derived the relation:[39]

$$E_{el} = -1/2 \int_{V_I} \sigma^I_{ij} e^o_{ij} dV_I \tag{2}$$

where V_I is the volume of the inclusion (of arbitrary shape), and σ^I_{ij} is the stress within the inclusion, given by

$$\sigma^I_{ij} = \sum_{kl} C^I_{ijkl}(e_{kl} - e^o_{kl}) \quad .$$

More generally, for a stress free strain, the strain energy density u is given by

$$u = \frac{1}{2} C_{ijkl}(e_{ij} - e^o_{ij})(e_{kl} - e^o_{kl})$$

or in matrix notation,

$$u = \frac{1}{2} \sum_{I=1}^{6} \sigma_I(\varepsilon_I - \varepsilon_I^o)$$

$$= \frac{1}{2} (\varepsilon - \varepsilon^o)^T \sigma = \frac{1}{2} (\varepsilon - \varepsilon^o) C(\varepsilon - \varepsilon^o)$$

$$= \frac{1}{2} (\varepsilon^T C\varepsilon - 2\varepsilon^T C\varepsilon^o + \varepsilon^o C\varepsilon^o)^*$$

Thus, the total strain energy is;

$$E_{el} = \int u dV = \frac{1}{2} \int (\varepsilon^T C\varepsilon - 2\varepsilon^T C\varepsilon^o + \varepsilon^o C\varepsilon^o)\, dV$$

$$= \frac{1}{2} \sum_m \int_m (\varepsilon^T \underline{C}_m \varepsilon - 2\varepsilon^T \underline{C}_m \underline{\varepsilon}_m^o)\, dV_m + \frac{1}{2} \int \varepsilon^o C\varepsilon^o dV$$

$$= \frac{A}{2}^T \sum_m \underline{J}_m^T \left\{ \int_m \underline{B}_m^T \underline{C}_m \underline{B}_m dV_m J_m A - 2 \int \underline{B}_m^T \underline{C}_m \underline{\varepsilon}_m^o dV_m \right\} + E_s$$

$$= \frac{1}{2} A^T (\underline{KA} - 2\underline{R}^o) + E_s$$

or, since KA = R,

$$E_{el} = \frac{1}{2} \underline{A}^T (\underline{R} - 2\underline{R}^o) + E_s$$

$$= E_{rx} + E_s$$

---

*The stiffness coefficients form a symmetric array.

where E_s is the self energy ($\frac{1}{2}\int \varepsilon^{o^T} C\varepsilon^o dV$) which is the total strain energy if the matrix were rigid and E_{rx} is the relaxation energy (defined to be $\frac{1}{2} A^T(\underline{R} - 2\underline{R}^o)$. E_{rx} is negative when the external load is zero.

When comparing with Eshelby's cutting, straining, welding and relaxation operations, the E_s term can be identified with the energy change during the straining operation, while the E_{rx} term is the energy change during relaxation; there is no energy change associated with the cutting and welding operations.

In the case of twinned martensite in which the stress free strains are constant within each twin, the self energy can be easily calculated by $E_s = \frac{1}{2}\underline{\varepsilon}^{o^T}\underline{C\varepsilon}^o V_I$. When the system is free from external load (and if we neglect gravity), $R = R_o$, the strain energy is given by

$$E_{el} = -\frac{1}{2}\underline{A}^T\underline{R}^o + \frac{1}{2}\underline{\varepsilon}^o\underline{C\varepsilon}^o V_I$$

In the above formulation, the effect of external loads is included in the term $\underline{R}$ (the interaction of the applied strain with the transformation is thus taken into account). In finite element procedures, $\underline{A}$, $\underline{R}$, or $\underline{R}^o$ can be readily established. The strain energy can thus be determined without difficulty.

2.2.4 Examples of the Finite Element Calculation

The finite element scheme described above was implanted into the existing finite element program SAP IV.[51] The reliability of the scheme was tested in a series of examples. The examples were

restricted to elastic isotropy because general analytic solutions for the strain energy of twinned martensite are not available. These restrictions, imposed on the input data, should not be regarded as limitations of the computer program.

1. Pure dilation of a spherical inclusion embedded in a spherical matrix (axisymmetric element)

In the first example, the pure dilation of a spherical inclusion embedded in a spherical matrix is considered. An analytic expression for the strain energy is (see Appendix E)

$$E_{el} = 2\mu V_I (e^T)^2 (1 + \nu) \left[1 - \left(\frac{r_I}{r_m}\right)^3\right] / 9(1 - \nu)$$

where μ is the shear modulus, V_I the volume of the inclusion, ν the Poisson's ratio, r_I the radius of the inclusion, r_m the radius of the matrix, e^T the unconstrained volume strain.

The isotropy of the geometry, of the stress free strain, and of the elastic constants, permits the strain energy to be analyzed by considering only a small portion of the system. The finite element mesh, shown in Fig. 1, consists of ten 4-node axisymmetric elements and ten boundary elements. The boundary elements[51] are used to assure the radial displacements of the points on line OB in Fig. 1 (by limiting their tangential displacement to zero). The ratio of the radius of the inclusion to that of the matrix is 1:2, and the azimuthal angle θ is 10^{-3} rad. Other numerical data needed for the computation

are given in Table 1. The strain energy of the system is calculated to be 5.58×10^7 J (or 44.4 percent); this compares with an analytic value of 5.50×10^7 J (or 43.85 percent E_s), where $E_s = 4\pi \times 10^7$ J. The deviation is less than 1.5 percent.

2. Pure dilation of a spherical inclusion embedded in a spherical matrix (3D brick element)

The second example (Ex. 2a) deals with the same dilational problem, except for the choice of the finite element and the size of the inclusion. Three-dimensional brick elements are used in order to evaluate their performance. This exercise is conducted because three dimensional elements are needed for the solution of twinned martensite problems, by virtue of the lack of axisymmetry. Due to symmetry considerations, only 1/8 of the sphere is analyzed. The mesh is given in Fig. 2. Thirteen three dimensional 20 node elements are used. The elastic energy is calculated to be 1.666×10^8 J (or 33.14 percent E_s, where $E_s = 16\pi \times 10^7$ J). Comparison with the analytic value of 1.662×10^8 J (or 33.07 percent E_s), indicates a deviation of less than 0.22 percent.

In another example (Ex. 2b) the capability of the finite element approach to handle problems involving elastic inhomogeneity was examined for the same stress free strain using the same mesh. As shown in Table 1, both the shear moduli and the Poisson's ratio are different for the inclusion and for the matrix. The matrix is extremely soft compared to the inclusion ($K_m/K_I = 0.025$, where K_m and K_I are

bulk moduli of the matrix and the inclusion respectively); hence, appreciable relaxation occurs. An analytic solution is given in Appendix E, eqn (E-9). The strain energy is 1.207×10^7 J (2.401 percent E_s, where E_s is the same as in Ex. 2a). The finite element result gave 1.209×10^7 J (2.406 percent E_s), a deviation from the analytic value of less than 0.2 percent. This represents a crucial test, because the strain energy is in the range of numerical error for a general numerical analysis. The capability of the finite element method is thus confirmed.

3. Spherical inclusion undergoing martensitic transformation

The third example considered is the martensitic transformation of a spherical inclusion embedded in an infinite matrix. The only non-zero transformation strain is γ_{13}^T, assumed to be 1 percent. In Ex. 3a no twinning is considered, but in Ex. 3b, one twin pair is included in the product phase. The numerical data, listed on Table 1, are identical to those used by Mura[43] et al. The infinite matrix is approximated by a spherical matrix with radius five times that of the inclusion. Thirteen 20-node elements are used. The mesh is similar to that used in Ex. 2 except that the boundary conditions are different. Example 3a (no twinning) and Ex. 3b (one twin pair) also differ only in the boundary condition on the xy plane. For Ex. 3a, the strain energy, 0.521 E_s, which deviates from the analytic value $(7-5\,\nu)/15/(1-\nu)\,E_s$, by 2.31 percent, where $E_s = (1/2)\,\mu\,(\gamma_{13}^T)^2\,V \equiv 2\pi/3 \times 10^7$ J. For Ex. 3b, the strain energy is determined as 0.413 E_s, which compares with Mura's value of 0.365 E_s. Successive

calculations, denoted as Ex. 3c (no twinning) and Ex. 3d (twinning), with further mesh subdivisions (using 19 elements), indicate respective strain energies of 0.533 E_s (only 0.013 percent from the analytic value) and 0.400 E_s (8.8 percent above Mura's result).

3. CONCLUSION

A strain energy formulation by the finite element method has been established. It can be implanted into existing finite element computer programs with little effort. The primary advantages of this method are the removal of limitations based on elastic isotropy of homogeneity, and its applicability to all types of stress-free strain (including twinning). Good numerical accuracy can be obtained with a reasonable number of elements. However, for the same mesh, the accuracy varies with the stress-free strain. Hence, for each case it is important to subdivide the mesh in order to test the convergence.

Appendix A: The Equivalent Inclusion Method

1. Ellipsoid with Uniform Transformation Strain

The concept of the equivalent inclusion was first introduced by Eshelby[39] to solve the transformation problem involving elastic inhomogeneity. Although his method was proposed for an isotropic matrix, the concept also applies to the most general anisotropic case. This method is an essential one for solving the transformation problem, because all analytic formulations are derived under the assumption of elastic homogeneity. The basic idea of Eshelby's method is that the true inclusion (with elastic constants C^*_{ijkl} and stress-free strain e^*_{ij}) is replaced by an equivalent inclusion with the same elastic constants C_{ijkl} as the matrix, and an equivalent stress-free strain e^T_{ij}, selected such that the usual analytic solution can be applied. However, displacement and stress continuity across the interface of the true inclusion and the matrix must be satisfied. This is achieved by requiring that the stresses within the true and the equivalent inclusions be identical. Thus the equivalent inclusion exists if the following equation has a solution

$$C_{ijkl}(e^c_{kl} - e^T_{kl}) = C^*_{ijkl}(e^c_{kl} - e^*_{kl})$$

or, by rearrangement of the terms,

$$(C^*_{ijkl} - C_{ijkl})\, e^c_{kl} + C_{ijkl}e^T_{kl} = C^*_{ijkl}e^*_{kl} \qquad \text{(A-1)}$$

For an ellipsoidal inclusion with a uniform stress-free strain e^T_{kl}, Kinoshita and Mura[40] have shown that, under homogeneity conditions, the constrained strain e^c_{kl} is also uniform, and symbolically, is related to e^T_{kl} as follows.

$$e^c_{ij} = S_{ijkl} e^T_{kl} \tag{A-2}$$

where S_{ijkl}'s are functions of the elastic constants and the geometric shape, but independent of e^T_{kl} and of location. By substituting (A-2) into (A-1), we have

$$(C^*_{ijkl} - C_{ijkl})\, S_{klmn} e^T_{mn} + C_{ijkl} e^T_{kl} = C^*_{ijkl} e^*_{kl} \tag{A-3}$$

Eqn (A-3) represents 6 simultaneous algebraic equations with 6 unknowns (e^T_{ij}), and can be solved for the equivalent stress free strain e^T_{ij}.

2. <u>Disc Martensite with a Periodic Transformation Strain</u>

Mura et al.[43] applied the equivalent inclusion method to solve the transformation problem of a twinned martensite disc. They expressed the true and the equivalent stress-free strain in the form of a Fourier Series.

$$e^*_{ij}(x) = \bar{e}^*_{ij}(0) + \sum_{n=1}^{\infty} \bar{e}^*_{ij}(n) \cos(2\pi nx/\lambda)$$

$$e^T_{ij}(x) = e^{**}_{ij}(0) + \sum_{n=1}^{\infty} e^{**}_{ij}(n) \cos(2\pi nx/\lambda)$$

where λ is the period of the alternating twins. They arrived at a set of equations to solve for $e^{**}_{ij}(n)$

$$C_{pqik}\left\{S_{ikmn}(0)\ e^{**}_{mn}(0) - e^{**}_{ik}(0)\right\} + C_{pqik}\left\{\sum_{J=1}^{\infty} S_{ikmn}(J)\ e^{**}_{mn}(J) - \sum_{J=1}^{\infty} e^{**}_{ik}(J)\ \cos(2\pi Jx/\lambda)\right\}$$

$$= C^{*}_{pqik}\left\{S_{ikmn}(0)\ e^{**}_{mn}(0) - \bar{e}^{*}_{ik}(o)\right\} + C^{*}_{pqik}\left\{\sum_{J=1}^{\infty} S_{ikmn}(J)\ e^{**}_{mn}(J) - \sum_{J=1}^{\infty} \bar{e}^{*}_{ik}(J)\ \cos(2\pi JX/\lambda)\right\} \qquad \text{(A-4)}$$

(for details of $S_{ikmn}(j)$, see eqn (43) in ref. 43).

Mura et al. assumed that $e^{**}_{ik}(0) = \bar{e}^{*}_{ik}(0)$, where $\bar{e}^{*}_{ik}(0)$ are chosen so that "all of the stresses produced by it vanish." Thus they claimed that the first terms in the left and right side of eqn (A-4) disappeared, and eqn (A-4) becomes

$$C_{pqik}\left\{\sum_{J=1}^{\infty} S_{ikmn}(J)\ e^{**}_{mn}(j) - \sum_{J=1}^{\infty} e^{**}_{ik}(j)\ \cos(2\pi Jx/\lambda)\right\}$$

$$= C^{*}_{pqik}\left\{\sum_{J=1}^{\infty} S_{ikmn}(J)\ e^{**}_{mn}(j) - \sum_{J=1}^{\infty} \bar{e}^{*}_{ik}(J)\ \cos(2\pi Jx/\lambda)\right\} \qquad \text{(A-5)}$$

To solve this equation, they invoked the experimental observation that $\lambda \ll$ disc dimension, and pointed out that, in the limiting case, $S_{ikmn}(J) = 0$. Thus the equation is further reduced to

$$C_{pqik} \sum_{J=1}^{\infty} e_{ik}^{**}(J) \cos(2\pi Jx/\lambda) = C_{pqik}^{*} \sum_{J=1}^{\infty} \bar{e}_{ik}^{*}(J) \cos(2\pi Jx/\lambda)$$

or, since the cosine functions are orthogonal,

$$C_{pqik} e_{ik}^{**}(J) = C_{pqik}^{*} \bar{e}_{ik}^{*}(J)$$

and $e_{ik}^{**}(J)$ can be solved.

However, in general, when the number of twins is finite, $S_{ikmn}(J) \neq 0$. Eqn (A-5) can then be decomposed into the following:

$$(C_{pqik}^{*} - C_{pqik}) \sum_{J=1}^{\infty} S_{ikmn}(J)\, e_{mn}^{**}(J) = 0 \qquad \text{(A-6)}$$

$$C_{pqik} e_{ik}^{**}(J) = C_{pqik}^{*} \bar{e}_{ik}^{*}(J) \qquad \text{(A-7)}$$

For each J, eqn (A-7) represents 6 equations with 6 unknowns $e_{ik}^{**}(J)$; thus, $e_{ik}^{**}(J)$ can be solved by eqn (A-7) alone. In general, $e_{ik}^{**}(j)$ solved from eqn (A-7) can not satisfy eqn (A-6). Thus eqn (A-5) has no solution and the equivalent inclusion does not exist.

However, this failure is due to the removal of the first terms on both sides of eqn (A-4) (eqn 43 in their paper[43]), as can be shown below. Rearrangement of eqn (A-4) gives;

$$(C^*_{pqik} - C_{pqik})\left\{S_{ikmn}(o)\ e^{**}_{mn}(o) + \sum_{J=1}^{\infty} S_{ikmn}(j)\ e^{**}_{mn}(J)\right\}$$

$$+ C_{pqik}\left\{e^{**}_{ik}(o) + \sum_{J=1}^{\infty} e^{**}_{ik}(J)\ \cos(2\pi Jx/\lambda)\right\}$$

$$= C^*_{pqik}\left\{\bar{e}^*_{ik}(o) + \sum_{J=1}^{\infty} \bar{e}^*_{ik}(J)\ \cos(2\pi Jx/\lambda)\right\} \qquad \text{(A-8)}$$

Then by the orthogonality of the cosine function, the x independent terms on both sides of eqn (A-8) should be equal, as should the terms containing $\cos(2\pi Jx/\lambda)$ for each J.

Then eqn (A-8) can be decomposed into the following:

$$(C^*_{pqik} - C_{pqik})\left\{S_{ikmn}(o)\ e^{**}_{mn}(o) + \sum_{J=1}^{\infty} S_{ikmn}(J)\ e^{**}_{mn}(J)\right\}$$

$$+ C_{pqik}e^{**}_{ik}(o) = C^*_{pqik}\bar{e}^*_{ik}(o) \qquad \text{(A-9)}$$

and

$$C_{pqik}e^{**}_{ik}(J) = C^*_{qpik}\bar{e}^*_{ik}(J)$$

The latter is the same as eqn (A-7), from which $e^{**}_{ik}(J)$ for $J \geq 1$ can be solved. Thus the only unknown in eqn (A-9) is $e^{**}_{mn}(o)$, which can be solved without difficulty.

Thus it is evident that without assuming $e^{**}_{mn}(o) = \bar{e}^*_{mn}(o)$, eqn (A-4) can be solved and the equivalent inclusion exists for the twinned martensite disc.

3. Ellipsoid with Non-Uniform Stress Free Strain

The equivalent inclusion method for an ellipsoid with a non-uniform stress free strain has not been seriously treated. In this section, a systematic procedure to set up the simultaneous equations will be described.

The transformation of an ellipsoid with a periodic strain has been solved by Mura et al.[43] under the assumption of elastic homogeneity. For a periodic strain $e^T_{mn}(\vec{k},\vec{x}) = e^{**}_{mn}(\vec{k}) \exp(i\vec{k}\cdot\vec{x})$, the constrained strain is given by

$$e^c_{ij}(\vec{k},\vec{x}) = S''_{ijmn}(\vec{k},\vec{x},\text{shape})\, e^{**}_{mn}(\vec{k}) \qquad \text{(A-10)}$$

where S''_{ijmn} is a function of $\vec{k}$, location $\vec{x}$, and inclusion shape.

Now suppose a_1, a_2, and a_3 are the lengths of the semi-axes of the ellipsoid. Then the ellipsoid can be considered to exist within an orthorhombic region having length $2a_1$, width $2a_2$, and height $2a_3$. One set of orthogonal functions for the orthorhombic region can be of the form:

$$\Psi_{hkl} = \Psi_1\left(\frac{\pi h x}{a_1}\right) \Psi_2\left(\frac{\pi k y}{a_2}\right) \Psi_3\left(\frac{\pi l z}{a_3}\right)$$

where Ψ_i's are sine or cosine functions and h, k, l are positive integers or zero. Due to the permutations of sine and cosine for Ψ_1, Ψ_2, and Ψ_3, there are eight orthogonal functions associated with each set of h, k, l. Thus a general expression for the orthogonal function is Ψ_{hklv} with h, k, l ≥ 0 and $1 \leq V \leq 8$. Since $\Psi_1\Psi_2\Psi_3$ can be

expressed as a linear combination of $e^{i\vec{k}\cdot\vec{x}}$, the constrained strain corresponding to a stress free strain of the form $\Psi_1\Psi_2\Psi_3$ can also be found as a linear combination of $e^c_{ij}(\vec{k}\cdot\vec{x})$ given in eqn (A-10). Take $\cos(rx)\cos(sy)\cos(tz)$ (where $r = \pi/h/a_1$, $s = \pi k/a_2$, and $t = \pi l/a_3$ respectively) for example,

$$\cos(rx)\cos(sy)\cos(tz) = \text{Real part of } 1/4\Big\{\exp i(rx + sy - tz)$$

$$+ \exp i(-rx + sy + tz) + \exp i(rx - sy + tz) + \exp i(rx + sy + tz)\Big\}$$

$$= \text{Real Part } \frac{1}{4}\Big\{\exp(i\vec{k}_1\cdot\vec{x}) + \exp(i\vec{k}_2\cdot\vec{x}) + \exp(i\vec{k}_3\cdot\vec{x}) + \exp(i\vec{k}_4\cdot\vec{x})\Big\}$$

$$= \text{Real Part } \left\{\frac{1}{4}\sum_{P=1}^{4}\exp(i\vec{k}_p\cdot\vec{x})\right\}$$

where

$$\vec{k}_1 = r\hat{i} + s\hat{j} - t\hat{k}$$
$$\vec{k}_2 = -r\hat{i} + s\hat{j} + t\hat{k}$$
$$\vec{k}_3 = r\hat{i} - s\hat{j} + t\hat{k}$$
$$\vec{k}_4 = r\hat{i} + s\hat{j} + t\hat{k}$$
$$\vec{x} = x\hat{i} + y\hat{j} + z\hat{k}$$

Thus the constrained strain corresponding to a stress-free strain of $e^{**}_{mn}(h,k,l)\cos(rx)\cos(sy)\cos(tz)$ can be found through eqn (A-10) as

$$e^{c}_{ij}(h,k,l,\vec{x}) = 1/4 \text{ Real part of } \sum_{P=1}^{4} S'_{ijmn}(k_p,\vec{x},\text{shape})\ e^{**}_{mn}(hkl)$$

Thus, in general, a relation similar to eqn (A-10) can be established for a stress free strain $e^{**}_{mn}(h,k,l,v)\ \Psi_{hklv}$ as shown.

$$e^{c}_{ij}(h,k,l,v,\vec{x}) = S_{ijmn}(h,k,l,v,x,y,z,\text{shape})\ e^{**}_{mn}(h,k,l,v)$$

Eqn (A-1) still applies for the case of a nonuniform stress-free strain. Suppose that the stress-free strain is given by

$$e^{*}_{ij}(x) = \sum_{hklv} \bar{e}^{*}_{ij}(k,h,l,v)\ \Psi_{hklv}$$

and the equivalent stress-free strain is expressed by

$$e^{T}_{ij}(x) = \sum_{hklv} e^{**}_{ij}(h,k,l,v)\ \Psi_{hklv}$$

Then, according to eqn (A-11), the constrained strain is given by

$$e^{c}_{ij}(x) = \sum_{hklv} S_{ijmn}(k,h,l,v,x,y,z,\text{shape})\ e^{**}_{mn}(h,k,l,v)$$

Substituting all the equations listed above into eqn (A-1), the following expression obtains;

$$(C^*_{ijst} - C_{ijst}) \sum_{hklv} S_{stmn}(h,k,l,v,x,y,z,shape)\, e^{**}_{mn}(h,k,l,v)$$

$$+ C_{ijst} \sum_{hklv} e^{**}_{st}(h,k,l,v)\, \Psi_{hklv} = C^*_{ijst} \sum_{hklv} \bar{e}^*_{st}(h,k,l,v)\, \Psi_{hklv} \quad \text{(A-12)}$$

$S_{stmn}(h,k,l,v,x,y,z,shape)$ is a function of x,y,z and can be expressed in terms of Ψ_{hklv}, or*

$$S_{stmn}(h,k,l,v,x,y,z,shape) = \sum_{pqu} S^*_{stmn}(h,k,l,v,p,q,u,w,shape)\ \Psi_{pquw}$$

By substituting this equation into eqn (A-12),

$$(C^*_{ijst} - C_{ijst}) \sum_{hkl} \sum_{pqu} S^*_{stmn}(h,k,l,v,p,q,u,w,shape)$$

$$\cdot\, e^{**}_{mn}(h,k,l,v)\, \Psi_{pquw} + C_{ijst} \sum_{hkl} e^{**}_{st}(h,k,l,v)\, \Psi_{hklv}$$

$$= C^*_{ijst} \sum_{hkl} \bar{e}^*_{st}(h,k,l,v)\, \Psi_{hklv}$$

Then by the orthogonality of Ψ_{hklv}, all of the coefficients of Ψ_{hklv} on both sides of the equation should be equal for each set of hklv, or

---

*S_{stmn}'s are not defined outside the inclusion. For the purpose of evaluating S^*_{stmn}, all the S_{stmn}'s outside the inclusion can be defined zero. However, to improve the numerical accuracy, a continuous variation of S_{stmn}'s is recommended.

$$(C^*_{ijst} - C_{ijst}) \sum_{pquw} S^*_{stmn}(p,q,u,w,h,k,l,v,\text{shape})$$

$$\cdot\, e^{**}_{mn}(p,q,u,w) + C_{ijst} e^{**}_{st}(h,k,l,v)$$

$$= C^*_{ijst} \bar{e}^*_{st}(h,k,l,v) \qquad \text{(A-13)}$$

This is the final form of the equations needed to solve for the equivalent stress free strain $e^{**}_{st}(h,k,l,v)$. In principle, the number of equations to be solved is infinite. However, when only finite accuracy is desired, a finite set of h,k,l,v are needed, and eqn (A-13) can be solved.

Appendix B: Twins and Uniformity

The martensite shown in Fig. 3 contains one twin pair, i.e., grain B is a twin of grain A. Thus the crystallographic axes in A and B exhibit mirror symmetry with respect to the twinning plane CD. The elastic constants of the grain A and B are the same when referenced to their own local coordinates. However, the elastic constants are different when referenced to a global coordinate O, unless they possess the same mirror symmetry. Thus the formation of the twins usually destroys the elastic uniformity.

Appendix C: Symbols and Notations

In the finite element method, most of the quantities have many components, and are represented by arrays. An array can be a vector or a matrix. When a quantity does not refer to any specific node, no superscripts or subscripts are used. On the other hand, a quantity which refers to a specific node is expressed by using the nodal number as a superscript. A quantity is global if it refers to all of the nodal points in the system, while it is local if it refers only to one element. Both arrays are underlined, but the local array has an element number as a subscript. All of the nodes in the system are globally numbered. Similarly, all of the nodes associated with an element are locally numbered. Thus a node has a unique global number and several local numbers. The local array is related to the global array by a connectivity array[46] $\underline{J}_m$ (or the destination array)[45] which is usually omitted in the literature. It is understood that whenever a local array is related to a global one, the connectivity array exists whether it is explicitly shown or not.

Take for example the nodal point displacement A for the system shown in Fig. 4

$$A = \begin{pmatrix} A_1 \\ A_2 \\ A_3 \end{pmatrix}$$

is the nodal point displacement without referring to any node,

$$A^3 = \begin{pmatrix} A_1^3 \\ A_2^3 \\ A_3^3 \end{pmatrix}$$ is the nodal point displacement for the global nodal point 3.

$\underline{A}_2^{(i)}$ is the nodal displacement for the local node i in element 2.

$\underline{A}_2$ is the array of nodal displacement of all the nodes in element 2. According to Fig. 4,

$$\underline{A}_2 = \begin{pmatrix} \underline{A}_2^{(1)} \\ \underline{A}_2^{(2)} \\ \underline{A}_2^{(3)} \\ A_2^{(4)} \end{pmatrix} = \begin{pmatrix} A^3 \\ A^4 \\ A^6 \\ A^5 \end{pmatrix}$$ with $\underline{A}_m^{(i)}$ and A^i defined above.

$\underline{A}$ is the array of the nodal displacement of all the nodes in the system. For Fig. 4,

$$\underline{A} = \begin{pmatrix} A^1 \\ A^2 \\ A^3 \\ A^4 \\ A^5 \\ A^6 \end{pmatrix}$$

$\underline{J}_2$ is the connectivity array for element 2. From Fig. 4,

$$\underline{J}_2 = \begin{pmatrix} 0 & 0 & 1 & 0 & 0 & 0 \\ 0 & 0 & 0 & 1 & 0 & 0 \\ 0 & 0 & 0 & 0 & 0 & 1 \\ 0 & 0 & 0 & 0 & 1 & 0 \end{pmatrix}$$

So that $\underline{A}_2 = \underline{J}_2 \, \underline{A}$

Appendix D: Decomposition of R^o to Surface and Body Force Terms

According to the definition $B \equiv LH$, where L is the strain operator defined in eqn (4). B^T is the transpose of B, and is expressed by $B^T = L^T H^T$, where

$$L^T = \begin{pmatrix} \frac{\partial}{\partial x} & 0 & 0 & 0 & \frac{\partial}{\partial z} & \frac{\partial}{\partial y} \\ 0 & \frac{\partial}{\partial y} & 0 & \frac{\partial}{\partial z} & 0 & \frac{\partial}{\partial x} \\ 0 & 0 & \frac{\partial}{\partial z} & \frac{\partial}{\partial y} & \frac{\partial}{\partial x} & 0 \end{pmatrix}$$

Let q stand for any of x, y, or z, then the non-zero components in L^T can be expressed as $\frac{\partial}{\partial q}$. Let h and p be scalars, and represent the components of H^T and $C\varepsilon^o$ respectively. Now consider the integral $\int \frac{\partial}{\partial q} (hp)\, dV$. By differentiation,

$$\int \frac{\partial}{\partial q} (hp)\, dV = \int \left(\frac{\partial}{\partial q} h\right) P dV + \int h \left(\frac{\partial}{\partial q} P\right) dV$$

Also, according to the divergence theorem,

$$\int \frac{\partial}{\partial q} (hP)\, dV = \int hP\, n_q\, dS$$

where n_q is the directional cosine of the outward normal. Thus,

$$\int_V \left(\frac{\partial}{\partial q} h\right) P dV = \int_S h\, n_q\, P\, dS - \int_V h \frac{\partial}{\partial q} P\, dV \qquad \text{(D-1)}$$

$\underline{R}^o$ is defined as

$$\underline{R}^o = \sum_m J_m^T \int \underline{B}_m^T \underline{C}_m \underline{\varepsilon}_m^o \, dV_m$$

or

$$\underline{R}^o = \sum_m J_m^T \int (L^T \underline{H}_m^T) \, \underline{C}_m \varepsilon_m^o dV_m$$

By applying eqn (D-1) for each component of $\underline{R}^o$,

$$\underline{R}^o = \sum_m J_m^T \left[\int_{S_m} \underline{H}_m^T \underline{n}_m \underline{C}_m \varepsilon_m^o dS_m - \int H_m^T L^T (\underline{C}_m \underline{\varepsilon}_m^o) \, dV_m \right]$$

where

$$\underline{n}_m = \begin{pmatrix} n_1 & 0 & 0 & 0 & n_3 & n_2 \\ 0 & n_2 & 0 & n_3 & 0 & n_1 \\ 0 & 0 & n_3 & n_2 & n_1 & 0 \end{pmatrix}$$

Appendix E: The Strain Energy of a Spherical Inclusion, in a Spherical Matrix, Subject to Uniform Expansion

The strain energy created by the uniform expansion of an isotropic spherical inclusion in a finite spherical matrix is established and compared with the analytic solution of Eshelby, $E_{el} = (2/9)(1+\nu)/(1-\nu)\cdot\mu(e^T)^2\ V$, for the case of an infinite matrix. Both the homogeneous and the inhomogeneous inclusions are discussed.

1. Homogeneous Inclusion

For a spherical inclusion in an infinite matrix, Eshelby showed that the constrained strains are given by the following expression,

$$e^c = \alpha e^T \quad \text{and} \quad {}'e^c_{ij} = \beta\, {}'e^T_{ij}$$

where

$$\alpha = \frac{1}{3}\left(\frac{1+\nu}{1-\nu}\right)$$

$$\beta = \frac{2}{15}\left(\frac{4-5\nu}{1-\nu}\right)$$

$$e^T = \text{stress-free volume strain} = \sum_m e^T_{mm}$$

$${}'e^T_{ij} = \text{deviatoric stress-free strain.}$$

For the case of a uniform expansion, ${}'e^T_{ij} = {}'e^c_{ij} = {}'\sigma^I_{ij} = 0$ while $\sum_m \sigma^I_{mm} = 3k(e^c - e^T) = 3k(\alpha - 1)\, e^T$. Hence

$$\sigma^I_{ij} = {}'\sigma^I_{ij} + \frac{1}{3}\left(\sum_m \sigma^I_{mm}\right)\delta_{ij} = k(\alpha - 1)\, e^T\delta_{ij} = -P^I\delta_{ij} \quad ; \quad (\text{for } r \lesssim a) \tag{E-1}$$

where k is the bulk modulus, σ^I_{ij} is the stress and P^I is the hydrostatic pressure within the inclusion. The stress distribution outside the inclusion is the same as that outside a spherical cavity subject to internal pressure P^I,[53]

$$\sigma_{rr} = -P^I \left(\frac{a}{r}\right)^3$$

$$\sigma_{\theta\theta} = \sigma_{\phi\phi} = (P^I/2) \left(\frac{a}{r}\right)^3$$

$$\sigma_{r\theta} = \sigma_{\theta\phi} = \sigma_{r\phi} = 0 \qquad \text{(for } r > a\text{)} \qquad \text{(E-2)}$$

where a is the radius of the cavity (or inclusion). According to eqn (A-2), the surface traction $\vec{t}$, on a surface, radius b, outside the inclusion, is given by

$$\vec{t} = \sigma_{rr}\,\hat{r} = -P^I \left(\frac{a}{b}\right)^3 \hat{r}$$

The stress distribution within $r \leq b$ is unchanged if the matrix outside the sphere $r = b$ is removed and the surface traction $\vec{t}$ is applied on the spherical surface.

The stresses within a finite matrix of radius b can be determined by removal of the surface traction. Thus a surface traction $\vec{t}' = -\vec{t}$ is applied on the spherical surface, leaving that surface traction

free. For elastic homogeneity, the stress distribution resulting from the surface traction $\vec{t}'$ is simply a hydrostatic stress

$$\sigma'_{rr} = \sigma'_{\theta\theta} = \sigma'_{\phi\phi} = P^I \left(\frac{a}{b}\right)^3 \tag{E-3}$$

The stress distribution associated with the transformation of a spherical inclusion in a spherical matrix is the sum of the stresses given in eqns (E-1), (E-2) and (E-3). The stress distribution is as follows,

$$\text{for } r \leq a \begin{cases} {}_b\sigma^I_{rr} = {}_b\sigma^I_{\theta\theta} = {}_b\sigma^I_{\theta\theta} = -P^I\left(1 - \dfrac{a^3}{b^3}\right) \\ {}_b\sigma^I_{r\theta} = {}_b\sigma^I_{\theta\phi} = {}_b\sigma^I_{r\phi} = 0 \end{cases}$$

$$\text{for } a \leq r \leq b \begin{cases} {}_b\sigma_{rr} = -P^I \left(\dfrac{a}{b}\right)^3 \left(\dfrac{b^3}{r^3} - 1\right) \\ {}_b\sigma_{\theta\theta} = {}_b\sigma_{\phi\phi} = P^I\left(\dfrac{a}{b}\right)^3 \left(\dfrac{b^3}{2r^3} + 1\right) \\ {}_b\sigma_{r\theta} = {}_b\sigma_{\theta\phi} = {}_b\sigma_{r\phi} = 0 \end{cases} \tag{E-4}$$

where the subscript b is used to indicate the finite matrix with radius b.

To evaluate the strain energy, only the stress within the inclusion is needed,[39]

$$E_{el} = -\frac{1}{2}\int {}_b\sigma^I_{ij} e^T_{ij}\, dV$$

$$= \frac{2}{9}\left(\frac{1+\nu}{1-\nu}\right)\mu\left(1-\frac{a^3}{b^3}\right)(e^T)^2\, V$$

The ratio of the strain energy of transformation of a particle embedded in the spherical matrix to that in the infinite matrix is thus $\left(1-\frac{a^3}{b^3}\right)$.

2. Inhomogeneous Inclusion

According to the equivalent inclusion method, the equivalent stress-free strain e^T_{ij} should satisfy the following equations:

$$k(e^c - e^T) = k^*(e^c - e^{T*}) \qquad \text{(E-5)}$$

$$\mu('e^c_{ij} - 'e^T_{ij}) = \mu^*('e^c_{ij} - 'e^{T*}_{ij})$$

where K^*, μ^*, and e^{T*}_{ij} are the bulk modulus, shear modulus, and stress free strain of the inclusion respectively.

For the case of uniform expansion, the deviatoric parts of the strains are zero, and only eqn (E-5) has to be satisfied. Eqn (E-5) can be rearranged as follows,

$$(k^* - k)(e^c) + ke^T = k^*e^{T*} \qquad \text{(E-6)}$$

In the previous section, it has been shown that the stress within a homogeneous inclusion is uniform, and

$$\sigma^I = -k(1 - \alpha)\left(1 - \frac{a^3}{b^3}\right)e^T \tag{E-7}$$

Since $\sigma^I = k(e^c - e^T)$, we have

$$e^c = \left[1 - (1 - \alpha)\left(1 - \frac{a^3}{b^3}\right)\right] e^T$$

Substituting this into eqn (E-6), we have

$$\left[k^* + (k - k^*)(1 - \alpha)\left(1 - \frac{a^3}{b^3}\right)\right] e^T = k^* e^{T*}$$

Thus

$$e^T = \xi e^{T*} \tag{E-8}$$

where

$$\xi = \left[1 + (\Omega - 1)(1 - \alpha)\left(1 - \frac{a^3}{b^3}\right)\right]^{-1}$$

$$\Omega = \frac{k}{k^*}$$

Substituting eqn (E-8) into eqn (E-7),

$$\sigma^I = -k(1 - \alpha)\left(1 - \frac{a^3}{b^3}\right)\xi e^{T*} = -P^I\left(1 - \frac{a^3}{b^3}\right)$$

where

$$P^I = k(1 - \alpha)\ \xi e^{T*}$$

The stress distribution for $a \leq r \leq b$ is shown in eqn (E-4) with P^I defined above.

Then the energy is given by

$$E_{el} = -\frac{1}{2}\int \sigma^I_{ij} e^{T*}_{ij}\, dV$$

$$= \frac{1}{2}k(1 - \alpha)\ \xi\left(1 - \frac{a^3}{b^3}\right)(e^{T*})^2\ V$$

$$= \frac{2}{9}\left(\frac{1 + \nu}{1 - \nu}\right)\mu\left(1 - \frac{a^3}{b^3}\right)\xi(e^{T*})^2\ V \qquad \text{(E-9)}$$

REFERENCES

1. R. P. Reed and J. F. Breedis, ASTM Spec. Tech. Publ. 387, 60 (1966).
2. R. C. Garvie, R. H. Hannink and R. T. Pascoe, Nature 258, 703 (1975).
3. D. L. Porter and A. H. Heuer, J. Am. Ceram. Soc. 60, 183 (1977).
4. E. Hornbogen, Acta Met. 26, 147 (1978).
5. J. Perkins, Shape Memory Effects in Alloys, J. Perkins ed., Plenum Press, New York and London (1975).
6. B. A. Billby and J. W. Christian, in "Mechanism of Phase Transformations in Metals," Monograph No. 18, p. 121. Institute of Metals, London, 1956.
7. J. W. Christian, "Theory of Transformations in Metals and Alloys." Pergamon, Oxford, 1965.
8. J. S. Bowles and J. K. Mackenzie, Acta Met. 2, 129, 224 (1954).
9. J. K, Mackenzie and J. S. Bowles, Acta Met. 2, 138 (1954); 5, 137 (1957).
10. M. S. Wechsler, D. S. Lieberman, and T. A. Reed, Trans. AIME 197, 1503 (1953).
11. M. S. Wechsler and H. M. Otte, Acta Met. 7, 793 (1959).
12. Z. Nishiyama, "Martensitic Transformation," M. E. Fine, M. Meshii, and C. M. Wayman, eds, Academic Press, p. 412-422 (1978).
13. H. M. Otte, Acta Cryst. 16, 8 (1963).
14. A. G. Crocker and B. A. Bilby, Acta Met. 9, 678, 992 (1961).
15. A. G. Crocker, Acta Met. 13, 815 (1965).

16. J. S. Bowles and D. P. Dunne, Acta Met. 17, 677 (1969).

17. A. G. Khachaturyan, Sov. Phys. Solid State 8, 2163 (1967).

18. M. Shibata and K. Ono, Acta Met. 23, 587 (1975); 25, 35 (1977).

19. See Part II of this dissertation.

20. S. H. Chen, Ph. D. Thesis, University of California, June 1979.

21. C. Zener, Elasticity and Anelasticity of Metals, University of Chicago, Press (1948).

22. E. Pytte, Phys. Rev. B4, 1094 (1971).

23. L. F. Mattheiss, Phys. Rev. B12, 2161 (1975).

24. P. C. Clapp, Phys. Status Solidi (b) 57, 561 (1973).

25. T. Suzuki and M. Wattig, Acta Met. 23, 1069 (1975).

26. J. Perkins, Scrip. Met. 8, 31, 439 (1974).

27. J. H. Hollomon and D. Turnbull, Progress in Metal Physics, Pergamon Press, London, vol. 4, p. 333 (1953).

28. G. V. Kurdjumov, "Problemi Metallovedenie i Fizika Metallov," vol. 1, p. 132, Metallurgizdat, Moscow (1949); ibid. vol. 3, p. 9, 1952.

29. J. C. Fisher, J. H. Hollomon, and D. Turnbull, Trans. Amer. Inst. Min. (Metall.) Engrs 185, 691 (1949).

30. M. Cohen, E. S. Machlin, and V. G. Paranjpe, "Thermodynamics in Physical Metallurgy," American Society of Metals, p. 242 (1949).

31. W. Kaufman and M. Cohen, "Thermodynamics and Kinetics of Martensitic Transformations" in Progress in Metal Physics, vol. 7, p. 165. Pergamon, Oxford (1958).

32. C. H. Shih, B. L. Averbach, and M. Cohen, Trans. Amer. Inst. Min. (Metall.) Engrs 203, 183 (1955).

33. H. Knapp and V. Dehlinger, Acta Met. 4, 289 (1956).

34. G. B. Olson and M. Cohen, Metall. Trans. 6, 1897, 1905, 1915 (1976).

35. K. E. Easterling and A. R. Thölen, Acta Met. 24, 333 (1976).

36. A. L. Roitburd, Sov. Phys.--Solid State 11, 119 (1969).

37. K. E. Easterling and P. R. Swann, Acta Met. 19, 117 (1971).

38. A. L. Roitburd, Solid State Physics 33, 317 (1978).

39. J. D. Eshelby, Proc. Roy. Soc. A241, 376 (1957); ibid A252, 561 (1959).

40. N. Kinoshita and T. Mura, Phys. Status Solidi 25, 759 (1971).

41. G. P. Sendeckyji, Ellipsoidal Inhomogeneity Problem, Ph. D. dissertation, Northwestern University, Evanston, Illinois (1967).

42. R. J. Asaro and D. M. Barnett, J. Mech. Phys. Solids 23, 77 (1975).

43. T. Mura, T. Mori and M. Kato, J. Mech. Phys. Solids 24, 305 (1976).

44. A. G. Khachaturyan and A. F. Rumynina, Phys. Stat. Sol. (a) 45, 393 (1978).

45. O. C. Zienkiewicz, "The Finite Element Method," 3rd ed., McGraw-Hill Book Co. (UK) Ltd. (1977).

46. K. J. Bathe and E. L. Wilson, "Numerical Methods in Finite Element Analysis," (1977).

47. G. Strang and G. J. Fix, An Analysis of the Finite Element Method, Prentice-Hall, 1973.

48. B. A. Finlayson, "The Method of Weighted Residuals and Variational Principles," Academic Press (1972).

49. For example, see p. 156, Ref. 45.

50. See p. 24, Ref. 45.

51. K. J. Bathe, E. L. Wilson and F. E. Peterson, "SAP IV, A Structural Analysis Program for Static and Dynamic Response of Linear System," University of California Structural Engineering Laboratory Report No. UC EERC 73-11, June 1973, Revised April 1974.

52. K. Robinson, J. Appl. Phys. 22, 1045 (1951).

53. S. P. Timoshenko and J. N. Goodier, "Theory of Elasticity," 3rd ed., p. 395, McGraw-Hill, New York (1970).

Table 1. Numerical data used in examples.

Example	r_I (m)	r_M (m)	μ_I/μ_M (GPa)	ν_I/ν_M	e^T (%)	γ_{13}^T (%)	E_{el}/E_s (FEM)(%)	E_{el}/E_s (analytic)(%)	Deviation (%)
1	1	2	50/50	0.2/0.2	3	0	44.38	43.75	1.5
2a	1	5	100/100	$\frac{1}{3}$ / $\frac{1}{3}$	3	0	33.14	33.07	0.22
2b	1	5	100/5	$\frac{1}{3}$ /0.2	3	0	2.406	2.401	0.20
3a	1	5	100/100	$\frac{1}{3}$ / $\frac{1}{3}$	0	1	0.521	0.5333	2.31
3b	1	5	100/100	$\frac{1}{3}$ / $\frac{1}{3}$	0	1 twinning	0.413	NA	
3c	1	10	100/100	$\frac{1}{3}$ / $\frac{1}{3}$	0	1	0.5333	8/15	0.013
3d	1	10	100/100	$\frac{1}{3}$ / $\frac{1}{3}$	0	1 twinning	0.400	NA	

FIGURE CAPTIONS

Fig. 1. Axisymmetric finite element mesh used in the analysis of the pure dilation of a spherical inclusion (example 1).

Fig. 2. Three dimensional finite element mesh used for the studies of the pure dilation, pure shear and twinning of a spherical inclusion (examples 2 and 3).

Fig. 3. A twinned martensite exhibiting nonuniform elastic properties.

Fig. 4. Nodes and elements in a finite element mesh.

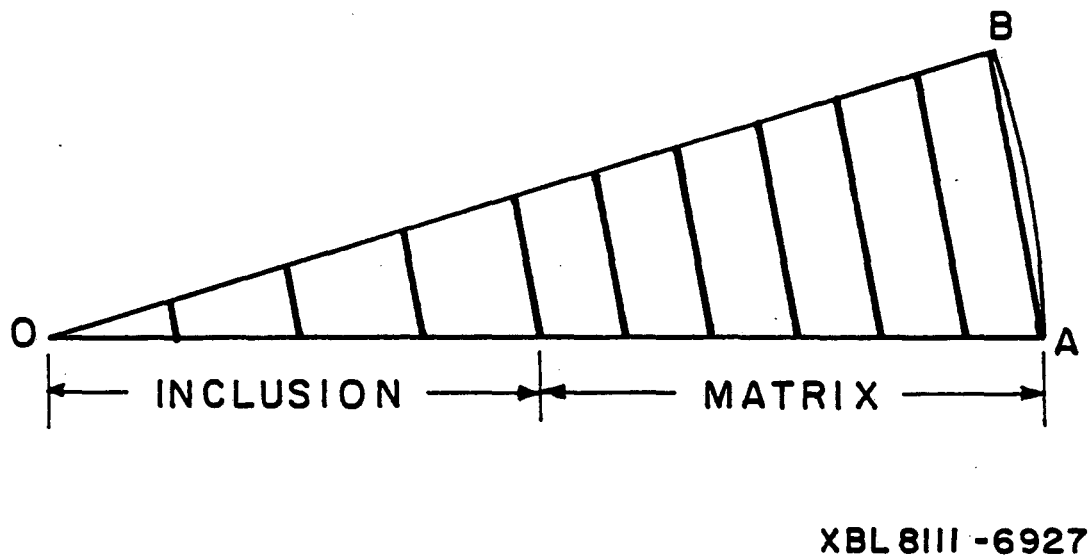

Fig. 1

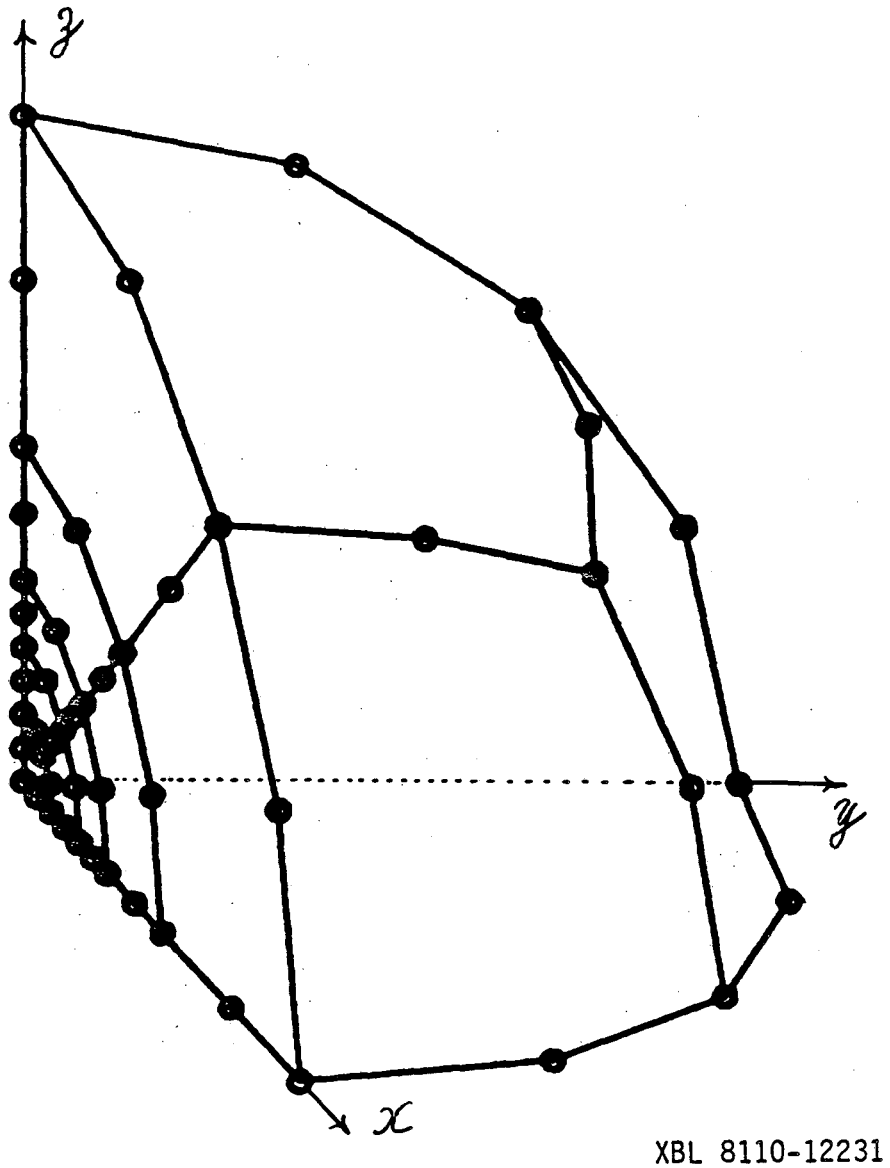

XBL 8110-12231

Fig. 2

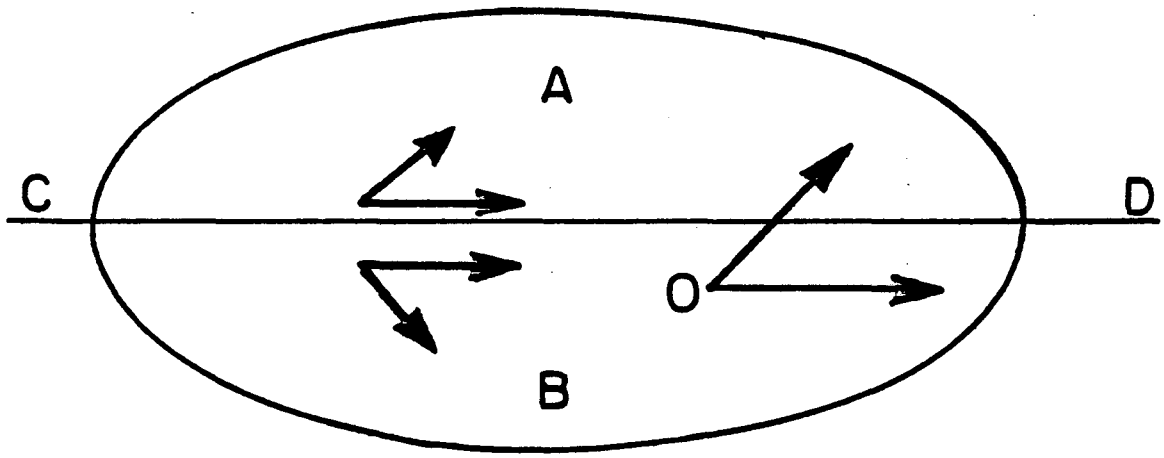

XBL 8111 -6929

Fig. 3

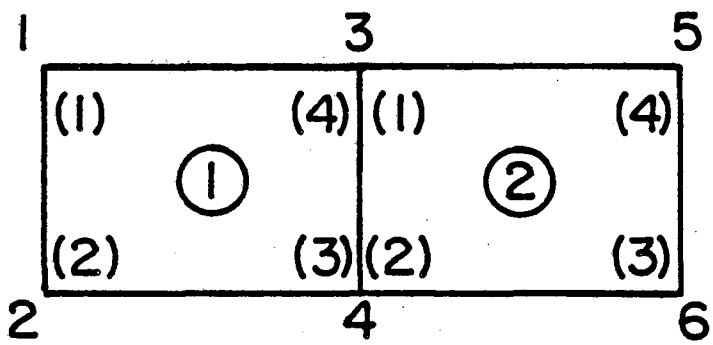

n GLOBAL NODAL NUMBER

(n) LOCAL NODAL NUMBER

(n) ELEMENT NUMBER

XBL 8111-6930

Fig. 4

PART II

STRAIN ENERGY OF TWINNED ZrO_2 MARTENSITE

ABSTRACT

The strain energy of an inhomogeneous (m)-ZrO_2 precipitate embedded in the (c)-ZrO_2 matrix has, for the first time, been determined using the finite element method. It was found that the total strain energy can be decoupled into two parts, one contributed by the diagonal stress free strain and the other by the shear stress free strain. These two strain energies are additive for an isotropic system. Twinning was found to reduce the shear strain energy and was thus justified as a relaxation mechanism. It was found that for a given precipitate, the orientation relationship which gave the minimum strain energy changed when twinning occurred. Thus twinning can not be neglected when making predictions based on the minimum energy approach. The active transformation mode was found to be predetermined by the precipitate shape and thus quite different from that in a larger grained pure ZrO_2. For PSZ, the minimum strain energy is related to the orientation relationship $(001)_m \parallel (001)_c$, $[100]_m \parallel (100]_c$; the lattice correspondence LCC, and the twinning mode $(001)_m$.

A minimum energy approach was used to estimate the bounds on the twinning boundary energy. It was found that $0.36 \leq \gamma_T \leq 0.89\ Jm^{-2}$. The twin width was found to be relatively insensitive to the particle size based on the free energy approach, consistent with the experimental observation.

1. INTRODUCTION

1.1. Zirconia and Transformation Toughening

The use of ceramics as structural materials has been limited by their inherent brittleness. In recent years, however, several toughening methods have been developed.[1] Among them, stable microcrack growth and transformation toughening are two of the most promising toughening methods. However, because of the introduction of microcracks in the former method, the mechanical strength is degraded. On the other hand, the transformation toughening method can improve the mechanical strength due to the presence of the compressive stresses resulting from the transformation. It thus seems that the transformation toughening method is more favorable and has been the subject of extensive investigation.[2-9]

Transformation toughening is a mechanism which enhances the fracture toughness by means of a stress-induced martensitic transformation. Systems which exhibit transformation toughening usually consist of two phases: e.g. precipitates of one phase embedded in the matrix of another. It is the martensitic transformation of the precipitates in the vicinity of the crack tip, induced by the stress field of the crack, that leads to the improvement of the fracture toughness. Two phase systems containing Zirconia, such as: partially stablized zirconia (PSZ), ZrO_2 in alumina, and ZrO_2 in mullite are the typical systems that can be toughened by transformation. The polymorphic nature of ZrO_2 is well known and has been the subject of many studies (see Ref. 10 for a recent review). At atmospheric pres-

sure, pure zirconia exists as three modifications: melt $\xrightarrow{2680\pm15^\circ C}$ cubic $\xrightarrow{2370^\circ C}$ tetragonal $\underset{700-1030}{\overset{1100-1200}{\rightleftharpoons}}$ monoclinic. The tetragonal to monoclinic transformation is martensitic[11] and accompanied by a ~5%[12,13] volume strain (which is normally deleterious). However, this transformation can be avoided by the formation of cubic solid solution with the stabilizing oxides, notably MgO, CaO, Y_2O_3 and CeO_2. A zirconia-rich portion of the phase diagram[14] for the ZrO_2-MgO system is shown in Fig. 1. The cubic solution can persist to room temperature because of the sluggish nucleation of the MgO; this structure is known as fully stabilized zirconia. Partially stabilized zirconia results when insufficient oxide solutes are added into zirconia. In this case, precipitation of the low solute content ZrO_2 phase with tetragonal symmetry occurs.[12] Larger precipitates usually transform martensitically to monoclinic symmetry. The transformed particles are internally twinned. However, the Ms temperature decreases with decrease in particle size and the smaller precipitates retain tetragonal symmetry.[4,15] Thus the PSZ consists of precipitates of monoclinic and tetragonal zirconia-rich phases in a matrix of the cubic solid solution. Experiments[2,3,4] indicate that the partially stabilized zirconia exhibits superior mechanical properties to the fully stabilized zirconia. Evidence has been presented to demonstrate that the retained tetragonal phase transforms martensitically to monoclinic symmetry in the vicinity of a stressed crack. The improvement in mechanical properties is believed to be attributed to the stress-induced transformation.[5-7,9]

1.2 The Role of Strain Energy in Transformation Toughening

1.2.1 Strain Energy and Transformation Zone

The retention of the tetragonal phase has been recognized to originate from the elastic constraint imposed by surrounding matrix. The transformation is prohibited because the strain energy increase can exceed the decrease in chemical free energy. However, under an applied tensile stress (especially in the vicinity of a crack tip) the constraint of the matrix can be relaxed, and the strain energy change reduced. In the extreme case, where the applied strain is larger than the transformation strain (e.g. near the crack tip for precipitates with small transformation strain) the strain energy decreases after transformation. Thus near the crack tip, there will be a region where transformation is energetically favorable i.e. the total change in the strain energy and the chemical free energy is negative. This region constitutes a transformation zone (in the case of many precipitates, some precipitates within this region may not be transformed because of the orientation dependence of the strain energy and interaction between precipitates). Since the transformation zone size is a key parameter in the fracture analysis, strain energy evaluation is indispensable in understanding the toughening mechanism.

1.2.2 Strain Energy and Optimal Size for Toughening

For the partially stabilized zirconia, the optimal fracture toughness[4] is obtained when tetragonal precipitates of a size near the critical size are fabricated. Thus it is important to know the critical size. Although the strain energy has been regarded as the major

restraining force that leads to the retention of the tetragonal phase, it alone can not explain the size effect, because precipitates of similar shape but different size have the same strain energy density (see Appendix A). In addition to the strain energy, the Helmholtz free energy change, the twinning boundary surface energy, and the inclusion-matrix interfacial energy all contribute to the total free energy change. To account for the size effect, all energy terms need to be considered. Mechanisms such as a size dependent chemical free energy change (due to possible compositional differences[5]), and surface energy effects[16] have been proposed.

1.2.3 Strain Energy and Transformation Toughening

In fracture mechanics,[17] the fracture toughness of a given material can be evaluated either by calculating the stress intensity factor or by determining the energy release rate under the application of the critical load. In the latter approach, the strain energy change during a crack increment needs to be analyzed. In the case of transformation toughening, the situation becomes more complex because both the transformation zone[7,18] and the strain energy change[7,22] are dependent on the applied stress. The fracture toughness can be evaluated if this critical applied stress is known. This stress is a function of the transformation strain, the chemical free energy change involved in transformation, and the precipitate size and spatial distribution. Currently, only limited information is available concerning these variables. Nevertheless the strain energy calculation provides the essential links between the transformation zone size, applied

stress, and the transformation strain, and can be used to place bounds on the problem and to elucidate theoretical concepts.

In the literature[5,7,9,16] the strain energy calculations have been limited to the case in which the transformed particles do not have internal twinning. Since internal twinning is almost invariably observed it must be included in the strain energy analysis. In the following, the finite element method is used to determine the strain energy, with emphasis on the existence of internal twinning. The size effect is then studied.

2. STRAIN ENERGY CALCULATIONS

The strain energy change involved in a martensitic transformation depends on several variables: the elastic constants of the precipitates and the matrix, the stress free strain of the transformation, the internal structure after transformation (e.g. number of twin pairs), the shape of the precipitates, the orientation relationship, and the applied stress. To study the effect of size on the retention of the tetragonal phase, the applied stress is set to zero. The respective choices of the remaining variables are considered in the following (for convenience, the monoclinic, tetragonal, and cubic zirconia solid solution will be referred as (m)-ZrO_2, (t)-ZrO_2. and (c)-ZrO_2, respectively).

2.1 Elastic Constants

The anisotropic stiffness coefficients of either (m)-ZrO_2, or (t)-ZrO_2, or (c)-ZrO_2 are not available; thus, isotropic elastic constants are used. Table 1 gives the values of the elastic constants

used in the calculation. Two matrices are considered: Mg-(c)-ZrO_2 and Ca-(c)-ZrO_2. The magnesia doped cubic solid solution has the higher value of Young's modulus.[19,20] Additionally, the monoclinic phase[21] has a higher Young's modulus than the cubic matrix. No data for the tetragonal phase are available at room temperature; hence, the elastic constants are assumed to be the same as those of the monoclinic phase. (Since the strain energy associated with the tetragonal precipitate in the cubic matrix is relatively small, this assumption introduces a minor error).

2.2 The Stress-Free Strain

Problems associated with transformations were first successfully treated by Eshelby.[22] In his analysis, the stress-free strain was used as the transformation strain based on the assumption that the transformed region was stress-free in the matrix before the phase transition. In the case of PSZ, this assumption does not apply (as exemplified by strain fringes observed around retained tetragonal precipitates[12,15]). Hence, in this study, the stress-free strain and the transformation strain are not considered to be identical. Specifically, the transformation strain is used to describe the dimensional change caused by the transformation in the absence of the constraint of the matrix, while the stress-free strain arises when two materials with different stress-free states are joined together. In general, the stress-free state of the matrix is used as the reference state, and a nonzero stress-free strain is assigned to the inclusions or the precipitates. For PSZ, the (t)-ZrO_2 and (m)-ZrO_2 have different non-

zero stress-free strains with respect to the (c)-ZrO_2 matrix. The difference is the tetragonal to monoclinic transformation strain. The stress-free strain of an inclusion in the matrix is determined by the dimensional change between a stress-free inclusion and the hole left behind in the matrix after the imaginary removal of the inclusion. The dimension of the former depends on the lattice parameters, the number of unit cells, and their spatial arrangement. The volume of the latter can be determined by the lattice parameters of the matrix and the number of matrix unit cells that will fill the hole. The ratio of the number of matrix unit cells to the number of inclusion unit cells is related to the coherency of the interface. The spatial arrangement of the unit cells is reflected in the internal structure (such as dislocations, internal twinning etc.), and the orientation relationship. Thus the stress-free strain is a function of the lattice parameters of the precipitate (after and before the transformation) and the matrix; the precipitate-matrix boundary coherency, the lattice correspondence in the transformation, and the orientation relationship.

2.2.1 The Lattice Constants

The lattice constants depend on composition. However, no information on the variation of lattice constants with composition is available for any of the three phases. In this study, lattice parameters reported by Hannink[12] for the (t)-ZrO_2 and (c)-ZrO_2 will be used. (The annealing temperatures used were 1420°C for Mg-PSZ, and 1300°C for Ca-PSZ, typical of optimally fabricated PSZ). The lattice constants for (m)-ZrO_2 at the same composition as (t)-ZrO_2 are not

available (the same composition is desirable because, according to the nature of the martensitic transformation, the composition is unchanged after the transition). Thus, the lattice constants of a nearly pure (m)-ZrO_2, reported by Patil et al.[13], are used. For comparison purposes, the lattice parameters for an essentially pure (t)-ZrO_2, reported by Patil et al., extrapolated to room temperature are also used. In the literature, two unit cells have been used to describe the tetragonal phase: face centered tetragonal[23] (fct) and body centered tetragonal[24] (bct). The relation between them is as follows: $A_{fct} = \sqrt{2}\, A_{bct}$ and $C_{fct} = C_{bct}$. The fct cell is used in this study. The lattice parameters are given in Table 2. It has to be pointed out, however, that the lattice constant reported by Hannink are constrained values. The "real" values can not be measured because the tetragonal phase is not stable without the constraint of the matrix (except for very tiny particles < 300 Å).[25] Estimated unconstrained lattice constants, obtained by an iteration method (see Appendix B), are also included in Table 2.

2.2.2 Boundary Coherency

The precipitate-matrix interface is fully coherent if the lattice planes are continuous across the interface. In this case, there is a unique correspondence between the atoms on both sides of the interface. If dislocations exist, the correspondence between the atoms is destroyed, and the interface is semicoherent. In the extreme case, when there is no correspondence, the interface becomes incoherent.

For a fully coherent or semicoherent interface, the ratio of the number of unit cells in the inclusion to that in the matrix which it replaces can be calculated and the stress-free strain is then determined. Fully coherent tetragonal and monoclinic phases in a cubic matrix constitute case A in this study. For fully incoherent tetragonal and monoclinic phases, the stress free strain is determined on the premise that the tetragonal phase is stress-free at the annealing temperature. The stress-free strain for the tetragonal-matrix system at room temperature is then just the thermal contraction mismatch strain. Upon subsequent transformation to the monoclinic phase, an additional transformation strain is introduced. This strain is determined from the correspondence between the tetragonal and the monoclinic unit cells (which enable the transformation strain to be evaluated directly from the lattice constants and lattice correspondence). The stress-free strain for the monoclinic-matrix system is the sum of the thermal strain and the transformation strain. This constitutes case B. Cases A and B represent upper and lower bound solutions.

2.2.3 Lattice Correspondence

In a cooperative diffusionless transformation, all atoms in the same position in a unit cell move in the same way. Thus there is lattice correspondence between the phases before and after transformation. The lattice correspondence defines the movement of the unit cell, from which the transformation strain is determined. The tetragonal to monoclinic transformation has three possible lattice correspondences, due to the symmetry of the lattices. The c-axis in the tetragonal lattice

can correspond to any of the a, b and c-axis of the monoclinic lattice, and are classified as lattice correspondences A, B, and C (symbolically LCA, LCB and LCC) respectively. The cubic to tetragonal transformation involves diffusion, and has no lattice correspondence. However, in case A, where atomic correspondence is imposed, lattice correspondence can be assigned to this transformation. Because of the lattice symmetry, there is only one lattice correspondence for the cubic to tetragonal transformation. In this way, atoms in the monoclinic lattice can also be correlated to those in the cubic lattice, and a cubic to monoclinic lattice correspondence can be established. There is only one cubic to monoclinic lattice correspondence due to symmetry considerations. From this correspondence, the stress-free strain involving a monoclinic phase in a cubic matrix can be determined.[26] There is another approach to evaluate this stress-free strain in case A. The stress free strain can be evaluated as the sum of the strains in the cubic to tetragonal and in the tetragonal to monoclinic transformation. The deviation between these two methods is less than 1%. In this study, the former method is used.

In case B, the transformation strain is determined by the tetragonal to monoclinic lattice correspondence.

2.2.4 Orientation Relationship[+]

The orientation relationship in a tetragonal-monoclinic transformation has been determined by various investigators.[10] Two posssible orientation relationships can be summarized as follows:

TYPE B: $(100)_m \parallel \{100\}_{fct}$

$[010]_m \parallel [001]_{fct}$

TYPE C: $(100)_m \parallel \{100\}_{fct}$

$[001]_m \parallel [001]_{fct}$

In particular, Bansal and Heuer[27] claimed that type B pertains for transformations which occur above 1000°C and type C applies below 1000°C. The orientation relationship usually suggests the lattice correspondence, especially when the angles between lattice axes of the two phases are small (as in the case of ZrO_2). Thus, type B suggests LCB and type C suggest LCC.

The orientation relationship[28] between the tetragonal participates and the cubic matrix were found to be

$$\{100\}_{fcc} \parallel \{100\}_{fct} \text{ and } (001)_{fct}$$

$$\langle 100\rangle_{fcc} \parallel \langle 100\rangle_{fct} \text{ and } [001]_{fct}$$

The orientation relationships between the monoclinic precipitates and the cubic matrix can be deduced from the relations mentioned above.

[+]The orientation relationship describes the orientations of the inclusion and the matrix, which is to be compared with the lattice correspondence which provides the identification of the atoms before and after a transformation.

However, it should be noted that neither type B nor type C uniquely determines the orientation relationship among a nonspheroidal monoclinic precipitate and the cubic matrix because there are two equivalent $(100)_{fct}$ in a tetragonal lattice. Since no pertinent data are available, both orientations are used in the calculation. Six orientation relationships between the (m)-ZrO_2 and the (c)-ZrO_2 are possible for an ellipsoidal precipitate, as shown in Fig. 2. These six O.R.'s are considered in this study.

2.2.5 The Stress-Free Strain

Given the lattice parameters, the lattice correspondence, and assuming full coherency, the stress-free strain between two lattices is determined by the following equation[26]

$$\{(Ac^TB)(B^*GB)(BCA) - \eta^2(A^*GA)\}[A:X] = 0$$

where A denotes the base vectors in the parent lattice, B those in the product lattice, (BCA) is the correspondence array (with successive columns referring to the basis B of the lattice vectors, CA, in the product lattice which corresponds with the base vector A in the parent lattice), (AC^TB) is the transpose of (BCA), (B^*GB) is the metric associated with the basis B, (A^*GA) is the metric associated with basis A, η is the principal strain, and [A:X] are the principal axes. A geometric method[29] and an approximation method[5,16] are also available in the literature.

The termal strains for case B are calculated using thermal expansion data reported by Patil et al.[13] and Burdick et al.[30] (in the latter, the thermal expansion coefficient of the stabilized zirconia

(matrix) is assumed to be the same as that during the first thermal cycle reported by Burdick et al. for the system ZrO_2 + 15.5 mole% MgO). All strains for cases A and B are listed in Table 3 for three orientation relationships. The other orientation relationships are considered by specifying the material axes during strain energy calculations (as an input to the computer program).

2.3 Twinning

Twinning has been recognized as a mechanism which reduces the strain energy.[27,31] In the literature,[10,31,32,33] $(100)_m$, $(110)_m$ and $(1\bar{1}0)_m$ twins have been observed both for the pure ZrO_2 and for precipitates in PSZ. The $(110)_m$ or $(1\bar{1}0)_m$ systems have the smaller shear component (~0.25 compared to 0.35 for $(100)_m$ twinning), and should be energetically favorable when the strain energy change completely dominates the surface energy. This mode of twinning has been primarily observed in severely overaged particles (>0.6 μ) and will not be considered in the present study. $(100)_m$ twinning[32,34] has been observed in slightly overaged precipitates (0.25~0.5μ). The traces of the twinning planes are perpendicular to the shortest axis and each precipitate contains only a few twins. The surface area is thus limited, and renders $(100)_m$ a favorable twinning mode for small precipitates.[+] In a recent study,[35] $(001)_m$ twinning has also been observed. Thus the $(100)_m$ and $(001)_m$ systems will be considered in this study. The traces of the experimentally observed twinning planes are perpendicular to the shortest axis. Taking the orientation relationships[28] between precipitates and matrix into consideration, the twinning plane normal

---

[+]The $(010)_m$ symmetry plane is not a twinning plane.

must be parallel to the shortest axis of the ellipsoidal precipitate. The twinning is considered herein to be limited to this case. Lattice correspondences A and C are assigned to $(100)_m$ and $(001)_m$ twins respectively, consistent with the experimental observations by Hannink[12] (i.e. $C_t \parallel$ to the shortest axis (see below)).

2.4 The Shape of the Precipitate

The shape of an intragranular Mg-(t)-ZrO_2 precipitate in a cubic matrix can be closely approximated by an ellipsoid with its principal axis parallel to the tetragonal lattice axes. Hannink[12] determined the aspect ratio and found $a_1:a_2:a_3 = 5.5:2.2:1$ where the a_i's are the lengths of the principal axes. The shortest principal axis was identified to lie parallel to the c_t axis. The precipitates of the Ca-(t)-ZrO_2 are plate-like. No specific aspect ratio was reported. Thus calculations of the strain energy of CaO doped precipitates have not been attempted. The elastic constant of the Ca-(c)-ZrO_2 is used for the matrix simply to test the effect of the elastic inhomogeneity on the strain energy. A spherical precipitate is also examined to understand the variation of the strain energy with shape.

2.5 Finite Element Calculations

The finite element method was developed in Part I. In the following, the additivity of the strain energy, symmetry considerations, and the meshes used in this study are discussed.

2.5.1 Additivity of the Strain Energy

The superposition principle applies to the stress, strain and the displacement field, but, in general, not to the strain energy.

Eshelby[22] showed that for an isotropic inhomogeneous ellipsoidal inclusion with twinning, the strain energy can be separated into two groups, one being contributed by the hydrostatic and the other by the deviatoric stress-free strain. These two strain energies are decoupled and additive. However, another possibility exists. The strain energy can also be separated into one part contributed by the diagonal and the other by the nondiagonal (i.e. the shear component) stress-free strain. The strain energies for these two parts are also decoupled and additive. In the case of internal twinning, the additivity of the strain energy has not been discussed in the literature. In this study, through the finite element calculation, it was found that the strain energy of a twinned isotropic inhomogeneous ellipsoidal inclusion is the sum of the strain energies contributed separately by the diagonal and the non-diagonal part of the stress-free strain. The additivity also applies to the twinned isotropic orthorhombic precipitate.

2.5.2 Symmetry Properties

Symmetry considerations can reduce the magnitude of the region to be analyzed in a finite element calculation and is an important factor with regard to the minimization of computation costs. To determine the symmetry in a transformation problem, all of the geometry, elastic stiffness coefficients, loading, and the stress-free strain must be considered. The ellipsoidal precipitate with the twinning plane parallel to two of the principal axes, has three symmetry planes. The isotropic elastic constants impose no limitation on symmetry. The external load is zero in this study. However the diagonal and the

shearing components of the stress-free strains have different symmetry. The diagonal part has three symmetry planes while the shear component has two symmetry planes and one antisymmetry plane (for an integer number of twin pairs) or one symmetry and two antisymmetry planes (for half integer numbers of twin pairs). Because of the additivity of the strain energy, the diagonal and the shearing components can be considered separately. In either case, only one octant of an ellipsoid needs to be analyzed.

2.5.3 Finite Element Mesh

According to the symmetry considerations, one-eighth of an ellipsoidal precipitate is studied. Some of the meshes used are shown in Figs. 3-6. Three dimensional twenty-node brick elements are used to describe the curved ellipsoidal surface. The infinite matrix is approximated by a finite matrix which is at least five times larger than the size of the inclusion in any direction. For the ellipsoidal inclusion, the aspect ratio is set to be 5.5:2.2:1, with the longest axis in the x direction, and shortest axis in the z direction. The twinning plane, whether it is $(100)_m$ or $(001)_m$ is always parallel to the xy plane. The accuracies of the meshes are estimated by comparison between those obtained by the finite element method and those by the Eshelby approach[22] for the case of no internal twinning. The deviation is less than 3% in all cases.

3. RESULTS

The energies associated with the diagonal terms of the stress free strains are determined by the Eshelby formulation (a computer

program based on the Eshelby approach is listed in Appendix C). The energies contributed by the nondiagonal terms are calculated by the finite element method, and are given in Table 4 and plotted in Fig. 7. The total strain energies determined by the formula $E_{tot}^{(n)} = E_{diag} + S^2 \times E_{shear}(n)$, where S is the shear strain and $E_{shear}(n)$ is the shear energy for unit shear strain for n twin pairs, are listed in Table 5 and plotted on Figs. 8, 9, and 10. Comparison of the total strain energies for different stress-free strains determined by different lattice parameters for the orientation relationship CXZ (Fig. 8) indicates a maximum deviation of 2% for case A, and of 9% for case B from the modified Hannink values. The following discussion is based on the stress-free strain calculated from the modified Hannink lattice parameters.

3.1 Influence of Twinning

From Fig. 7, it is noted that the strain energy decreases as the number of twin pairs increases. This confirms the concept that the twinning is a mechanism to relax and to reduce the strain energy, as pointed out by previous investigators.[27,31] The variation of the strain energy is determined by a least square curve fitting method as

$$E_{sh}(n) = \frac{1}{a\sqrt{n} + b}$$

The asymptotic shearing strain energy as $n \to \infty$ is zero, which is consistent with physical expectations.

3.2 Precipitate Shape Effects

Comparison of the diagonal strain energies between spherical and ellipsoidal precipitates (Table 6) indicates that the strain energy of an ellipsoidal precipitate can be smaller or larger than that of a spherical precipitate, depending on the orientation relationship and the lattice correspondence. However, the shearing strain energy of a spherical precipitate is invariably larger than that of an ellipsoid (Table 4). The total strain energy for a small number of twin pairs, in which the shearing strain energy dominates, is lower for an ellipsoidal inclusion. As the number of twin pairs increases, the diagonal strain energy dominates and the spherical precipitate may have a lower total strain energy (for example, in the case of LCA). The comparison is shown in Fig. 11.

3.3 Effect of the Shearing Plane

Suppose the longest axis of an ellipsoid is along the x axis and the shortest along the z axis. Without internal twinning, shearing on the y-z plane gives the minimum energy. However, in the case of internal twinning, shearing on the x-z plane has a strain energy less than that associated with shearing on the y-z plane. It is thus evident that neglect of the existence of internal twinning (as is the case for most strain energy calculations in the literature) obviates effective prediction of the orientation relationships and the habit plane.

3.4 Differences Between Transformation in Single Crystal (Large Grained) ZrO_2 and ZrO_2 Precipitates in PSZ

The orientation relationship, $(100)_m \parallel (100)_{fct}$ and $[010]_m \parallel [001]_{fct}$ has been observed by most investigators[10] in large grained monoclinic ZrO_2. However, this orientation relationship is energetically unfavorable in PSZ. The major difference lies in the shape of the transformed region. For the former, the shape of the transformed region is probably determined by minimum energy considerations without spatial restrictions. According to the stressfree strain data given in Table 3, a minimum energy results if the transformed region is plate-like, and the b_m (or C_t) is parallel to the plane of the plate. In the latter, the shape of the precipitate is predetermined, and the C_t axis is perpendicular to the plane of the plate. Thus the lattice correspondence, orientation relationships of the tetragonal to monoclinic transformation and the twinning plane are predetermined. This study indicates that lattice correspondence C (LCC), the orientation relationship $(001)_m \parallel (001)_{fct}$, $[100]_m \parallel [100]_{fct}$, and the twinning plane $(001)_m$ give the minimum strain energy.

3.5 The Effect of the Matrix

The shear energy for the transformation in Ca-(c)-ZrO_2 is given in Table 4. It is noted that for a softer matrix (Ca-(c)ZrO_2), the strain energy is less. The ratios of the strain energies for a Mg-(c)-ZrO_2 matrix to that for a Ca-(c)-ZrO_2 matrix are 1.19, 1.12, and 1.16 for no twins, one twin pair, and two twin pairs respectively. This result indicates that the strain energy ratio for different matrices and a spec-

ified number of twin pairs can be approximated by the strain energy ratio in the absence of twins. The strain energy contributed by the diagonal terms of the stress-free strain can be evaluated by the Eshelby approach (see Appendix C). Thus, for a given inclusion shape, once the strain energies for a given inhomogeneity are determined for a number of twins, the strain energy for another inhomogeneity can be quickly estimated. This information is useful in material selection and microstructure design.

4. DISCUSSION

4.1 Bounds on the Strain Energy

The total strain energy changes for LCC and shearing on the xz plane are plotted in Fig. 8. The energy in case A is 30% higher than in case B, primarily because the full coherency assumption overestimates the stress-free strain. The values obtained in case A are thus regarded as an upper bound. In case B, the stress free strains in the tetragonal precipitates are compressive, compared with a large tensile strain in the C_t direction in case A. The difference resides from the relatively high thermal expansion coefficients of the tetragonal phase, which cause a reduction in the total stress-free strain. Case B constitutes the lower bound. The actual strain energy is probably closer to the lower bound, because diffusive stress relaxation can proceed at the annealing temperature, in the presence of excess vacancies formed during the precipitation.

4.2 The Twin Boundary Energy

Thermodynamic considerations of martensitic transformations involve considerations of the twin boundary and precipitate/matrix interface energies, in addition to strain and chemical energies. The total change in thermodynamic potential following transformation is given by:

$$\Delta F = [\Delta\mu + \Delta E(n)]V + \gamma_T A_T + \Delta\gamma_p A_p$$

or

$$(\Delta F/V) = \Delta\mu + \Delta E(n) + (\gamma_T A_T^o + \Delta\gamma_p A_p^o)/(kV^o) \qquad (1)$$

where ΔF is the total free energy change, $\Delta\mu$ is the chemical free energy change per unit volume, $\Delta E(n)$ is the strain energy change per unit precipitate volume (which is a function of the number of twin pairs, n), V is the volume of the precipitate, γ_T is the twin boundary energy per unit surface area, A_T is the total twinning boundary area, $\Delta\gamma_p$ is the change in the precipitate-matrix interfacial energy, A_p is the precipitate-matrix interface area, the superscript o indicates that the value is for a reference size (for example, 1 μ in length in the longest axis), and k is a ratio of the linear precipitate dimension to the reference size. For very small precipitates, k is small, and the surface energy terms may dominate the free energy change. Conversely, for larger precipitates (larger k values) the surface energy terms become negligible. The precipitate volume dependence of $\Delta\mu V$ and $\Delta E(n)V$, coupled with the area dependence of $\gamma_T A_T$ and $\Delta\gamma_p A_p$, and the influence of the number of twin pairs on ΔE and $\gamma_T A_T$, results in a precipitate size dependent ΔF. Hence, by associating transformation with a specific excess driving force, $-\Delta F$,

(e.g. in order to nucleate the transformation), the incidence of transformation becomes precipitate size dependent. For example, a lower bound critical size can be estimated by requiring that $\Delta\dot{F} = 0$.[+] The characteristics of the critical size are exemplified by performing calculations for PSZ. However, it is noted at the outset that several of the quantities in Eq. (1) can only be estimated at this juncture. In particular, since the tetragonal phase is metastable, the chemical energy can not be determined in the absence of strain. Thus only an estimated value (usually invoking the assumption of a temperature independent entropy change) is available for pure ZrO_2. The chemical energy can be approximated as follows. For pure ZrO_2 $\Delta H = -1420$ cal/mole at 1478°K.[36] Hence by setting $\Delta\mu = 0$ at the unconstrained transformation temperature ΔS can be determined. Thereafter it follows that $\Delta\mu$ at room temperature ≈ -230 MPa (with respect to the tetragonal phase which has a density of 6.1 g/cm^3[10]). A lower value of $\Delta\mu$ must obtain in the presence of solutes. However, the energies of the cubic-tetragonal and the cubic monoclinic interfaces are not available (the solid/vapor interface has an energy of 0.4/m^2).[25] Similarly, the twin boundary energy has not been experimentally measured or estimated.

A minimum free energy approach for estimating bounds on the twinning boundary energy is described in this study. This approach is based on the assumption that, for a specified transformation, (i.e.

[+]In the real world, acoustic waves carrying energy Q are emitted during the course of the martensitic transformations, thus it would require $\Delta F \leq -Q$ for the transformation to proceed. In this case, the inclusions with size satisfying $\Delta F = 0$ will not be transformed. Thus the condition of $\Delta F = 0$ constitutes the lower bound critical size.

fixed composition, chemical free energy change and the interfacial surface energy change), the system will possess the number of twins that minimize the total free energy. The energy terms that vary with the number of twin pairs are the strain energy (specifically, the shear energy), and the overall twinning surface energy. According to this approach, and the experimental observation that there are usually two twin pairs, the following inequality is established:

$$\Delta E_{k2}\, V + \gamma_T\, \Delta A_{k2} \geq 0 \qquad (2)$$

where ΔE_{k2} is the change in the strain energy between k and 2 twin pairs, V is the volume of the precipitate experimentally observed, and ΔA_{k2} is the change in total twin surface between k and 2 twin pairs. Equation 2 can be separated into two groups, depending on the sign of ΔA_{k2}, as follows

$$\left|\frac{\Delta E_{k2} V}{\Delta A_{k2}}\right| \geq \gamma_T \qquad (\text{for } k < 2)$$

$$\left|\frac{\Delta E_{k2} V}{\Delta A_{k2}}\right| \leq \gamma_T \qquad (\text{for } k > 2)$$

These two inqualities constitute the upper and the lower bounds respectively. For an accurate estimation, the size, the shape and the number of twin pairs should be obtained by experiment. In this study, the aspect ratio determined by Hannink[12] (5.5:2.2:1) is used, the critical size is considered to be 0.2 μm[15] and the two twin pairs observed[4,15] in the slightly overaged particles and the stress-induced transformed particles are presumed. The minimum free energy

result then yields $0.36 \leq \gamma_T \leq 0.89$ J/m^2. The estimation could be improved by using information concerning the size, shape and number of twins obtained from the same particle.

4.3 Size Effects

If the value of the twin boundary energy is chosen to be 0.40 J/m^2 and the $\Delta\gamma_p$ is estimated to be 0.2 J/m^2, the effect of size on the transformation is shown on Fig. 12. The free energy curve versus the number of twin pairs exhibits a minimum. For a low number of twin pairs the strain energy dominates, and the total free energy decreases as the number of twins increases; while, for a large number of twins, the surface energy dominates and the total free energy increases as number of twins increases. For a small particle, the total free energy is positive for any number of twin pairs, and the transformation is energetically unfavorable. As the particle size increases, the total free energy becomes negative for a range of twin pairs and the transformation is then energetically favorable.

4.4 The Twin Thickness

From Fig. 12, it is noted that the free energy minimum displaces to a larger number of twin pairs as the particle size increases. This minimum may be used to estimate the twin widths as a function of the particle size. The results are plotted in Fig. 13. The twin widths are found to be relatively insensitive to the particle size, as demonstrated in Fig. 13. The latter has been used by others to argue that the martensitic transformation is nucleation controlled. However, this study indicates that it is a natural consequence of the system attempting to minimize its total free energy.

4.5 The $(110)_m$ Twinning

As discussed in section 2.3, the $(110)_m$ twins are not consistent with the experimental observation[12] that the C_t axis is parallel to the shortest axis, when the trace of the twinning planes are perpendicular to the shortest axis of the ellipsoid as generally observed in slightly overaged precipitates. However, it is of interest to see whether the $(110)_m$ twins are energetically favorable when the inconsistency is neglected. To remove the inconsistency, an imaginary precipitate with its shortest axis parallel to $(110)_m$ (or $(011)_t$, $(101)_t$ and $(110)_t$ before transformation for lattice correspondence LCA, LCB and LCC respectively) is assumed. Since the precipitate-matrix lattice orientation relationship is assumed to be unchanged, the stress-free strain is the same (as shown in Table 3) when referring to a coordinate system with x, y, z axes parallel to the $\{100\}_{fcc}$ axes. The stress free strain referring to a new coordinate system with the x, y, z axes parallel to the principal axes of the ellipsoid can be obtained by a tensor transformation. If the twinning plane $(110)_m$ is the xy plane, the shear strain $e_{12}^T = S/\sqrt{2}$, where S is the shear strain shown in Table 3. According to Table 3, $e_{12}^T \geq 5.8\%$. This strain does not change sign in the presence of twins. Hence the strain energy contributed by this stress free strain can not be reduced by twinning. According to Table 4, the strain energy per precipitate volume contributed by 1% shear on xy plane is 12.4 MPa. Therefore, for $e_{12}^T \gtrsim 5.8\%$ the strain energy $\geq$ 420 MPa. This strain energy is far too large compared to the chemical free energy change of 230 MPa. Thus the $(110)_m$ twinning is energetically unfavorable.

The result is consistent with the experimental observation that when $(110)_m$ is the twinning mode, the twinning plane is parallel to the shortest axis of the ellipsoid.[32,37].

5. CONCLUSIONS

The strain energy of an inhomogeneous (m)-ZrO_2 precipitate embedded in the (c)-ZrO_2 matrix has, for the first time, been determined using the finite element method. It was found that the total strain energy can be decoupled into two parts, one contributed by the diagonal stress-free strain and the other by the shear stress-free strain. These two strain energies are additive. Twinning was found to reduce the shear strain energy and was thus justified as a relaxation mechanism. It was found that, for a given precipitate, the orientation relationship which gave the strain energy minimum changed when twinning occurred. Thus twinning can not be neglected when making predictions based on the minimum energy approach. The active transformation mode in PSZ was found to be predetermined by the precipitate shape and thus quite different from that in a larger grained pure ZrO_2. For PSZ, the minimum strain energy is related to the orientation relationship $(001)_m \parallel (001)_c$, $[100]_m \parallel [100]_c$; the lattice correspondence LCC; and the twinning mode $(001)_m$. $(110)_m$ twins are energeticaly unfavorable if the twinning plane is perpendicular to the shortest axis of the ellipsoid.

A minimum energy approach was used to estimate the bounds on the twinning boundary energy. It was found that $0.36 \leq \gamma_T \leq 0.89$ J/m^{-2}. However, the shear strain used in the estimation was an upper bound

value, thus the actual bounds on the twinning boundary energy may be lower. The twin width was found to be relatively insensitive to the particle size based on the minimum free energy approach, consistent with the experimental observation.

APPENDIX A: The Scaling Factor for The Strain Energy Calculation

Let systems A and B both consist of m twinned inclusions in an infinite matrix. The twinned particles can be regarded as consisting of several grains with uniform stress-free strain within each grain. Assume that there are n grains in either system. In system A, the surfaces of the grains are described by

$$g_i^A(\vec{x}) = 0 \qquad \text{for } 1 \leq i \leq n.$$

Assume that the distribution and the shapes of the n grains in system B are similar to those in A, except for a scaling factor k (a scaling factor is the ratio of the length between two points in system B to that between two corresponding points in system A). In other words, the surfaces of the grains in system B are described by

$$g_i^B(\vec{x}) = g_i^A(\vec{x}/k) = 0 \qquad \text{for } 1 \leq i \leq n. \tag{A-1}$$

Figure 14 shows an example of systems A and B with $m = 2$, $n = 4$, and $k = 2$.

Under the assumption of no body force, the strain energy in system B is k^3 times that in system A, as shown below.

Let $\sigma^A(x)$ be the stress distribution in system A. Then σ^A must satisfy the following conditions:

(i) The equilibrium equation $\sigma^A_{ij,j} = 0$ (A-2)

(ii) Continuity of surface tractions across the grain boundary,

$$f(\sigma^A(x), \epsilon_i) = 0 \quad \text{on } g_i^A(x) = 0 \text{ surface} \tag{A-3}$$

(iii) The condition of compatibility within each grain

$$h\ (\sigma^A(x)_{,ij}) = 0$$

(iv) $\lim_{x\to\infty} \sigma^A(x) = 0$

Now consider the stress distribution $\sigma^B(x) = \sigma^A(x/k)$ in system B. According to Eq. (A-2)

$$\sigma^B(x)_{ij,j} = \sigma^A_{ij,j}\ (x/k)/k = 0,$$

thus the equilibrium equations are satisfied. On the i-th grain boundary in system B, the surface is described by $g_i^A(x/k) = 0$ according to Eq. (A-1). Then it follows from Eq. (A-3) that

$$f(\sigma^A[(x/k)],\ \epsilon_i) = 0 \quad \text{on } g_i^A\ (x/k) = 0$$

or

$$f(\sigma^B(x),\ \epsilon_i) = 0 \quad \text{on} \quad g_i^B\ (x) = 0.$$

Thus the second condition is also satisfied. Compatibility condition contains only second derivatives of the stress component. Since $\sigma^B_{,ij} = (1/k^2)\ \sigma^A(x/k)_{,ij}$, $h(\sigma^B(x),ij) = (1/k^2)h\ (\sigma^A(x/k)_{,ij}) = 0$ and thus, $\sigma^B_{ij}(x)$ satisfies the condition of compatibility. The fourth condition is also satisfied.

Let E^A and E^B be the strain energies for system A and B respectively. Then

$$E^A = \frac{1}{2}\int(\epsilon^A(x) - \epsilon^{\circ A}(x))\ \sigma^A(x)\ d^3x$$

and

$$E^B = \frac{1}{2}\int(\epsilon^B(x) - \epsilon^{\circ B}(x))\ \sigma^B(x)\ d^3x$$

$$= \frac{1}{2}\int(\epsilon^A(\tfrac{x}{k}) - \epsilon^{\circ A}(\tfrac{x}{k}))\ \sigma^A(\tfrac{x}{k})\ d^3x$$

$$= \frac{1}{2} k^3 \int (\varepsilon^A(y) - \varepsilon^{\circ A}(y))\ \sigma^A(y)\ d^3y$$

$$= k^3\ E^A\ .$$

Thus the strain energy for inclusions of similar shape is proportional to the cube of the scaling factor k. For one inclusion problem, the strain energy can, therefore, be normalized with respect to the inclusion volume, and E/V is a constant for a given shape independent of the inclusion size.

Appendix B: An Iterative Method To Determine the Unconstrained Lattice Parameters Of the (t)-ZrO_2

For an ellipsoidal inclusion, a uniform constrained strain is developed if the stress-free strain is uniform. Because of the uniformity of the constrained strain, the constrained inclusion responds to the x-ray as if it consisted of a lattice with different lattice constants. Thus the lattice constants determined by the x-ray diffraction method can be different from the real or the unconstrained values. The relations between the lattice parameters of the cubic matrix (a^o), of the measured constrained inclusion (a_i^c) and of the unconstrained inclusion (a_i) are shown in Fig. 15 (the notation of the strains follow Eshelby's, i.e. the superscripts T* and C denote the true stress-free strain and the constrained strain respectively). It follows that e_{ii}^{T*} can be solved from the iterative equation

$$ {}^{(n)}e_{ii}^{T^*} = \left(\frac{a_i^c}{a^o}\right)\left(\frac{1 + {}^{(n-1)}e_{ii}^{T^*}}{1 + {}^{(n-1)}e_{ii}^{c}}\right) - 1 \qquad \text{(B-1)} $$

where the superscript n and n-1 denote the nth and (n-1)th iteration. The constrained strain ${}^{(n-1)}e_{ii}^{c}$ is a function of the true stress-free strain ${}^{(n-1)}e_{ii}^{T*}$, which was established by Eshelby.[22] Thus, in principle, Eq. (B-1) can be solved.

For (t)-ZrO_2, additional constraint has to be imposed because of $e_{11}^{T*} = e_{22}^{T*}$ which comes directly from $a_1 = a_2$ for a tetragonal lattice. However, the resulting constrained strains e_{11}^{c} and e_{22}^{c} are

different for an ellipsoidal inclusion. Consequently, the calculated e_{11}^{T*} and e_{22}^{T*} from Eq. (B-1) are not the same. Thus the average value is used in the next iteration. Furthermore, because of the difference in e_{11}^{c} and e_{22}^{c}, the measured constrained lattice constants a_1^c and a_2^c can not be the same. Thus the lower and the upper bound of the measured lattice parameters are used as a_1^c and a_2^c respectively (where a_1 corresponds to the direction of the longest principal axis of the ellipsoid). According to Hannink's data, $a_1^c = 5.075$ Å, $a_2^c = 5.079$ Å, $a_3^c = 5.183$ Å, and $a^o = 5.080$ Å. The iteration method converges rapidly to the following values: a = 5.0766 and c = 5.2037. The same values are obtained if $a_1^c = 5.076$ and $a_2^c = 5.078$ are used for the measured lattice constants.

APPENDIX C: Listing of a Computer Program for Strain Energy Calculation Based on Eshelby Method

```
      PROGRAM TRANSF(INPUT,OUTPUT,TAPE5=INPUT,TAPE6=OUTPUT)
C  ------
C  --                AUTHOR   MING-DER HUANG
C  --           UNIVERSITY OF CALIFORNIA,BERKELEY
C  --                      MARCH 1981
C  --
C  ****************** THE ESHELBY METHOD ******************************
C  --
C  -- ***INPUT FORMAT***
C  -- GIVE THE FOLLOWING DATA AND THE PROGRAM WILL RETURN EQUIVALENT
C  -- TRANSFORMATION STRAIN,S TENSOR ,STRESS INSIDE THE INCLUSION, AND
C  -- THE TOTAL STRAIN ENERGY
C  --
C  --      1. LS,LEC,LABEL.          (2A1,3X,7A10)
C  --            IF LS IS NOT BLANK,THE S TENSOR IS PRINTED
C  --            IF LEC IS NOT BLANK,THE CONSTRAINED STRAIN IS PRINTED
C  --      2. A, B, C,ISHAPE,ICOR(3),NDIV)  (3F10.0,1X,A4,4I5)
C  --            (A,B,C IN ARBITARY ORDER)(IF ISHAPE IS SPECIFIED,ICOR
C  --            SPECIFIES THE AXIS NUMBER IN THE ORDER OF DECREASING
C  --            LENGTH . IF ISHAPEIS IS BLANK, ICOR IS IGNORED.)
C  --             (DEFAULT FOR NDIV=50)
C  --            (ISHAPE,ICOR,AND NDIV ARE DESIGNED TO BE LEFT BLANK
C  --            AND A,B,C,TO BE IN ARBITARY ORDER)
C  --
C  --                INCLUSION SHAPE        ISHAPE CODE
C  --
C  --                     SPHERE                BALL
C  --                     OBLATE                CAKE
C  --                     PROLATE               POLE
C  --                      OTHER            (ANY NONBLANK)
C  --
C  --      3. G(M),V(M),G(INC),V(INC))IN CASE OF HOMOG LEAVE G(INC)BLANK
C  --      4. THE TRANSFORMATION STRAIN E1 E2 E3 R4 R5 R6  (6F10.0)
C  --      5. MORE DATA) USE A , G AND E TO INDICATE THE RE-ENTRY POINT
C  --         LS,LEC,CODE,LABEL.                  (2A1,2X,A1,7A10)
C  --
C  ------
      COMMON /INT/TK2
      DIMENSION A(3),G(2),V(2),T(3),TT(3,3),S(6,6),CI(6,6),CM(6,6)
     1  ,EI(6),ET(6),A2(3),ICY(3),AA(6,6),BB(6),RLUMDA(2),LABEL(7)
     2  ,ICOR(3),AX(3)
      LOGICAL MHOMOG
      DATA ICY/2,3,1/
C  ----  PI4=4PI   -----
      PI4=ATAN(1.)*16.
      PI43=PI4/3.
C  ---- NDIV IS USED TO EVALUATE ELLIPTIC INTEGRAL  -------
      NDIV=50
      READ(5,1009)LS,LEC,MORE,LABEL
1     READ(5,1000) AX,ISHAPE,ICOR,I
C  --   AX   ORIGINAL INPUT.     A   ORDERED AXES  --------
      IF(I.NE.0) NDIV=I
      IF(ISHAPE.EQ.4H    ) GO TO 610
C  -------  NONBLANK ISHAPE WILL SKIP SORTING  -----
      DO 620 I=1,3
      J=ICOR(I)
      IF(J.NE.0) GO TO 620
```

```
      J=I
      ICOR(I)=I
620   A(I)=AX(J)
      GO TO 700
610   A(1)=AX(1)
      A(3)=AX(1)
      ICOR(1)=1
      ICOR(3)=1
      DO 600 I=2,3
      IF(AX(I).GT.A(1)) GO TO 601
      IF(AX(I).LT.A(3)) GO TO 602
      A(2)=AX(I)
      ICOR(2)=I
      GO TO 600
601   A(2)=A(1)
      ICOR(2)=ICOR(1)
      A(1)=AX(I)
      ICOR(1)=I
      GO TO 600
602   A(2)=A(3)
      ICOR(2)=ICOR(3)
      A(3)=AX(I)
      ICOR(3)=I
600   CONTINUE
C  ---  TEST FOR  SPECIAL CASE  ----
      IF(AX(1).EQ.AX(2)) ICOR(2)=2
      IF(A(1).EQ.A(2)) ISHAPE=4HCAKE
      IF(A(2).EQ.A(3)) ISHAPE=4HPOLE
      IF(A(1).NE.A(3)) GO TO 700
      ISHAPE=4HBALL
      ICOR(3)=3
700   DO 10 I=1,3
10    A2(I)=A(I)*A(I)
      DUM=SQRT(1.-A2(3)/A2(1))
      THEDA=ASIN(DUM)
      DAB=A2(1)-A2(2)
      DAC=A2(1)-A2(3)
      DBC=A2(2)-A2(3)
      DACH=SQRT(DAC)
      IF(ISHAPE.EQ.4HBALL) GO TO 4
      IF(ISHAPE.EQ.4HCAKE) GO TO 5
      IF(ISHAPE.EQ.4HPOLE) GO TO 5
C  ----- TK2=K**2)T(I)=I(I))TT(I,J)=I(I,J) THIS WAY RELATES TO ESHELBYS
      TK2=DAB/DAC
      CALL ELLIPS(THEDA,NDIV,F,E)
      DUM=PI4*A(1)*A(2)*A(3)/DACH
      T(1)=DUM/DAB*(F-E)
      T(3)=DUM/DBC*(A(2)*DACH/A(1)/A(3)-E)
      T(2)=PI4-T(1)-T(3)
      DO 20 I=1,2
      K=I+1
      DO 20 J=K,3
      TT(I,J)=(T(J)-T(I))/3./(A2(I)-A2(J))
20    TT(J,I)=TT(I,J)
      DO 30 I=1,3
      J=ICY(I)
      K=ICY(J)
```

```
30    TT(I,I)=PI43/A2(I)-TT(I,J)-TT(I,K)
2     READ(5,1001) G(1),V(1),G(2),V(2)
      DO 60 I=1,6
      DO 60 J=1,6
      S(I,J)=0.0
      CI(I,J)=0.0
60    CM(I,J)=0.0
C  --- DEFAULT IS THE INHOMOGENEOUS AND MHOMOG=FALSE.---------
      MHOMOG=.FALSE.
      IF(G(2).NE.0.) GO TO 61
C  ----   BLANK G(INCLUSION) IS USED TO INDICATE HOMOGENEOUS CONDITION--
      MHOMOG=.TRUE.
      G(2)=G(1)
      V(2)=V(1)
61    VM=1.-V(1)
      Q=0.5/PI43/VM
      R=(1.-2.*V(1))*0.5/PI4/VM
C  ---- T AND TT USE ORDERED AXES (AX) AS INDEX,HOWEVER S USES THE INPUT
C  ----  ORDER (A)
C---     DEFINE S IN THE FOLLOWING  ------
      DO 40 I=1,2
      IR=ICOR(I)
      RI=R*T(I)
      K=I+1
      DO 40 J=K,3
      JR=ICOR(J)
      S(IR,JR)=Q*A2(J)*TT(I,J)-RI
40    S(JR,IR)=Q*A2(I)*TT(I,J)-R*T(J)
      DO 50 I=1,3
      IR=ICOR(I)
      S(IR,IR)=Q*A2(I)*TT(I,I)+R*T(I)
      K=IR+3
      J=ICY(I)
      M=ICY(J)
50    S(K,K)=Q*(A2(J)+A2(M))*TT(J,M)+R*(T(J)+T(M))
C  -------S DEFINITION END  -----
C  -------- DEFINE C(INCLUSION) AND C(MATRIX)-------
      DO 65 I=1,2
65    RLUMDA(I)=2.0*G(I)*V(I)/(1.-2.0*V(I))
      DO 70 I=1,3
      DO 70 J=1,3
      IF(I.EQ.J) GO TO 71
      CI(I,J)=RLUMDA(2)
      CM(I,J)=RLUMDA(1)
      GO TO 70
71    CI(I,I)=RLUMDA(2)+2.0*G(2)
      CM(I,I)=RLUMDA(1)+2.0*G(1)
      K=I+3
      CI(K,K)=G(2)
      CM(K,K)=G(1)
70    CONTINUE
3     READ(5,1001) EI
      WRITE(6,1002)AX
      WRITE(6,1003)G(1),V(1),G(2),V(2)
      IF(LS.NE.1H )WRITE(6,1004) ((S(I,J),J=1,3),I=1,3),(S(I,I),I=4,6)
      WRITE(6,1005) EI
      IF(MHOMOG) GO TO 150
```

```
C  ------  THE EQUIVALENT INCLUSION METHOD  -------
      CALL MTPL(CI,EI,ET,6,6,1)
C  ------  THE FOLLOWING USE THE FISH LIKE PATTERN OF C S AND S -------
      DO 80 I=1,3
      DO 80 J=1,3
      DUM=0.0
      DO 90 K=1,3
90    DUM=DUM+(CI(I,K)-CM(I,K))*S(K,J)
80    AA(I,J)=DUM+CM(I,J)
      CALL GAUSS(AA,ET,3,6)
      DO 100 I=4,6
100   ET(I)=ET(I)/((CI(I,I)-CM(I,I))*S(I,I)+CM(I,I))
      WRITE(6,1006) ET
      GO TO 200
150   DO 110 I=1,6
110   ET(I)=EI(I)
200   IF(LEC.EQ.1H )  GO TO 201
      CALL MTPL(S,ET,BB,6,6,1)
      WRITE(6,1100)BB
201   DO 210 I=1,6
210   S(I,I)=S(I,I)-1.
      CALL MTPL(S,ET,BB,6,6,1)
      CALL MTPL(CM,BB,ET,6,6,1)
C  ----- ET IS NOW THE STRESS -------
      WRITE(6,1007) ET
      CALL MTPL(EI,ET,ENG,1,6,1)
      ENG=-0.5*ENG
      WRITE(6,1008) ENG
      WRITE(6,1010) LABEL
      READ(5,1009)LS,LEC, MORE,LABEL
      IF(EOF(5).NE.0.0) STOP
      IF(MORE.EQ.1HA) GO TO 1
      IF(MORE.EQ.1HG) GO TO 2
      IF(MORE .NE.1HE)STOP
      DO 220 I=1,6
220   S(I,I)=S(I,I)+1.
      GO TO 3
C--  FOR   SPHERE
4     E=PI4/5./A2(1)
      F=E/3.
      DO 400 I=1,3
      T(I)=PI43
      TT(I,I)=F
      DO 410 J=1,3
      IF(I.EQ.J) GO TO 410
      TT(I,J)=F
410   CONTINUE
400   CONTINUE
      GO TO 2
5     E=PI4*0.5*A(1)*A(3)/DAC/DACH
      IF(ISHAPE.EQ.4HPOLE) GO TO 6
      F=A(3)/A(1)
      T(1)=E*A(1)*(ACOS(F)-F/A(1)*DACH)
      I=3
      GO TO 560
6     I=1
      F=A(1)/A(3)
```

```
      THEDA=ALOG(F+DACH/A(3))
      T(2)=E*A(3)*(F/A(3)*DACH-THEDA)
560   J=ICY(I)
      K=ICY(J)
      T(I)=PI4-T(J)-T(J)
      T(K)=T(J)
      TT(I,J)=(T(J)-T(I))/3./(A2(I)-A2(J))
      TT(J,I)=TT(I,J)
      TT(I,K)=TT(I,J)
      TT(K,I)=TT(I,J)
      TT(J,K)=(PI43/A2(J)-TT(I,J))*0.25
      TT(K,J)=TT(J,K)
      TT(J,J)=TT(J,K)*3.
      TT(K,K)=TT(J,J)
      TT(I,I)=PI43/A2(I)-TT(I,J)-TT(I,J)
      GO TO 2
1000  FORMAT(3F10.0,1X,A4,4I5)
1001  FORMAT(8F10.0)
1002  FORMAT(1X,51H***** NEW SETS OF DATA ************************** /
     11X,*THE LENGTH OF THE SEMI-AXES ARE*,3F16.8)
1003  FORMAT(3X,*THE ISOTROPIC ELASTIC CONSTANTS ARE AS FOLLOWS*/3X,*MU(
     1MTX) = *,1PE18.8,*  NU(MTX) = *,0PF10.7,*  MU(INC) = *,1PE18.8,*
     2NU(INC) = *,0PF10.7//)
1004  FORMAT(3X,*THE S TENSOR IS AS FOLLOWS9*/3(1X,1P3E18.8//),54X,E18.8
     1//73X,E18.8//91X,E18.8//)
1005  FORMAT(38X,2HE1,14X,2HE2,14X,2HE3,13X,3HR23,13X,3HR13,13X,3HR12/3X
     1,*TRUE TRANSFORMATION STRAIN = *,1P6E16.6//)
1006  FORMAT(3X,*EQUIVALENT TRANSFORMATION STRAIN = */30X,1P6E16.6//)
1007  FORMAT(3X,*THE STRESS INSIDE THE INCLUSION IS */30X,1P6E16.6//)
1008  FORMAT(3X,*THE ENERGY IS *,1PE18.9///)
1009  FORMAT(2A1,2X,A1,7A10)
1100  FORMAT(3X,*THE CONSTRAINED STRAIN IN INCLUSION = */30X,1P6E16.6//)
1010  FORMAT(* ---- THE ABOVE CALCULATION IS FOR LABEL9*/1X,7A10///)
      END
      SUBROUTINE ELLIPS(XU,N,F,E)
      COMMON /INT/TK2
C  ---- F = ELLIPTIC INTEGRAL OF THE FIRST KIND) E=2ND KIND ---------
      LOGICAL IDX
      FINT(SNX2)=SQRT(1.-TK2*SNX2)
C  -----   N IS THE SECTION NUMBER AND SHOULD BE EVEN
C  -----   IDX TRUE X4 , FALSE X2  ------
      IF(N.NE.N/2*2) N=N+1
      NM=N-1
      H=XU/FLOAT(N)
      DUM=SIN(XU)
      DUM=DUM*DUM
      DUM=FINT(DUM)
      F=1.+DUM
      F=1.+1./DUM
      X=0.0
      IDX=.TRUE.
      DO 10 I=1,NM
      X=X+H
      DUM=SIN(X)
      DUM=DUM*DUM
      DUM=FINT(DUM)
      IF(IDX) GO TO 1
```

```
      E=E+2.*DUM
      F=F+2./DUM
      IDX=.TRUE.
      GO TO 10
1     E=E+4.*DUM
      F=F+4./DUM
      IDX=.FALSE.
10    CONTINUE
      H3=H/3.
      E=E*H3
      F=F*H3
      RETURN
      END
      SUBROUTINE MTPL(A,B,C,L,M,N)
      DIMENSION A(L,M),B(M,N),C(L,N)
C  ----- C=AB
      DO 10 I=1,L
      DO 10 J=1,N
      X=0.0
      DO 20 K=1,M
20     X=X+A(I,K)*B(K,J)
      C(I,J)=X
10    CONTINUE
      RETURN
      END
      SUBROUTINE GAUSS(A,B,NEQ,NDM)
C  ----  GAUSS ELIMINATION  ----------
      DIMENSION A(NDM,NDM),B(NDM)
      DO 400 N=1,NEQ
      B(N)=B(N)/A(N,N)
      IF(N.EQ.NEQ) GO TO 500
      NL=N+1
      DO 300 J=NL,NEQ
300   A(N,J)=A(N,J)/A(N,N)
      DO 400 I=NL,NEQ
      B(I)=B(I)-A(I,N)*B(N)
      DO 400 J=NL,NEQ
400   A(I,J)=A(I,J)-A(I,N)*A(N,J)
500   NL=N
      N=N-1
      IF(N.EQ.0) RETURN
      DO 600 J=NL,NEQ
600   B(N)=B(N)-A(N,J)*B(J)
      GO TO 500
      END
'00
'17
```

REFERENCES

1. A. G. Evans, A. H. Heuer and D. L. Porter, Proc. Fourth Int. Conf. on Fracture, Vol. I, 529 (1977).

2. R. C. Garvie, R. H. Hannink and R. T. Pascoe, Nature 258, 703 (1975).

3. N. Claussen, J. Am. Ceram. Soc. 59, 49 (1976).

4. D. L. Porter and A. H. Heuer, J. Am. Ceram. Soc. 60, 183 (1977).

5. D. L. Porter, A. G. Evans and A. H. Heuer, Acta Met. 27, 1649 (1979).

6. A. G. Evans and A. H. Heuer, J. Am. Ceram. Soc. 63, 241 (1980).

7. A. G. Evans, N. Burlingame, M. Drory and W. M. Kriven, Acta Met., in press.

8. T. K. Gupta, F. F. Lange and J. H. Bechtold, J. Mat. Sci. 13, 1464 (1978).

9. F. F. Lange, Science Center Report Sc 5117.6TR (Oct. 1979).

10. E. C. Subbarao, H. S. Maiti, and K. K. Srivastava, Phys. Status Solidi A, 21, 9 (1974).

11. G. M. Wolten, J. Am. Ceram. Soc. 46, 418 (1963).

12. R. H. Hannink, J. Mater. Sci. 13, 2487 (1978).

13. R. N. Patil and E. C. Subbarao, J. Appl. Cryst. 2, 281 (1969).

14. C. F. Grain, J. Am. Ceram. Soc. 50, 288 (1967).

15. D. L. Porter and A. H. Heuer, J. Am. Ceram. Soc. 62, 298 (1979).

16. F. F. Lange, Science Center Report SC 5117.8 TR (Oct. 1980).

17. R. W. Hertzberg, "Deformation and Fracture Mechanics of Engineering Materials," page 255, John Wiley & Sons, New York (1976).

18. E. Hornbogen, Acta Met. 26, 147 (1978).

19. Data supplied by Zirconia Div., Corning Glass Works, Solon, Ohio.

20. S. M. Lang, U. S. Natl. Bur. Stand., Mono. 6 (1960).

21. C. F. Smith and W. B. Crandall, J. Am. Ceram. Soc., 47, 624 (1964).

22. J. D. Eshelby, Proc. Roy. Soc. A 241, 376 (1957).

23. O. Ruff and F. Ebert. Z. Anorg. Allg. Chem. 180, 19 (1929).

24. G. Teufer, Acta Cryst. 15, 1187 (1962).

25. R. C. Garvie, J. Phys. Chem. 69, 1238 (1965).

26. J. K. Mackenzie and J. S. Bowles, Acta Met. 2 138 (1954).

27. G. K. Bansal and A. H. Heuer, Acta Met. 20 1281 (1972), ibid. 22, 409 (1974).

28. G. K. Bansal and A. H. Heuer, J. Am. Ceram. Soc. 58 235 (1975).

29. W. L. Fraser, Ph.D. dissertation, University of Adelaide, August 1974.

30. R. Bardick and W. Hoskins, Aerospace Research Laboratories, ARL-63-170 (1963).

31. J. E. Bailey, Proc. Roy. Soc. A 279, 395 (1964).

32. D. L. Porter, Ph.D. Thesis, Case Western Reserve Univ., Cleveland, Ohio, 44106 (1977).

33. D. K. Smith and H. W. Newkirk, Acta Cryst. 18, 983 (1965).

34. W. M. Kriven, "On Martensite Theory and Twinning in Composite Zirconia Ceramics", submitted to Proc. 1st Intl. Conf. on ZrO_2, CWRU, Cleveland, Ohio, USA. June 16-18, 1980, for publication in Advances in Ceramics.

35. W. M. Kriven, private communication.

36. J. P. Coughlin and E. G. King, J. Am. Chem. Soc. 72, 2262 (1950).

37. Larry H. Schoenlein, MS Thesis, Case Western Reserve Univ., Jan. 1979.

Table 1
Isotropic Elastic Constants

Material	Young's Modulus E(GPa)	Shear Modulus G(GPa)	Poisson's Ratio ν
Mg-(c)-ZrO_2	192	73.7	0.302
Ca-(c)-ZrO_2	149	58.4	0.279
(m)-ZrO_2	244	96.5	0.265
(t)-ZrO_2	244	96.5	0.265

Table 2(a)
Lattice Constants

Material	Reference	A(Å)	b(Å)	c(Å)	β(degree)
Mg-(c)-ZrO_2	Hannink	5.080	-	-	-
(m)-ZrO_2	Hannink	5.1415	5.2056	5.3128	80.7
Mg-(t)-ZrO_2	Hannink	5.077	-	5.183	-
	Modified Hannink	5.0766	-	5.2037	-
(t)-ZrO_2	Patil and Subbarao	5.0893	-	5.1752	-

Table 2(b)
Thermal Expansion Coefficient

Material	α_1 ($x10^6$)	α_3 ($x10^6$)
Mg-(c)-ZrO_2	11.49	-
(t)-ZrO_2	11.6	16.08

Table 3. The Stress-Free Strain ($x10^2$)

Case+	O.R.+	System	Data*	e_{11}	e_{22}	e_{33}	e_{13}
A	CXZ	C-m		0.86595	2.47244	4.24915	8.34572
		C-t	H	-0.059055	-0.059055	2.02756	0.
		C-t	M	-0.06750	-0.06750	2.43530	0.
		C-t	P	0.18307	0.18307	1.87402	0.
B	AXZ	C-m	H	4.30253	2.51779	-1.78559	8.26297
	(LCA)	C-m	M	4.31272	2.52646	-2.18044	8.24638
		C-m	P	4.04910	2.26999	-1.63528	8.25961
	BXY_L						(e_{12})
B	(LCB)	C-m	H	0.91035	4.29555	-2.04119	-8.35065
		C-m	M	0.91888	4.30437	-0.60390	-8.35136
		C-m	P	0.66643	4.04345	-0.05274	-8.33047
	CXZ	C-m	H	0.91734	2.51779	1.53037	8.26578
B	(LCC)	C-m	M	0.92724	2.52646	1.12232	8.24975
		C-m	P	0.67208	2.26999	1.68568	8.26189
B		C-t		-0.01520	-0.01520	-0.64016	0.

+In Case A, all the precipitate-matrix interfaces are fully coherent, while in Case B, the (t)-ZrO_2 precipitate is stress-free at the annealing temperature.
+The orientation relationships are defined in Fig. 2.
*Data indicate the data source for the lattice constants of (t)-ZrO_2: H for Hannink, m for modified Hannink, and P for Patil et al.

Table 4. Shear Energy per Unit Precipitate Volume (in MPa) for 1% Shear Stress-Free Strain

Shape	Matrix	Shear	S.E. (no twin)	S.E.(1)	S.E.(2)	S.E.(3)	S.E.(4)
Ellipsoid (5.5:2.2:1)	Mg-(c)-ZrO_2	XZ	5.87917	2.0796	1.28952	0.99315	0.83267
		YZ	5.48827	2.87697	1.57579	1.19083	0.98462
		XY	12.40154	12.40154	12.40154	12.40154	12.40154
	Ca-(c)-ZrO_2	XZ	4.92790	1.85574	1.11566	0.87616	0.73521
Sphere	Mg-(c)-ZrO_2	XZ	8.82230	6.59681	3.57199	2.52702	2.04090

(The data are plotted in Figs. 7a, 7b, 7c)

Table 5(a). Total Strain Energy+ Per Unit Precipitate Volume (in MPa) (ellipsoidal inclusion 5.5:2.2:1)

Twinning plane	Orientation Relationship	Case	ΔE(no Twin)	ΔE(1)	ΔE(2)	ΔE(4)
100	AXZ	A	694.75	430.11	375.08	343.26
		B	670.87	412.49	358.76	327.69
100	AYZ	A	623.09	441.21	350.58	309.41
		B	598.22	420.64	332.16	291.96
001	CXZ	A	534.81	270.16	215.13	183.37
		B	476.01	217.41	163.64	132.55
001	CYZ	A	526.85	344.97	254.34	213.17
		B	469.83	292.11	203.56	163.32
010 (Symmetry plane) (no Twinning)	BXY(L)	A	1046	not applicable		
		B	1015			
010 (Symmetry plane) (no Twinning)	BXY(S)	A	1110	not applicable		
		B	1081			

+The values are based on modified tetragonal lattice constants measured by Hannink. The matrix is Mg-(c)-ZrO_2.

Table 5(b). Total Strain Energy Per Unit Precipitate Volume (in MPa) (spherical inclusion)

Twinning plane	Orientation Relationship	Case	ΔE no Twinning	ΔE(1)	ΔE(2)	ΔE(4)
100	AXZ	A	785.22	630.21	419.53	312.89
	or AYZ	B	764.68	613.34	407.65	303.53
001	CXZ	A	785.22	630.21	419.53	312.89
	or CYZ	B	670.23	518.77	312.91	208.70
010 (Symmetry plane) (no Twinning)	BXY(L) or BXY(S)	A	785.22	not applicable		
		B	735.33	not applicable		

Table 6. Strain Energy Per Unit Precipitate Volume (in MPa) Contributed by the Diagonal Stress-Free Strain (for Monoclinic inclusion in Cubic Matrix)

Orientation Relationship	Case	E_{diag} Ellipsoidal inclusion	E_{diag} Spherical inclusion
AXZ	A	299.74	205.74
	B	272.17	167.30
AYZ	A	255.31	205.74
	B	226.10	167.30
CXZ	A	139.80	205.74
	B	76.98	72.36
CYZ	A	159.07	205.74
	B	97.41	72.36
BXY(L)	A	197.24	205.74
	B	151.28	122.58
BXY(S)	A	260.94	205.74
	B	217.56	122.58

FIGURE CAPTIONS

Fig. 1. Zirconia-rich portion of the phase diagram for the ZrO_2-MgO system.

Fig. 2. Six possible orientations of the ellipsoidal monoclinic phase embedded in the cubic phase. The X and Z axes are parallel to the longest and the shortest axes of the ellipsoid respectively. The X, Y, Z directions are the ⟨100⟩ directions in the cubic phase.

Fig. 3-6. Finite element meshes used in the study of the strain energy of the twinned martensite.

Fig. 7. The shear strain energy per unit precipitate volume per 1% stress-free shear strain for the ellipsoidal precipitate with aspect ratio 5.5:2.2:1.

7(a) the effect of the shearing plane (for Mg-(c)-ZrO_2 matrix)

7(b) the effect of the different matrices (XZ shear plane)

7(c) the effect of the precipitate shapes (XZ shear plane).

Fig. 8. Comparison of the total strain energies per unit precipitate volume of the ellipsoidal particle (5.5:2.2:1) embedded in Mg-(c)-ZrO_2 for different stress-free strains based on different lattice parameters for orientation relationship CXZ.

Fig. 9. Total strain energy per unit precipitate volume for an ellipsoidal particle with the aspect ratio (5.5:2.2:1).

9(a) coherent particle (Case A)

9(b) incoherent particle (Case B).

Fig. 10. Total strain energy per unit precipitate volume for a spherical particle.

Fig. 11. Comparison of the total strain energies between a spherical and an ellipsoidal incoherent particles.

Fig. 12. The variation of the total strain energy of an ellipsoidal particle (5.5:2.2:1) as a function of the particle size and internal twinning.

Fig. 13. The twin width as a function of the particle size.

Fig. 14. Similar systems A and B with $m = 2$, $n = 4$, $k = 2$.

Fig. 15. The relation between the constrained and the unconstrained lattice constants.

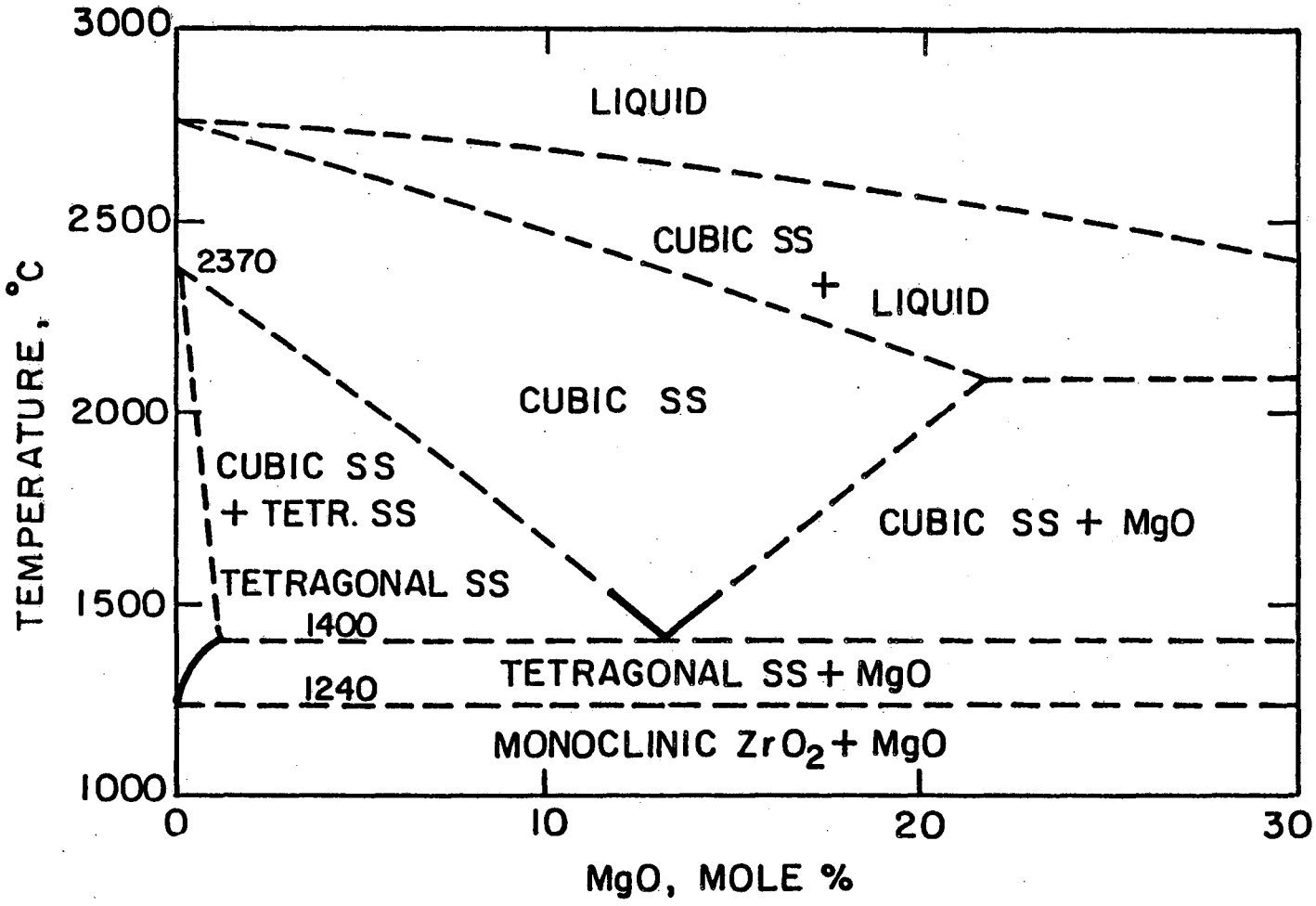

Fig. 1

XBL 8111 -6928

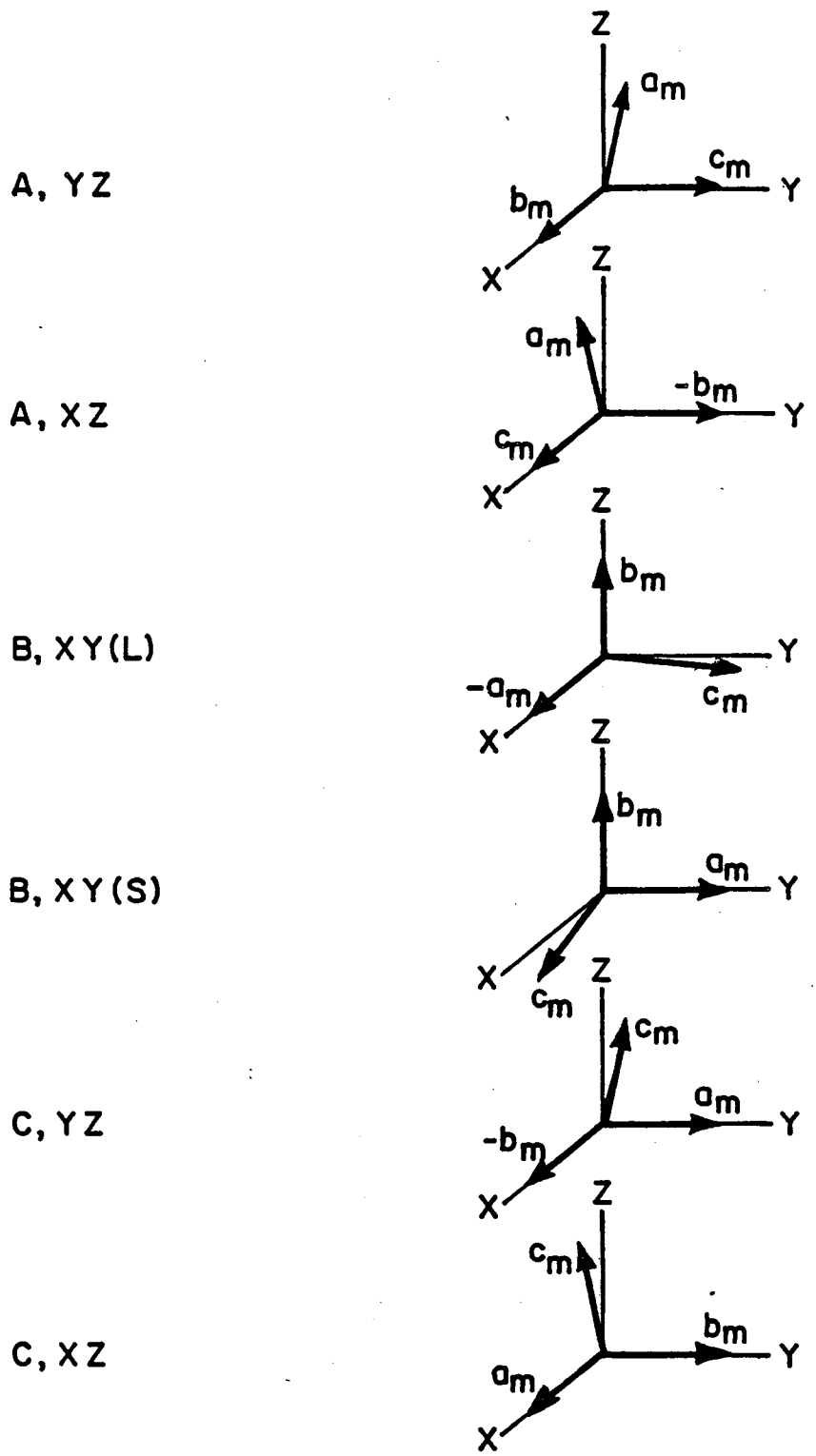

XBL 8111-6931

Fig. 2

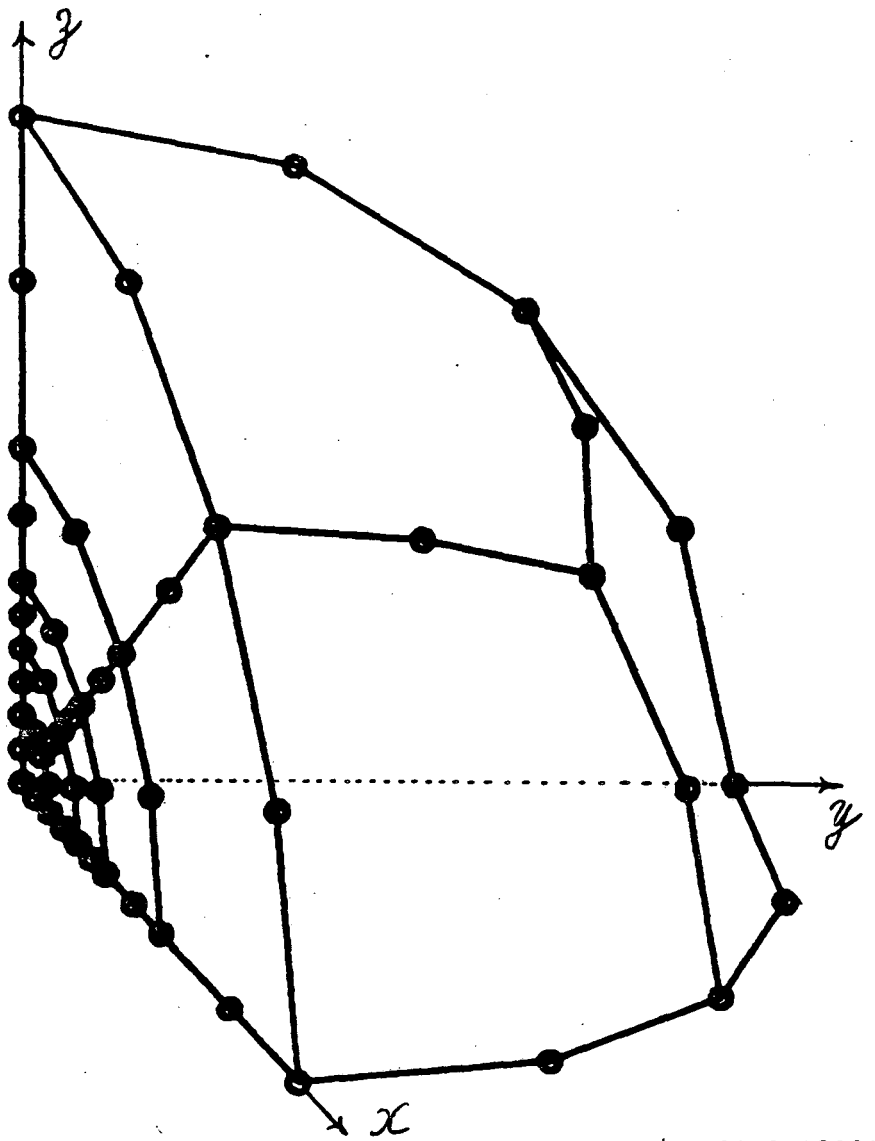

XBL 8110-12231

Fig. 3

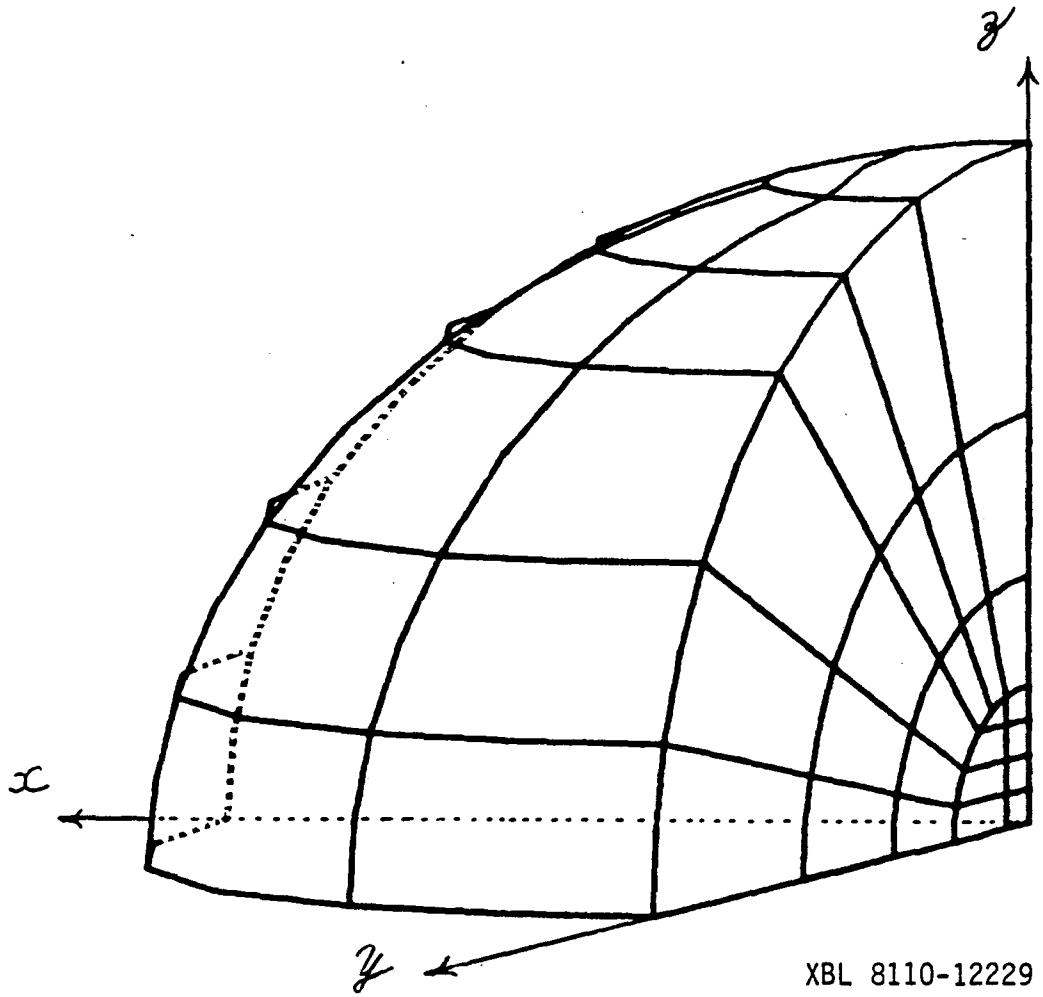

XBL 8110-12229

Fig. 4

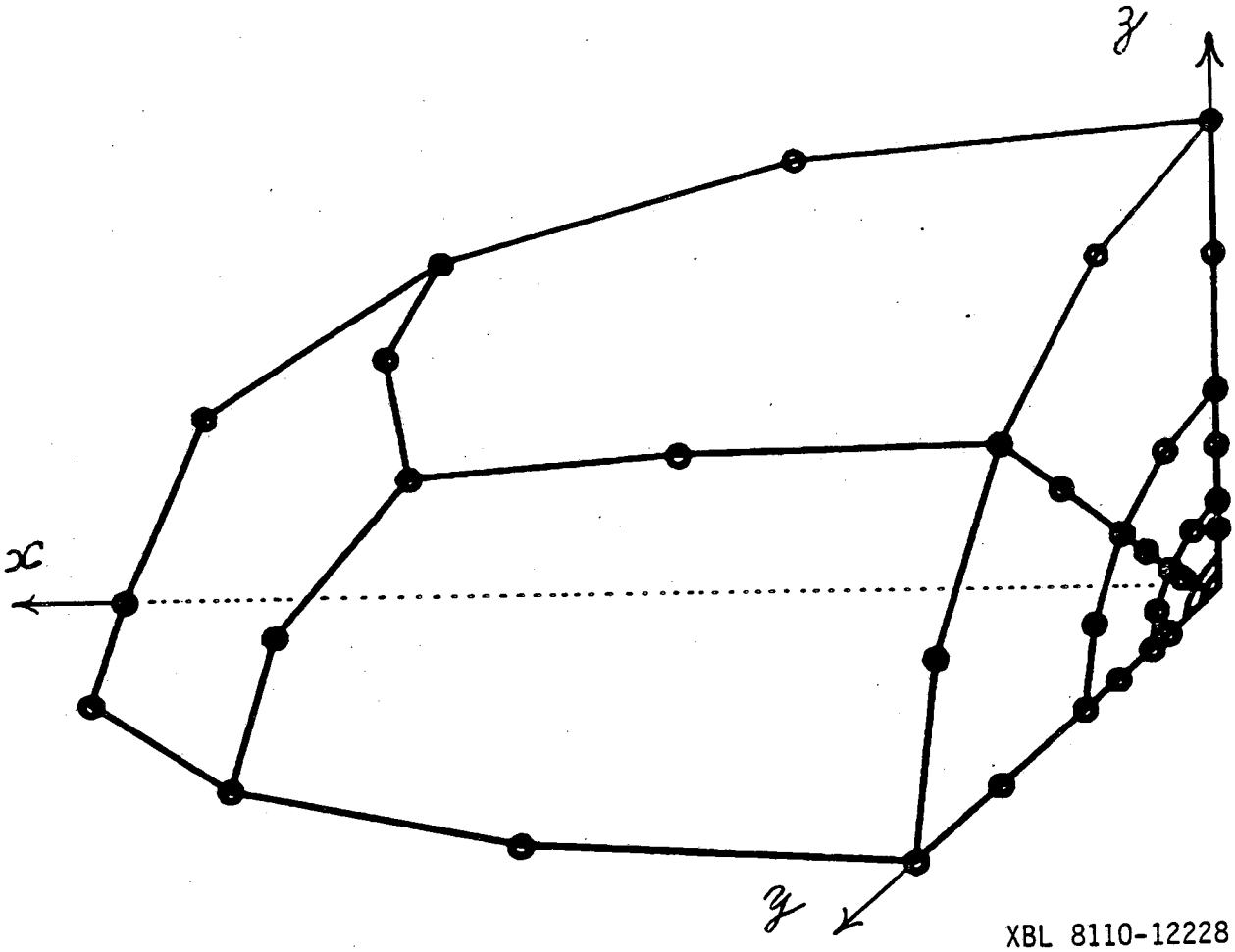

XBL 8110-12228

Fig. 5

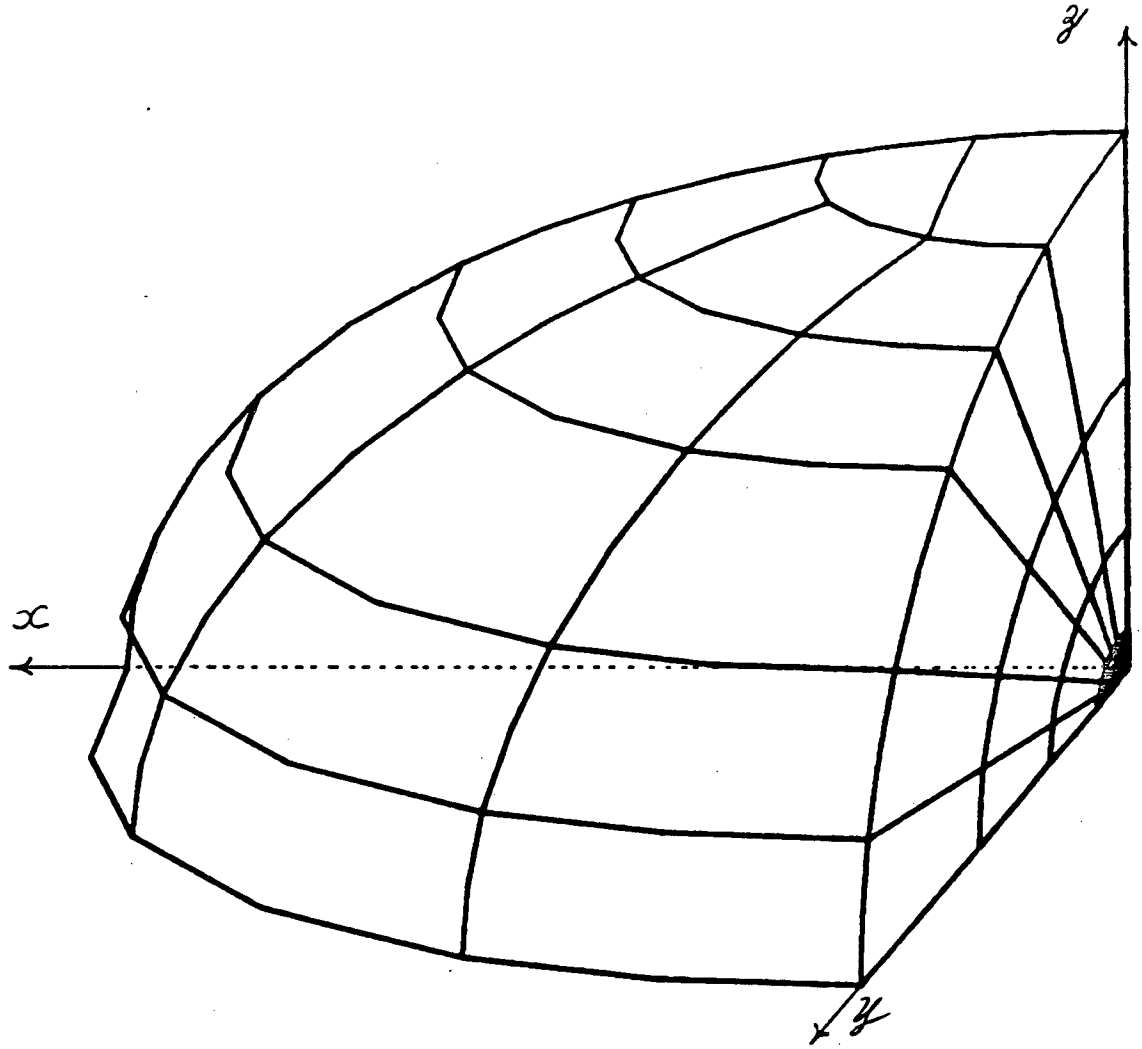

XBL 8110-12230

Fig. 6

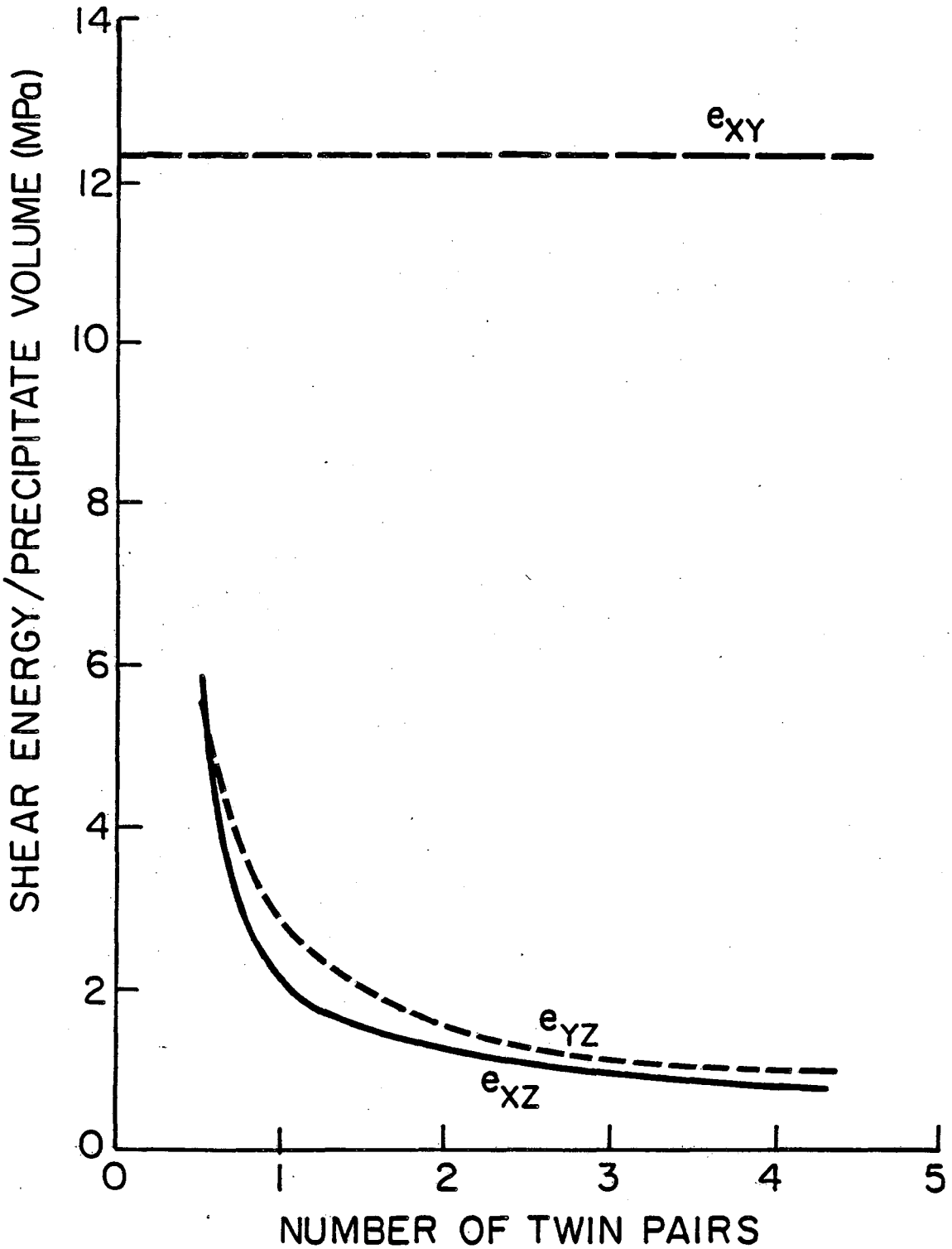

Fig. 7a

XBL 816-5867

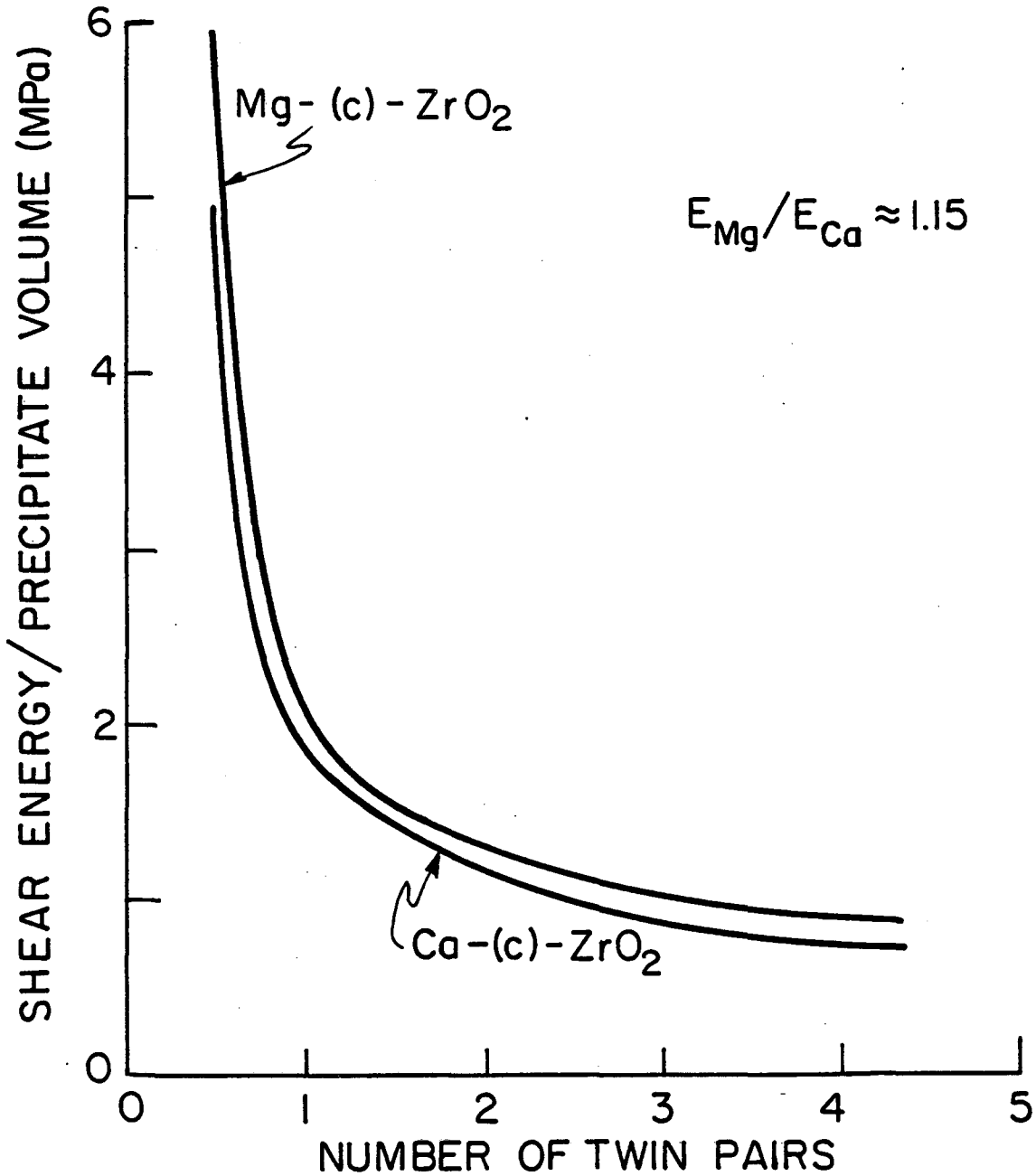

XBL 816-5868

Fig. 7b

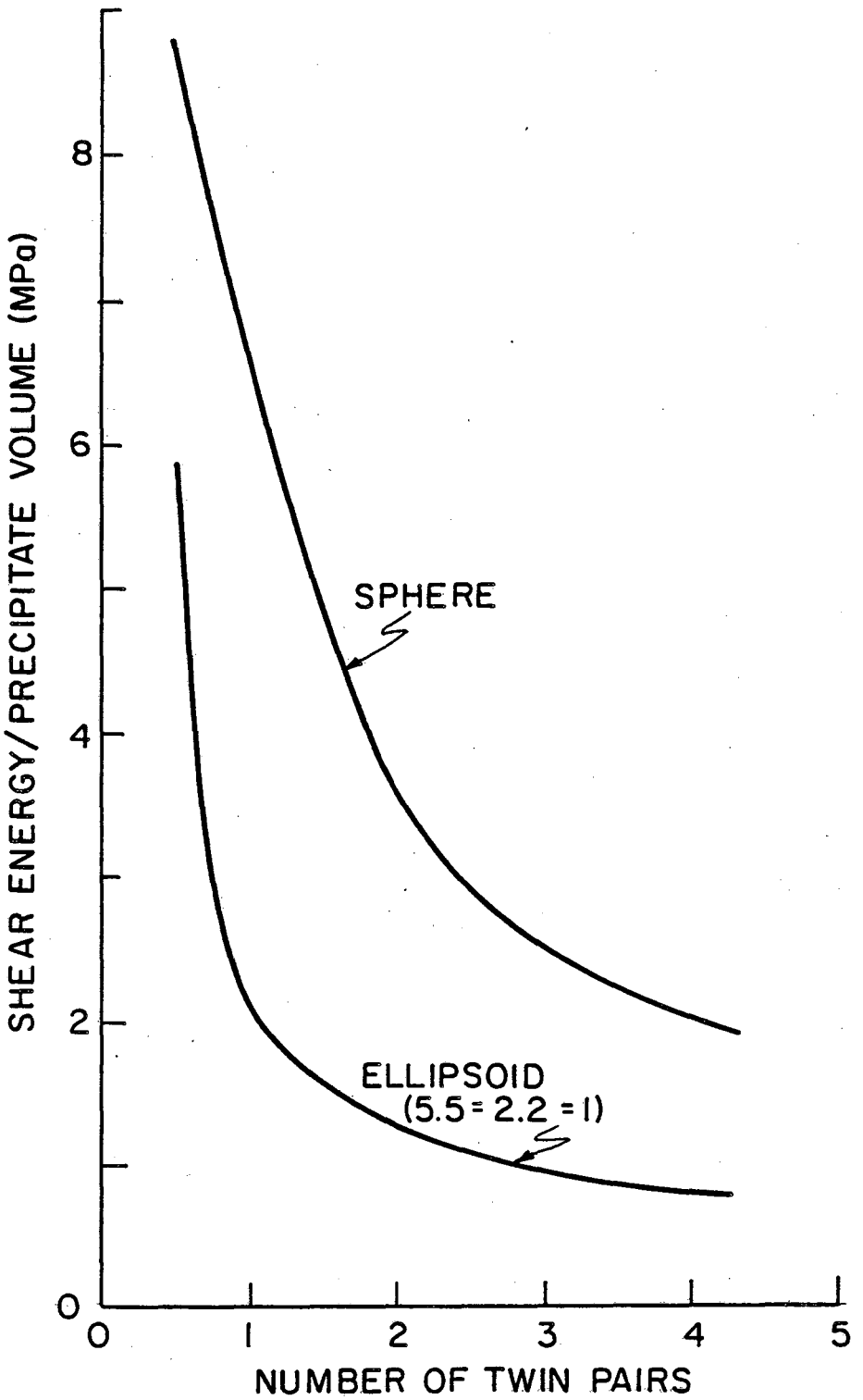

XBL 816-5869

Fig. 7c

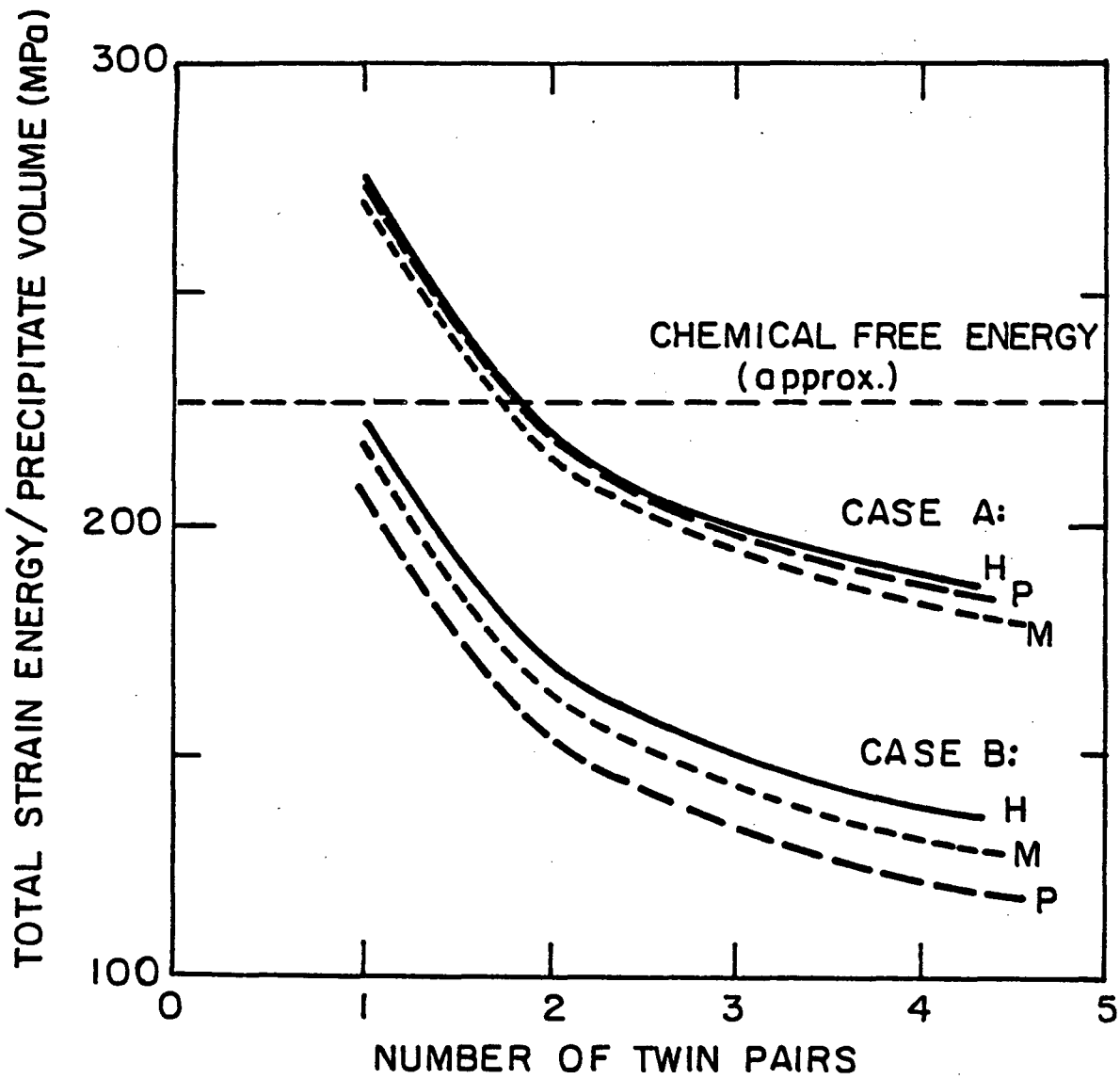

XBL8111-6932

Fig. 8

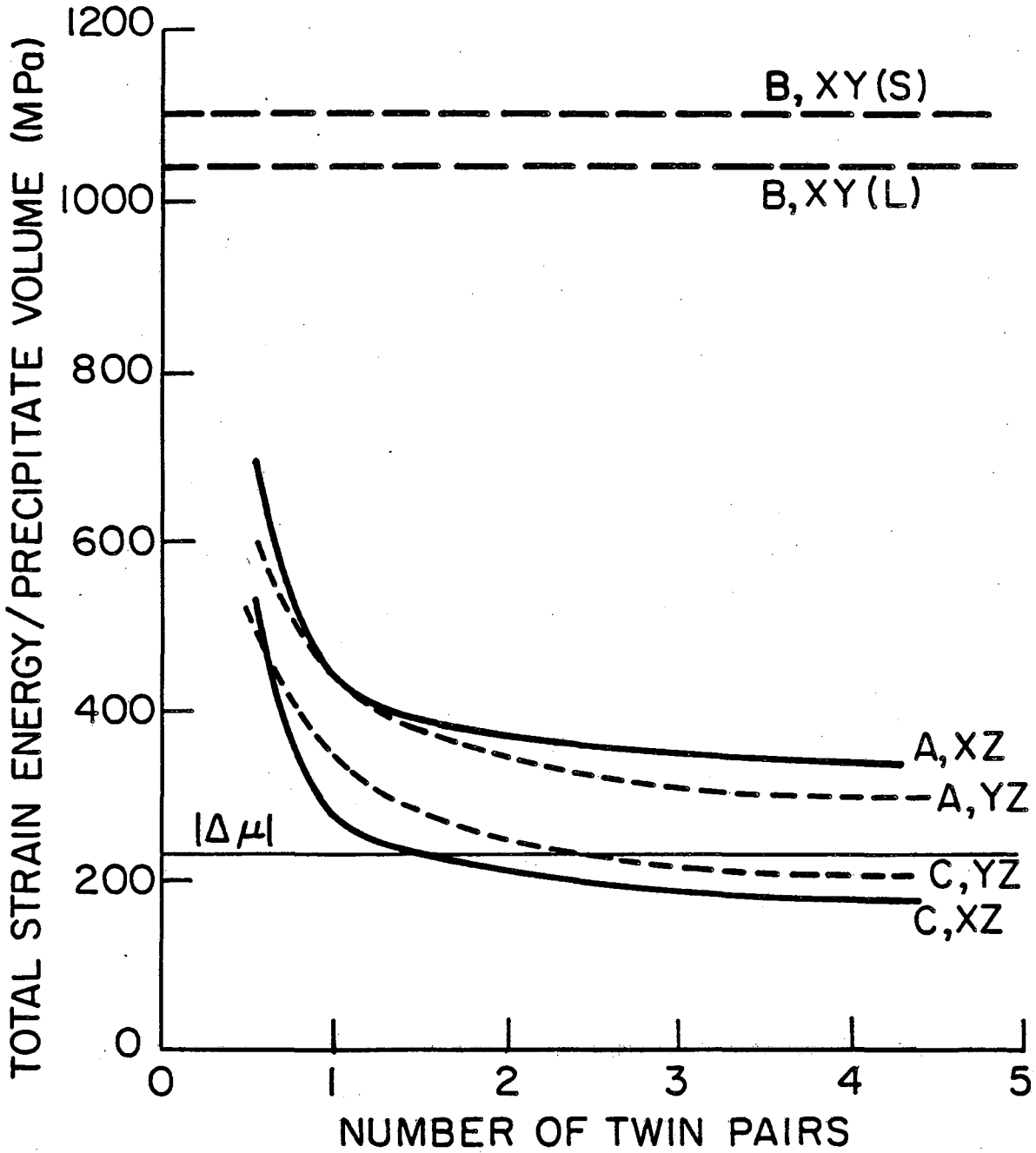

XBL816-5870

Fig. 9a

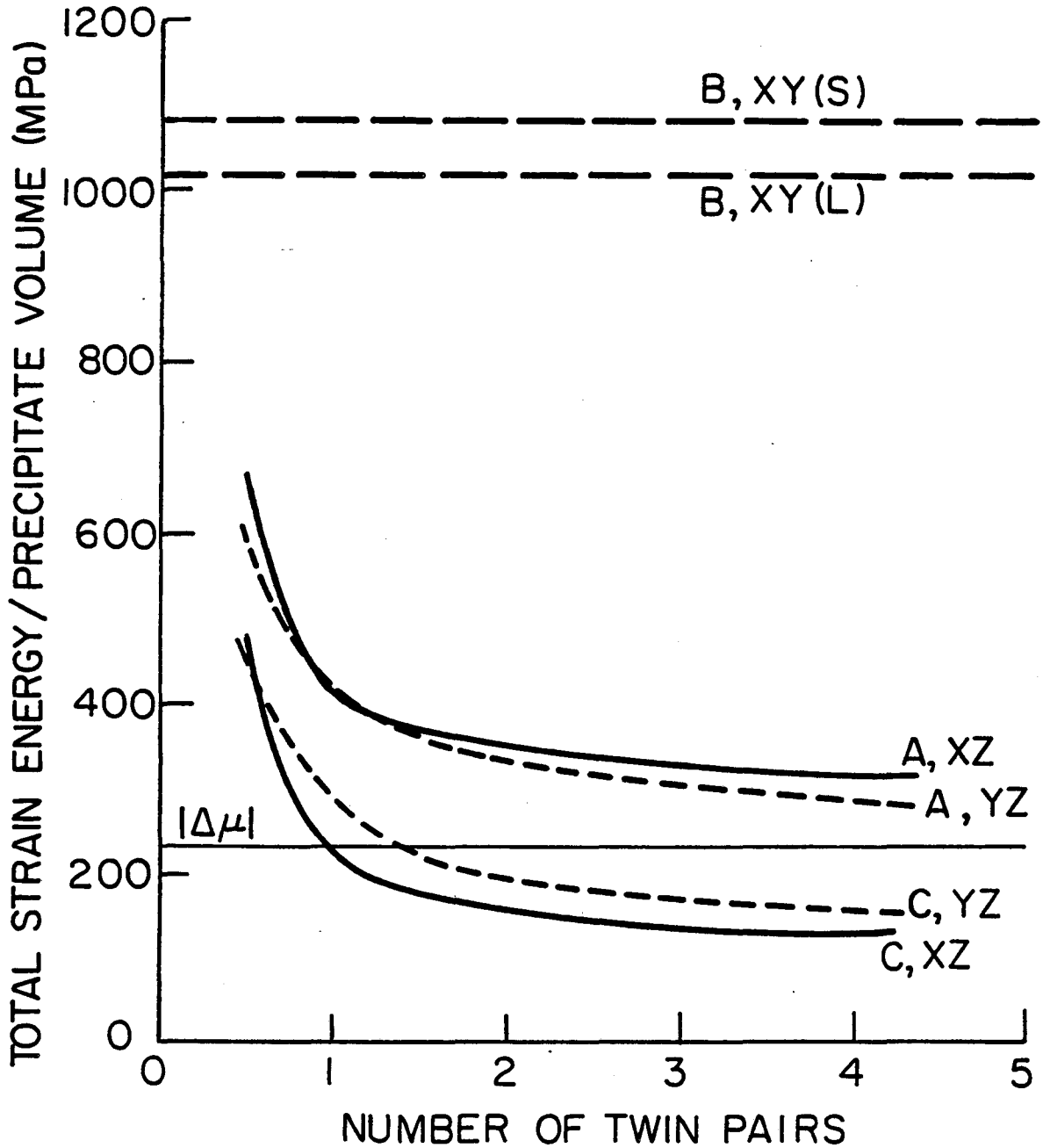

XBL 816-5871

Fig. 9b

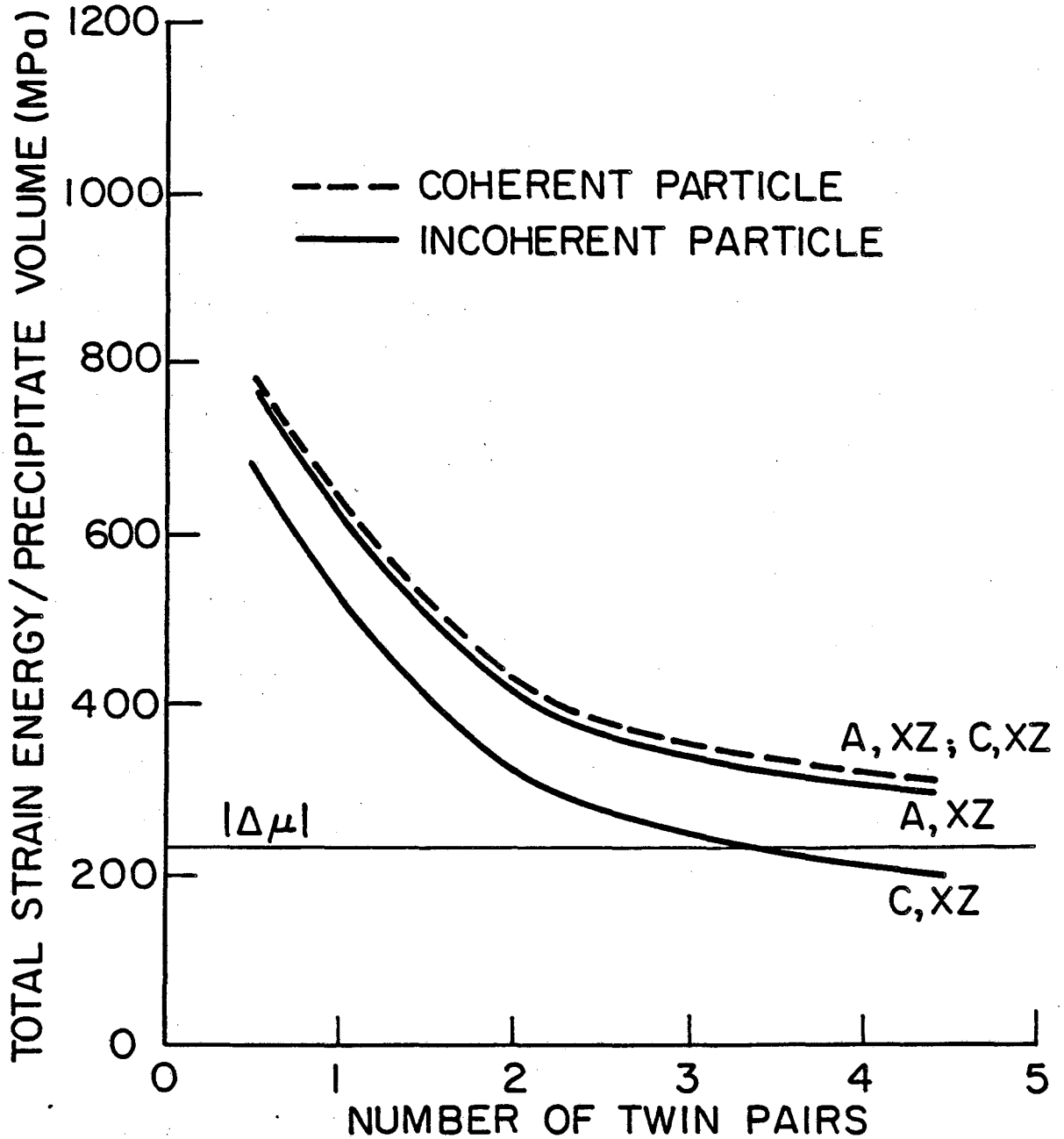

XBL816-5872

Fig. 10

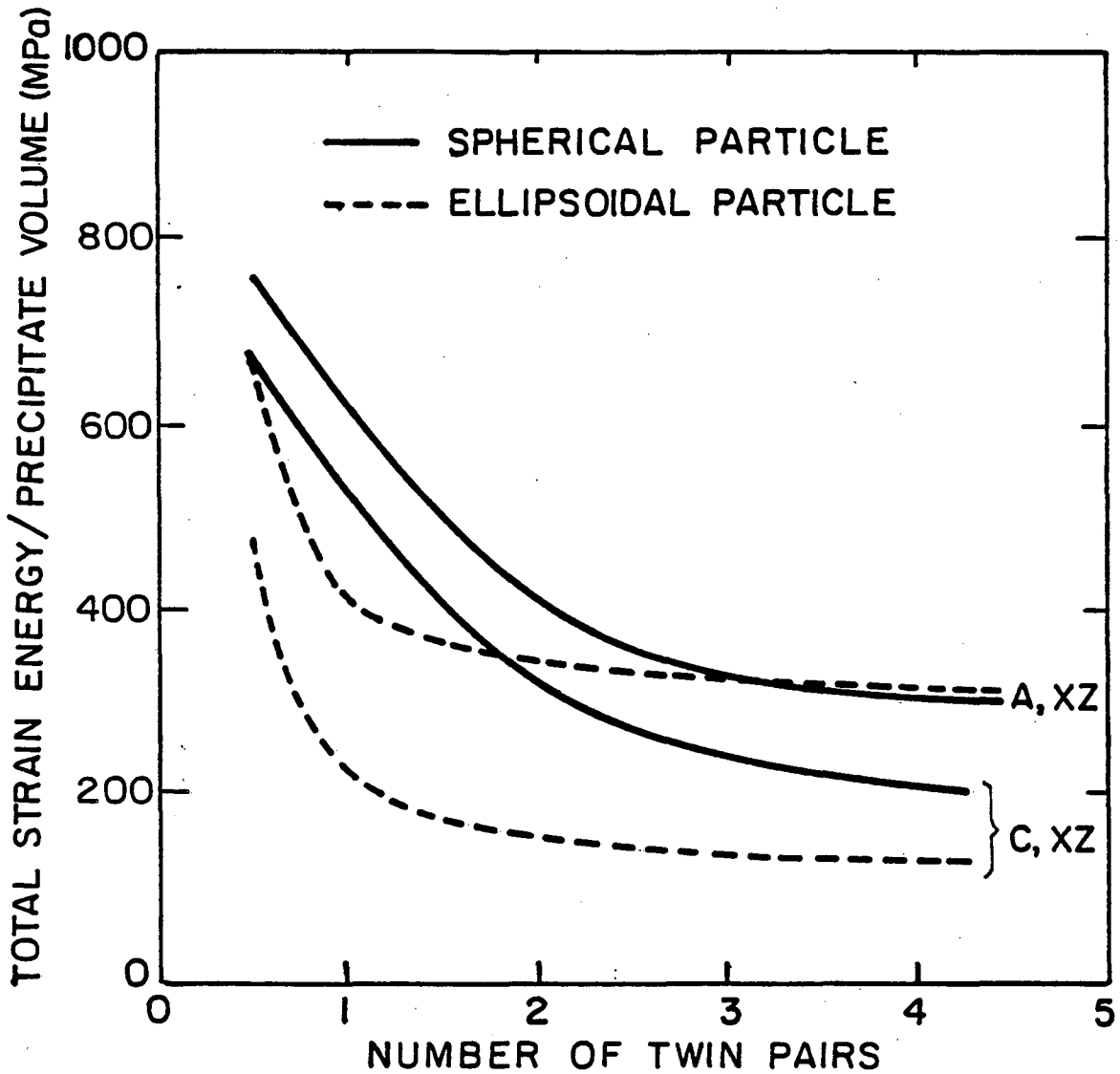

XBL8111-6933

Fig. 11

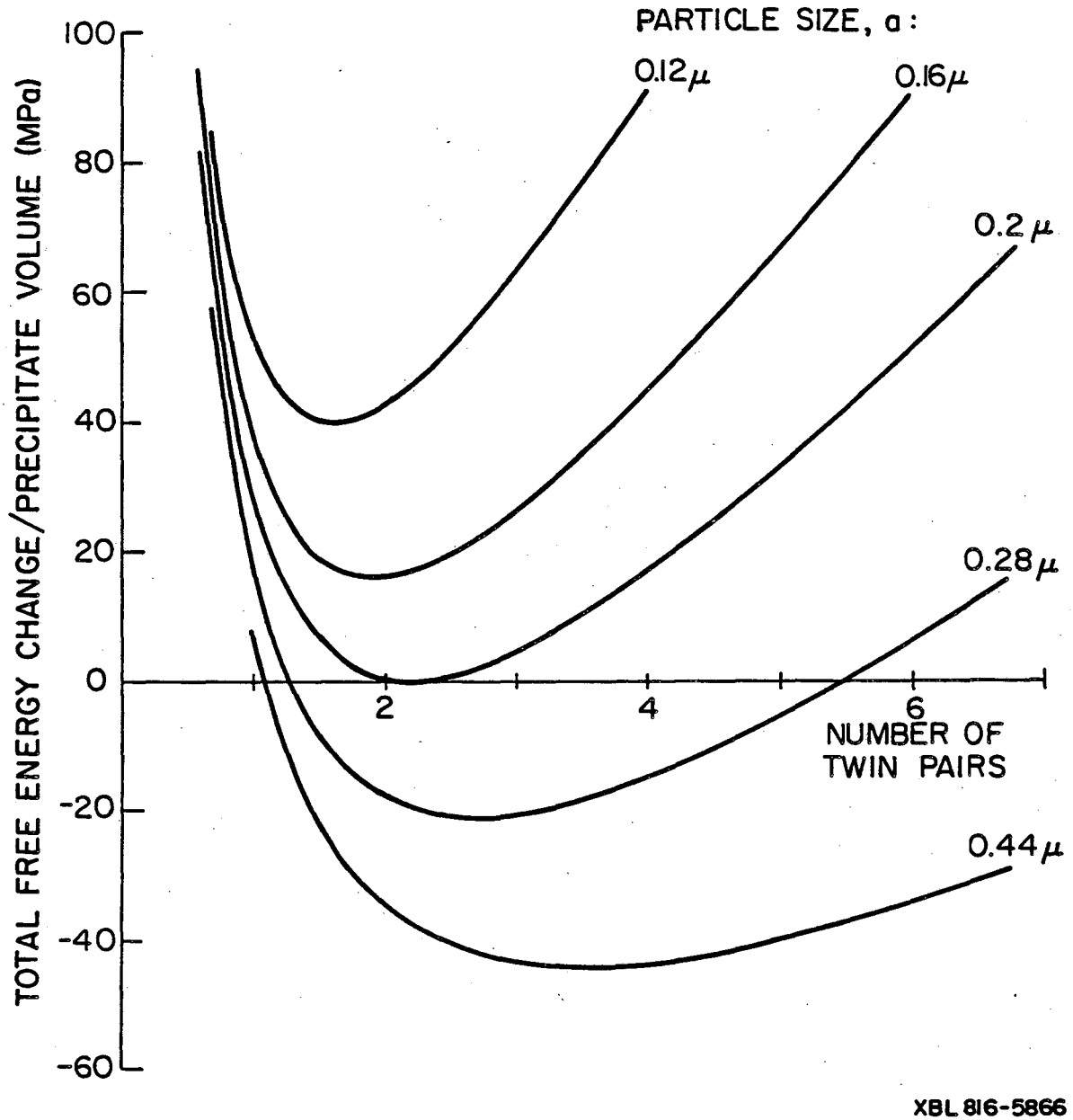
PARTICLE SIZE, a:
0.12μ
0.16μ
0.2μ
0.28μ
0.44μ
TOTAL FREE ENERGY CHANGE/PRECIPITATE VOLUME (MPa)
100
80
60
40
20
0
-20
-40
-60
2
4
6
NUMBER OF TWIN PAIRS
XBL 816-5866

Fig. 12

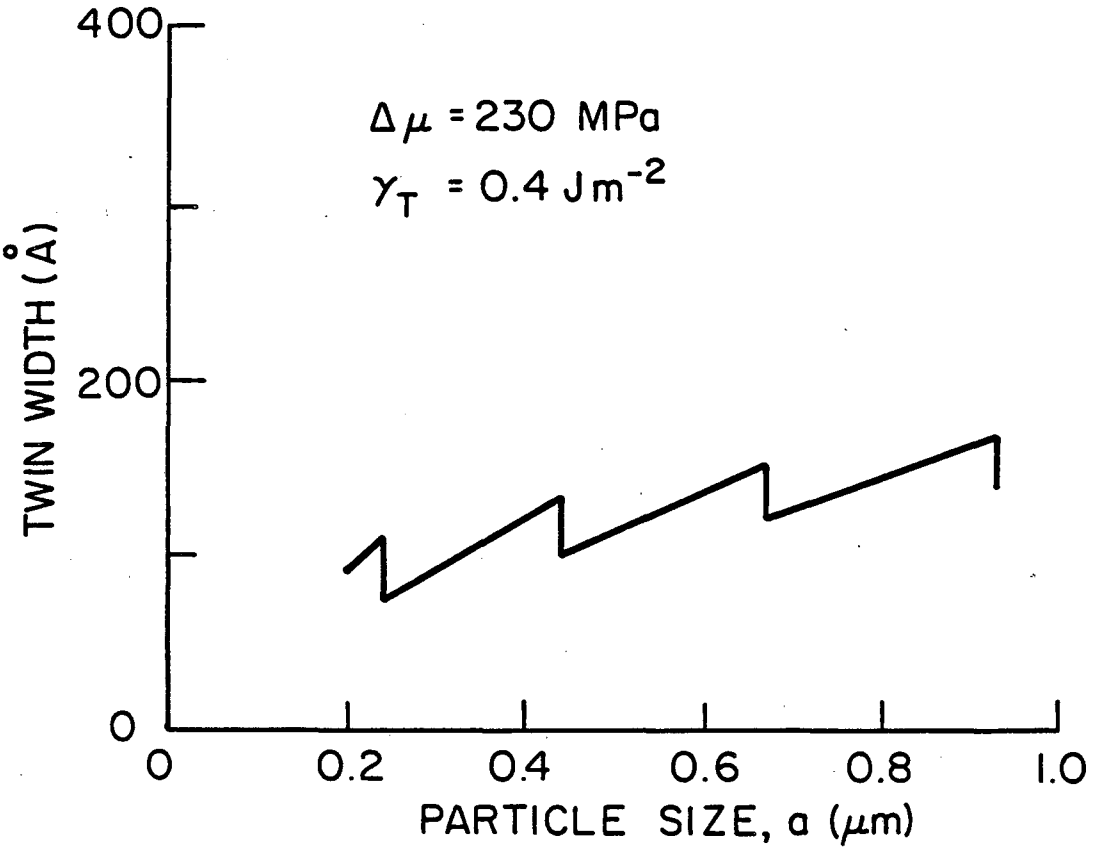

Fig. 13

XBL816-5873

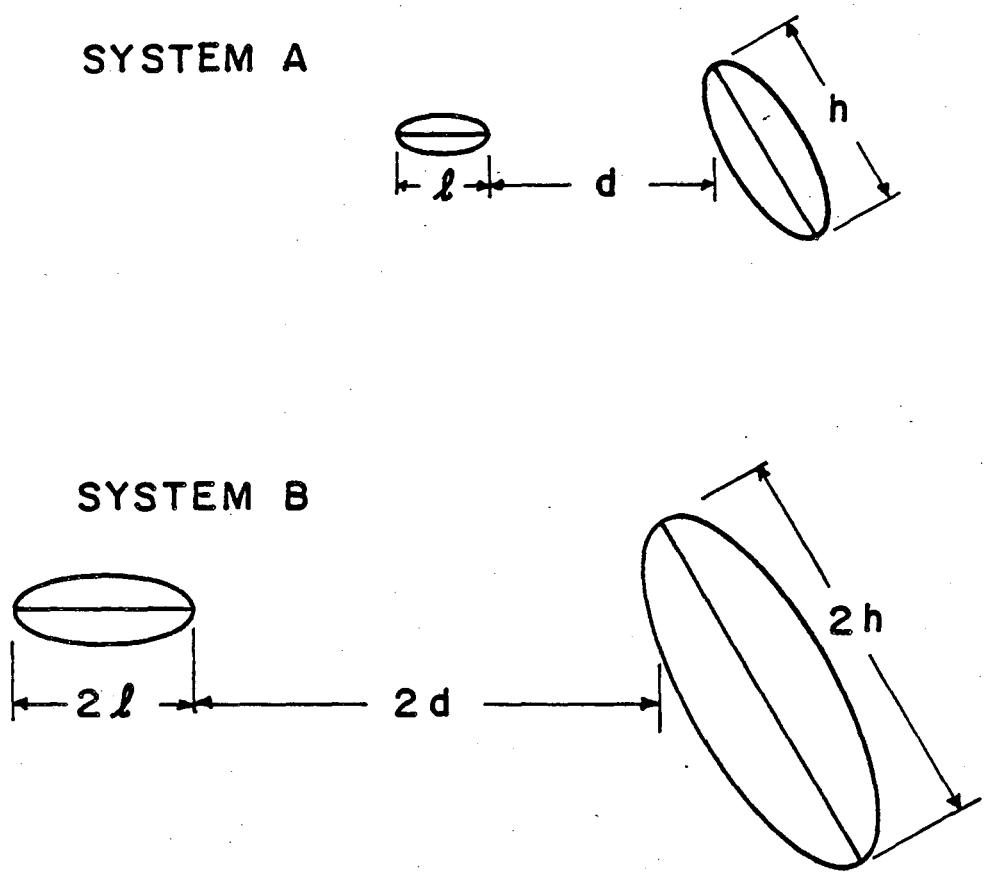

Fig. 14

XBL 8111-6934

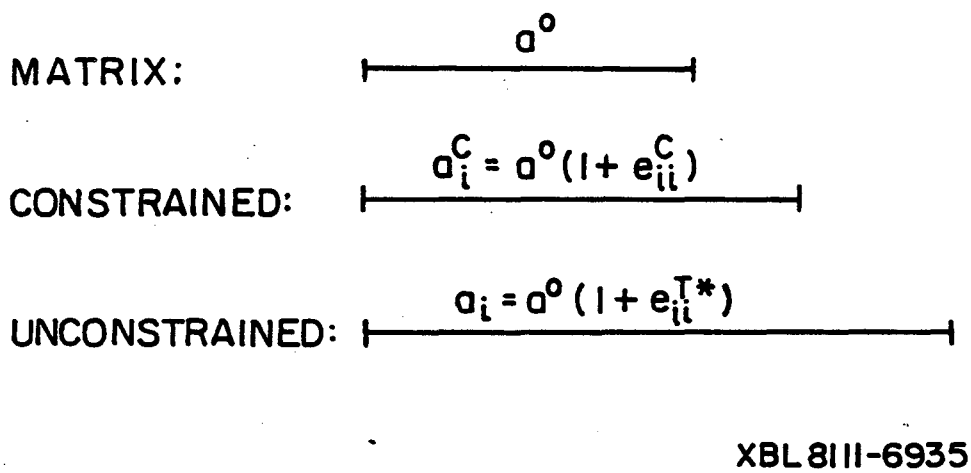

XBL8111-6935

Fig. 15

To my parents, my wife Lily, and my daughter Emily

Acknowledgement

The farmer can not take all the credit for the harvest. He would thank God and Goddess for the abundant year. He would thank the sun, the moon, the rain, and the earth for providing the energy, nutrition, and support needed for the proper growth of the crops. He would also thank the people who make the farming tools and chemicals for their products which make farming feasible. In fact, with appreciation for what he experienced and recognizing that no event in the world can be isolated from the others, he is thankful to everyone for everything.

This work has been inspired, encouraged and supported by the people around me in Berkeley. Without their contribution, this work would not have been possible. I find myself feeling the same way as the farmer.

Among all, I would like to express my deepest gratitude to my advisor, Professor Anthony G. Evans and to Professor Alan W. Searcy for their able guidance, encouragement and support. Their stimulating inspiration and enthusiasm brought this work into being.

I would also like to express my sincere thanks to Professor Iain Finnie and Professor Didier R. Defontaine for their valuable advice and stimulating discussions on this work.

The computer program developed in this study is based on the finite element program SAP IV. I am in debt to the authors of the PROGRAM SAP IV, Professor K. J. Bathe, Professor E. L. Wilson, and Professor F. E. Peterson. Special thanks must go to Mr. Ken Wang of the Department of Civil Engineering, who made the program available to me.

I am pleased to thank Mr. Francis C. Lin who first advised me to use SAP IV. A special deep appreciation is extended to Dr. Y. C. Chen and Dr. Paul F. Chen for their kindly assistance during the early development of the computer program. Without their help, this work would have been dead in its initial stage.

Many thanks to the colleagues in our research group and department, who provided interesting discussions and a pleasant working atmosphere. I would like especially to thank Dr. Keh-Minn Chang, Dr. Stephen T. Tso, Dr.Shu-Sheng Chiang and Dr. Ming-Hwei Hong for the very fruitful discussions and constant encouragement.

I am pleased to thank Ms. Mary Besser for her kindly assistance with the typing of the first draft. Many thanks to the technical typing staff, Jean Wolslegel and June DeLaVergne, for the careful preparation of this manuscript.

I would like especially to thank my parents, my brothers, and most of all my wife. Without their love, understanding, and encouragement, this work would not have been possible.

I am in debt to Venerable C. M. Chen. His encouragement inspired me with the confidence that there must be a solution, which is the key to the persistent research that finally leads to success.

This work was supported by the Director, office of Energy Research, Office of Basic Energy Sciences, Materials Science Division of the U. S. Department of Energy under Contract No. W-7405-ENG-48.

This report was done with support from the Department of Energy. Any conclusions or opinions expressed in this report represent solely those of the author(s) and not necessarily those of The Regents of the University of California, the Lawrence Berkeley Laboratory or the Department of Energy.

Reference to a company or product name does not imply approval or recommendation of the product by the University of California or the U.S. Department of Energy to the exclusion of others that may be suitable.

TECHNICAL INFORMATION DEPARTMENT
LAWRENCE BERKELEY LABORATORY
UNIVERSITY OF CALIFORNIA
BERKELEY, CALIFORNIA 94720